One-Dimensional Mathematical Model for Quantum Particles in Weakly Curved Optical Lattices

Diplomarbeit

in

Theoretischer Physik

von

Sandro Gödtel

durchgeführt am

Fachbereich Physik

der Technischen Universität Kaiserslautern

unter Anleitung von

Prof. Dr. James R. Anglin

Mai 2017

Zusammenfassung

In nahezu allen theoretischen und experimentellen Arbeiten zu ultrakalten Quantengasen wurden diese in flachen Geometrien wie z.B. flache und homogene Gitter untersucht. Erst in den letzten Jahren untersuchten einige Arbeitsgruppen anhand spezieller Beispiele Quantengase auf gekrümmten Oberflächen wie z.B. Kugeloberflächen. Hierdurch motiviert, beschäftigt sich die vorliegende Diplomarbeit mit dem Verhalten von Quantenteilchen in gekrümmten optischen Gittern.

Zunächst gehen wir genauer auf das flache Bose-Hubbard Modell ein und berechnen sowohl analytisch als auch numerisch den Tunnelparameter für beliebige Distanzen. Anschließend verifizieren wir unsere Ergebnisse im Rahmen eines Kontinuumslimes. Dafür rekonstruieren wir ausgehend von dem Hamilton-Operator des Bose-Hubbard Modells im Limes einer verschwindender Gitterkonstanten den zweitquantisierten Hamilton-Operator im Kontinuum, der ursprünglich der Ausgangspunkt für die Herleitung des Bose-Hubbard Modells war.

Um ein Quantenteilchen in einem schwach gekrümmten optischen Gitter beschreiben zu können, beschäftigen wir uns nach einer Einführung in die Riemannsche Differentialgeometrie mit der Störungstheorie. Die Annahme einer Störung der Metrik führt dazu, dass sowohl der Hamilton Operator als auch das Skalarprodukt gestört werden. Dadurch ist die bekannte Rayleigh-Schrödinger Störungstheorie, die nur eine Störung des Hamilton Operators vorsieht, nicht mehr anwendbar. Deshalb erweitern wir diese Störungstheorie auf gekrümmte Mannigfaltigkeiten.

Die erweiterte Störungstheorie nutzen wir dann, um ein Quantenteilchen in einem gekrümmtem Gitter zu beschreiben. Im Rahmen eines eindimensionalen Modells zeigen wir für eine beispielhafte lokale Deformation des Gitters, dass der Tunnelparameter räumlich abhängig ist. Analog zum Vorgehen beim flachen Bose-Hubbard Modell überprüfen wir auch für das gekrümmte Modell den Kontinuumslimes.

Abstract

Nearly every theoretical and experimental research work on ultracold quantum particles treats the case of flat geometries, e.g. flat and homogeneous lattices. In recent years a few groups analyzed particular examples of quantum gases on curved surfaces like spheres. Motivated by this the present diploma thesis deals with the properties of quantum particles in curved optical lattices.

First we treat in detail the flat Bose-Hubbard model and determine analytically as well as numerically the hopping parameter for arbitrary hopping distances. Then we verify our results by a continuum limit. Based on the Hamiltonian of the Bose-Hubbard model we perform the limit of vanishing lattice constant and reconstruct with this the second quantized Hamiltonian in the continuum, which was initially used to derive the Bose-Hubbard model.

After an introduction of the Riemannian differential geometry we investigate the perturbation theory in order to describe a quantum particle in a weakly curved optical lattice. Due to the assumption of perturbing the metric, it turns out that both the Hamiltonian and the scalar product are perturbed. Thus the common Rayleigh-Schrödinger perturbation theory, which is based only on a perturbed Hamiltonian, can not be applied. Therefore we have to extend the perturbation theory on curved manifolds.

With the extended perturbation theory we are then able to describe a quantum particle on a curved lattice. In a one-dimensional model we show for an example of a local deformation of the lattice that the hopping parameter becomes spatially dependent. Analogous to the approach of the flat Bose-Hubbard model we test the continuum limit for the curved model afterwards.

Contents

1. Introduction

In the first chapter of this diploma thesis we give a review about the subject of ultracold quantum gases. We begin in Section 1.1 with a brief summary of the research achievements of quantum gases. In Section 1.2 we specialize to the subdomain of optical lattices, their realization, and their properties. A special property of bosonic gases in optical lattices is the quantum phase transition between a superfluid and a Mott-insulating phase which can be explained theoretically by the Bose-Hubbard model. Ultracold quantum gases are often used to simulate physical systems, for instance from solid-state physics, which exist in flat spaces. Therefore, we ask in Section 1.3 and Section 1.4 the question if it is possible to simulate also systems in curved space and curved optical lattices, respectively. To this end we refer to some current experimental and theoretical research in this topic. At the end of this chapter, in Section 1.5 we give an overview of the structure of this diploma thesis.

1.1. Ultracold quantum gases

Although predicted in the year 1925 by Einstein [1], based on a work of Bose from 1924 [2], it lasted seven decades until the macroscopic phenomenon of Bose-Einstein condensation (BEC) was experimentally realizable. Within a few months three groups succeeded 1995 to condense ultracold quantum gases of rubidium-87 [3], lithium-7 [4, 5], and sodium [6]. In the following years many other atoms beside the alkali metals were condensed, e.g. ytterbium-174 [7] and chromium-52 [8].

The technique used in the experiments is a clever combination of a magneto-optical trap (MOT) with both laser and evaporative cooling. A MOT contains a magnetic field which traps an atomic cloud. Additionally three pairs of laser beams cool down the cloud by the effect of stimulated emission. Further cooling is reached by decreasing the trap depth so that the hottest atoms leave the cloud, thus the rest of the atom cloud has a smaller kinetic energy which is equivalent to a lower temperature. This process is called evaporative cooling and was investigated in the first experiments of BEC. Rubidium-87

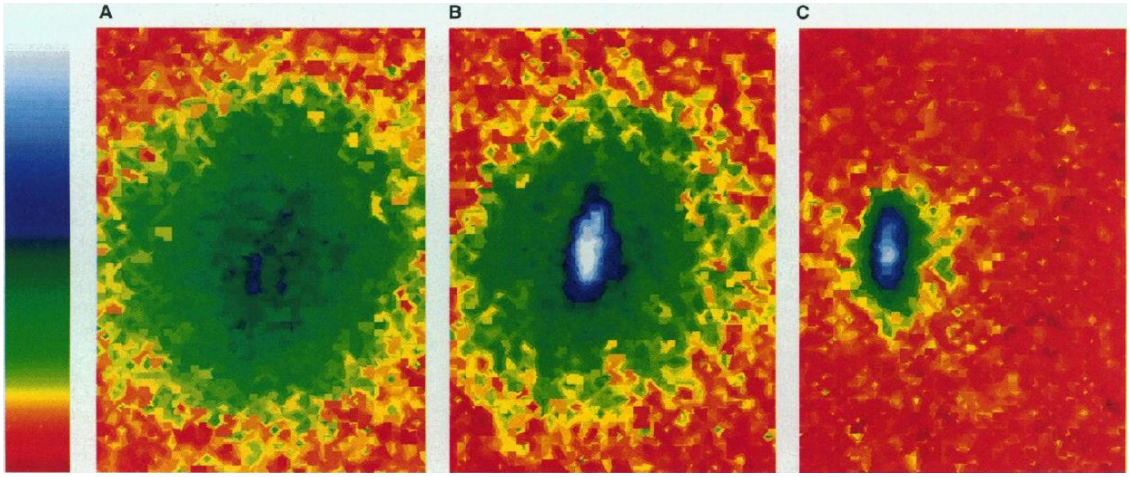

Figure 1.1.: Time-of-flight pictures (false color image) from the first experimentally realized BEC according to Ref. [3]: **A** before the condensation, **B** right after the moment of condensation, and **C** after further evaporating. The blue and white elliptic form represents the BEC while the green and yellow part is the non-condensed thermal atom cloud.

for example can be cooled down to 170 nK using these methods [3].

At such low temperatures the trapped gas shows completely new properties compared to an ideal gas at room temperature. Especially one has to distinguish between fermionic and bosonic gases. A bosonic gas can form a BEC, where nearly all atoms occupy the ground state [9]. Via Feshbach resonance it is also possible to condensate dimers of fermionic atoms [10, 11].

To investigate the behavior of an ultracold quantum gas, so called time-of-flight pictures are taken. For this the trap is turned off so that the atoms fall down due to gravity and expand due to non-zero temperature. After a certain amount of time the velocity distribution is measured which is depending on the temperature. This measurement destroys the sample but it is possible to repeat the condensation process under the same conditions. An example of time-of-flight pictures is shown in Fig. 1.1 which shows the results of the experiment in Ref. [3].

1.2. Optical lattices

An important subdomain of quantum gases physics is the behavior of ultracold atoms in optical lattices predicted in 1998 [12] and realized in 2002 [13]. To this end up to three pairs of laser beams, depending on the dimensionality of the lattice, are used additionally to the MOT to create a periodic potential for the quantum gas. There are

many advantages of optical lattices: By changing the laser frequencies and intensities, the lattice depth and lattice constant can be varied. Using one or two pairs of laser beams leads to one- and two-dimensional lattices [14, 15] and it is possible to create more complicated lattice structures like the Kagome lattice [16] by changing the angles of the laser directions. Thus even more exotic lattice structures can be simulated in the experiment while staying highly controllable. Today it is even possible to address a single site of an optical lattice and manipulate the occupation without loss at the neighboring sites [17, 18]. This technique is based on scanning electron microscopy [19].

A special phenomenon of bosons in an optical lattice is the quantum phase transition which originates from quantum fluctuations. Thermal fluctuations are negligible due to the low temperature, thus phase transitions caused by thermal fluctuations do not appear. In an optical lattice with low lattice depth the Bose gas is after the cooling process a BEC, thus it can be described by one matter wave with longe-range phase coherence [13]. Due to the small lattice depth the bosons can tunnel between the lattice sites, so that their number in each lattice site is fluctuating. Releasing the BEC leads to a characteristic interference pattern in the time-of-flight pictures [15]. In the other limit i.e. deep lattices, the tunneling rate decreases. The number of particles in one lattice site is now fixed and after releasing no interference can be seen. Figure 1.2 shows the time-of-flight pictures for increasing lattice depths, thus revealing the quantum phase transition between the superfluid and the Mott-insulating phase, while Fig. 1.3 illustrates both extreme limits.

The theoretical basis of the behavior of bosonic gases in optical lattices is described by the Bose-Hubbard model, where the Hamiltonian is given by

$$\hat{H}_{\mathrm{BHM}} = -\sum_{<i,j>} J_{ij}\hat{a}_i^\dagger\hat{a}_j - \sum_i \mu_i\hat{a}_i^\dagger\hat{a}_i + \sum_i \frac{U_i}{2}\hat{a}_i^\dagger\hat{a}_i^\dagger\hat{a}_i\hat{a}_i. \tag{1.1}$$

The numbers i and j enumerate the respective lattice sites and $< i, j >$ indicates that the sum is performed over the nearest neighbors. The hopping matrix J_{ij} describes the tunneling of a quantum particle from one lattice site i to another j, μ_i denotes the effective chemical potential at site i, and U_i stands for the interaction strength between two bosons at the same lattice site i. The dominant parameter U_i/J_{ij} determines the phase of the bosonic gas. For weak interaction $U_i/J_{ij} \ll 1$ the tunneling dominates so that the atoms are delocalized over the whole lattice. Thus the condensate is superfluid. In the other case of strong interaction $U_i/J_{ij} \gg 1$, the condensate is in the Mott-insulating phase, where the atoms are strongly correlated and localized to single lattice

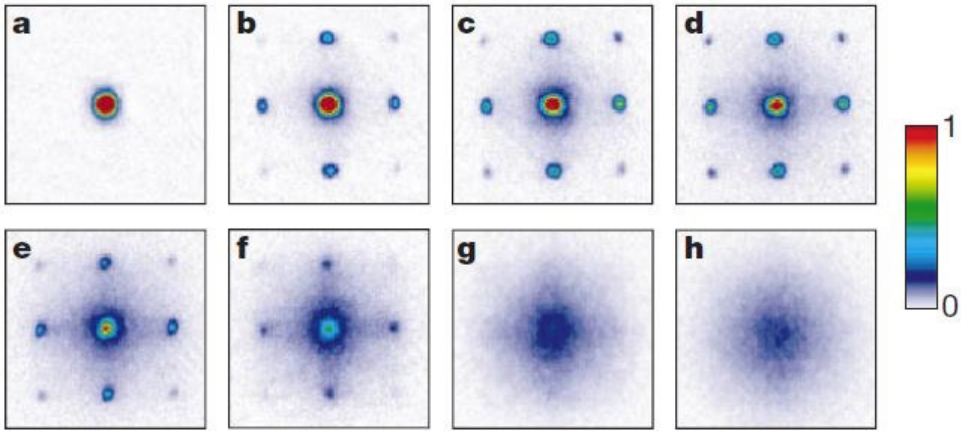

Figure 1.2.: Time-of-flight pictures 15 ms after releasing the atom cloud from an optical lattice with lattice depths V_0 **a** $V_0 = 0\ E_\mathrm{R}$, **b** $V_0 = 3\ E_\mathrm{R}$, **c** $V_0 = 7\ E_\mathrm{R}$, **d** $V_0 = 10\ E_\mathrm{R}$ **e** $V_0 = 13\ E_\mathrm{R}$, **f** $V_0 = 14\ E_\mathrm{R}$, **g** $V_0 = 16\ E_\mathrm{R}$, and **h** $V_0 = 20\ E_\mathrm{R}$ according to Ref. [13]. The recoil energy $E_\mathrm{R} = \hbar^2\pi^2/(2ma^2)$ with the lattice constant a is a typical energy scale depending on the lattice constant and the mass of the atoms of the cloud.

sites [13, 15, 20].

Most of the theoretical calculations are done for the ideal case at temperature $T = 0$ but there are also investigations for finite and thus more realistic temperatures [21, 22].

1.3. Ultracold quantum gases on curved manifolds

So far the overwhelming majority of experimental and theoretical investigations of ultracold quantum gases has been focused on flat spaces. Therefore, the natural question arises whether the field of ultracold quantum gases could also be used to simulate many-body quantum physics in curved spaces. With this one could investigate, which properties quantum particles have in curved geometries.

Initial experimental attempts were focused on analyzing superfluid helium on spheres. Superfluid helium is the most known example of a quantum fluid. Below a temperature of 2.172 K the bosonic isotope He-4 transits from a normal fluid to a superfluid phase, where quantized vortices appear [23]. In this phase the superfluid has also high thermal conductivity and small viscosity [24]. This phase also appears with fermionic He-3 atoms at much lower temperature, when they form pairs similar to Cooper pairs of electrons in superconductors. Another possibility to simulate experimentally quantum gases on a hard sphere is to use two different bosonic species. The idea is that one BEC forms

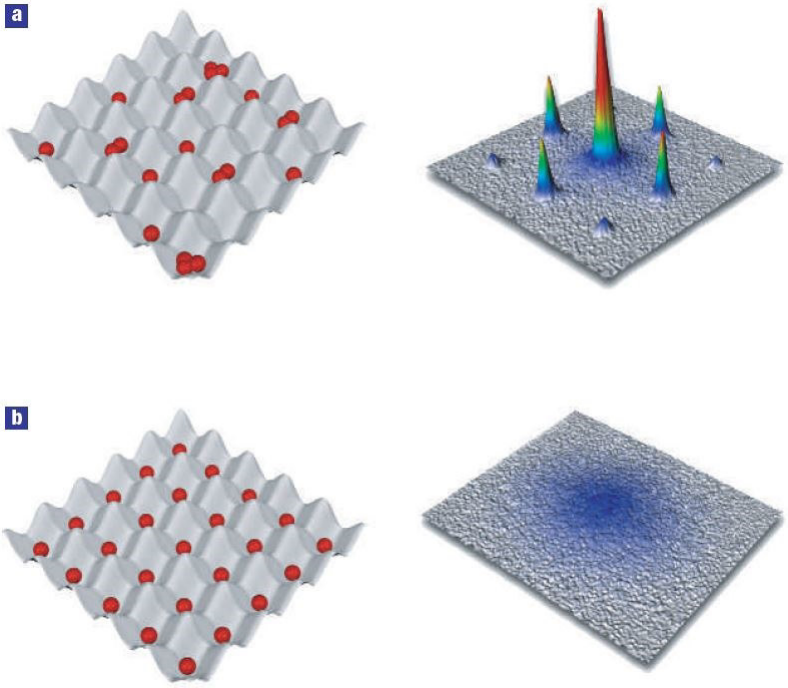

Figure 1.3.: Illustration of **a** superfluid phase and **b** Mott-insulating phase in the optical lattice and as time-of-flight picture [15].

a rigid sphere, while the other lies on top of the first as a thin film which can then be treated as a BEC on a curved surface. Therefore it is necessary that both BEC species do not mix, which is realized provided that the condition

$$g_{11}g_{22} - g_{12}^2 > 0 \tag{1.2}$$

is fulfilled. Note that (1.2) follows, for instance, from an energetic argumentation, where g_{11}, g_{22} and g_{12} denote intra- and inter-species interaction strengths, respectively. These interaction strengths are proportional to the corresponding s-wave scattering lengths, which are tunable via Feshbach resonances [11].

There are many groups working with Bose-Bose mixtures, which are realized for example with two different spin states of rubidium-87 [25] or so called spinor bosons, where different hyperfine states are occupied [26]. Other investigations have also been performed with Bose-Fermi mixtures, which contain both bosons and fermions [27, 28].

In Ref. [29] the density of superfluid He-4 absorbed in porous Vycor glass was studied. It was found out that the density follows a power law in reduced temperature similar to the bulk value of He-4, which was supposed to be a result of the three-dimensional geometry of the substrate. Motivated by this experiment, first theoretical investigations

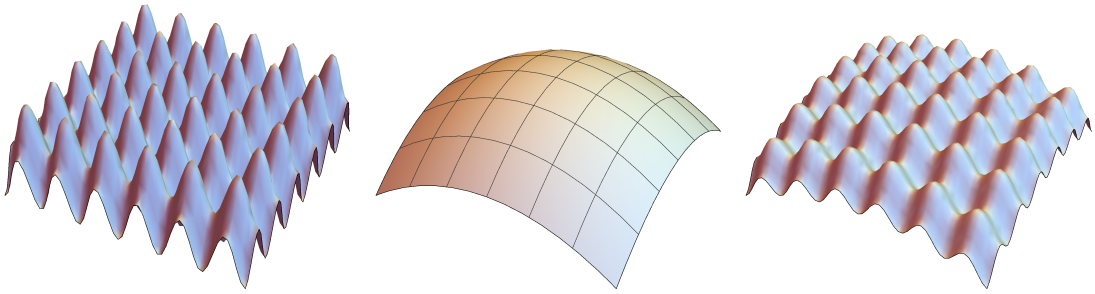

(a) (b) (c)

Figure 1.4.: (a) a typical two-dimensional optical lattice, (b) an illustration of a curved surface, and (c) the deformation of the optical lattice due to the curvature.

were performed in Ref. [30], where the theory of superfluid phase transition is generalized on spherical surfaces. The theory is applied on the experiment of Ref. [29], which leads to the reinterpretation that the power law is a size effect of the spherical structure instead of the three-dimensional geometry.

Furthermore, in the end of 2016 Fan *et al.* obtain for a system of spinless fermions living on a sphere three different phases depending on the radius of the sphere [31]. One phase shows a vortex pair on the poles, the other two phases have a domain wall between two superfluid phases, where the domain wall is in one phase located on the northern or southern hemisphere while in the other phase it is located on the equator. In this year spherical structures were numerically simulated with superfluid helium by Herdman *et al.* [32]. It was found out that the quantum gas shows in this case an entanglement area law, which is similar to black holes [33, 34].

1.4. Curved optical lattices

Another interesting realm of ultracold quantum gases is basically unexplored. Every optical lattice realized experimentally so far is flat. Thus the question is how to simulate curved optical lattices and what effects would occur if quantum particles are loaded into them.

As a first theoretical approach, in Ref. [35] an analogy between the Schrödinger field in discrete curved space and ultracold atoms in an optical lattice was developed. An inhomogeneous hopping term is then directly related to the spatially dependent metric, which describes the curvature. An illustration of such a curved optical lattice is shown in Fig. 1.4. A typical two-dimensional optical lattice in Fig. 1.4a can be deformed by

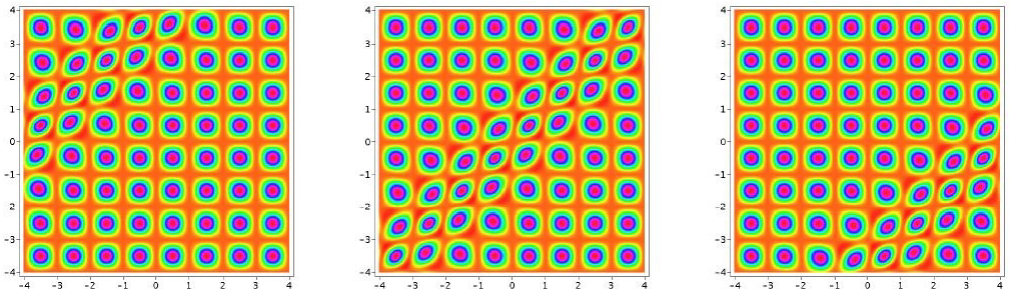

Figure 1.5.: An illustration of a regular optical lattice, which is deformed by a passing metric wave according to Ref. [35].

assuming a certain curvature as in Fig. 1.4b. The result shown in Fig. 1.4c represents then a curved optical lattice.

Furthermore, an example of mimicking metric waves, e.g. gravitational waves, is also given, which is illustrated schematically in Fig. 1.5. Such waves can possibly be created by an additional time-depending laser beam which locally deforms the optical lattice in a periodic way and thus modifies locally the hopping parameter periodically.

The behavior of atomic gases on curved surfaces as well as in curved optical lattices is part of the current research and so far barely explored. However, the realm of ultracold quantum gases offers many advantages including analogue models of solid-state physics and other theories. Even models of astrophysics and cosmology like cosmological strings [36], black holes [37], Hawking radiation [38] as well as gravity itself [39, 40] can be tested within a few seconds in a vacuum chamber instead of many years in the universe. Especially constructing analogue models can lead to a better understanding of physics and maybe some new effects will be found in this way.

1.5. Overview

The aim of this diploma thesis is to investigate a model for quantum particles in curved optical lattices. To this end we apply the concepts of the Riemannian differential geometry to the Bose-Hubbard model and find that a curved lattice is related to an inhomogeneous hopping term. Additionally we assume weak curvature so that we can treat the resulting problem within perturbation theory.

We begin this thesis with reviewing the flat Bose-Hubbard model in Chapter 2. After a short derivation of the Bose-Hubbard Hamiltonian, we discuss the method of continued fraction to derive the form and special properties of both the Bloch and the Wannier functions. These functions are essential for determining the hopping parameter and the

onsite energy. We conclude Chapter 2 by calculating the continuum limit of the Bose-Hubbard model for vanishing lattice constant in order to reconstruct the continuous Hamiltonian of an ultracold quantum gas.

Subsequently, Chapter 3 treats the Riemannian differential geometry, where we introduce the structure elements of a manifold, which are the metric tensor and the affine connection as well as the covariant derivative. With this we investigate the Laplace-Beltrami operator as an extension of the Laplace operator for curved manifolds, which leads us to the formulation of the underlying Hamiltonian. Furthermore, we investigate the volume element, which appears in the scalar product and which turns out to depend in general on the metric tensor. We also show that in one dimension and under an appropriate coordinate transformation the Hamiltonian with the Laplace-Beltrami operator becomes the common Hamiltonian of a quantum particle in the flat space, which contains the Laplace operator plus an additional effective potential. With the same coordinate transformation the general scalar product goes over to the Euclidean scalar product. This means that in one dimension no physical curvature exists.

In Chapter 4 we discuss the Rayleigh-Schrödinger perturbation theory. Since we investigate a perturbation of the metric itself, we know from the previous chapter that the metric influences both the Hamiltonian by the Laplace-Beltrami operator and the scalar product via the volume element. This means that we can not apply the common form of the Rayleigh Schrödinger perturbation theory. Therefore, we work out an extended form of perturbation theory of a quantum theory on a curved manifold, which contains a perturbation in the Hamiltonian as well as a perturbation in the scalar product.

As a first approach, Chapter 5 contains the calculations of the Bose-Hubbard model in one dimension with a perturbed metric. Although we know that there is no physical curvature in one dimension, this represents a mathematical model, which indicates how to deal with curvature in more than one spatial dimension. Nevertheless, we use the formalism of the metric tensor introduced in Chapter 3 and the perturbation theory developed in Chapter 4 to get a formally correct description of quantum particles in such a one-dimensional slightly bent chain model. The results of Chapter 2 are supposed to represent the unperturbed limit. For a perturbation given by a Lorentz function, which can be experimentally realized, we compute both the hopping parameter and the onsite energy. Furthermore, we perform the continuum limit of the Hamiltonian for the bent chain model in close analogy to Chapter 2.

Finally, we conclude the thesis with Chapter 6 by a summary of the important results and an outlook with further possible investigations.

2. Bose-Hubbard model

In this chapter we review the Bose-Hubbard model and its properties. We start with deriving the lattice model from a continuum many-body theory in Section 2.1. Afterwards, we introduce in Section 2.2 the method of continued fraction with which we calculate in Section 2.3 the Bloch and Wannier functions for non-interacting bosons and discuss some of their special properties. With this we compute the hopping parameter as well as the onsite energy in Section 2.4. In Section 2.5 we investigate the continuum limit for the hopping parameter by performing the limit of vanishing lattice constant.

2.1. Derivation of the Bose-Hubbard Hamiltonian

A bosonic gas in an optical lattice is usually described by the Bose-Hubbard model. For the derivation of the Hamiltonian of the Bose-Hubbard model we start with the standard continuum model for a bosonic many-body quantum system in second quantization

$$\begin{aligned}\hat{H} = &\int d^3x\ \hat{\psi}^\dagger(\mathbf{x}) H_{\text{free}} \hat{\psi}(\mathbf{x}) \\ &+ \frac{1}{2}\int\int d^3x_1 d^3x_2 \hat{\psi}^\dagger(\mathbf{x}_1)\hat{\psi}^\dagger(\mathbf{x}_2) V_{\text{int}}(\mathbf{x}_1,\mathbf{x}_2)\hat{\psi}(\mathbf{x}_1)\hat{\psi}(\mathbf{x}_2),\end{aligned} \tag{2.1}$$

where $\hat{\psi}^\dagger(\mathbf{x})$ and $\hat{\psi}(\mathbf{x})$ are bosonic field operators fulfilling the commutator relations

$$[\hat{\psi}(\mathbf{x}),\hat{\psi}(\mathbf{x}')]_- = 0, \quad [\hat{\psi}^\dagger(\mathbf{x}),\hat{\psi}^\dagger(\mathbf{x}')]_- = 0, \quad [\hat{\psi}(\mathbf{x}),\hat{\psi}^\dagger(\mathbf{x}')]_- = \delta(\mathbf{x}-\mathbf{x}'), \tag{2.2}$$

where $[\cdot,\cdot]_-$ stands for the common commutator. The one-particle Hamiltonian is given by

$$H_{\text{free}} = -\frac{\hbar^2}{2m}\Delta + V_{\text{ext}}(\mathbf{x}) - \mu', \tag{2.3}$$

where μ' marks the chemical potential, and the contact interaction in the s-wave approximation is given by

$$V_{\text{int}}(\mathbf{x}_1, \mathbf{x}_2) = g_{\text{BB}}\delta(\mathbf{x}_1 - \mathbf{x}_2). \tag{2.4}$$

Here the strength of the contact interaction g_{BB} is related to the s-wave scattering length a_{BB} via

$$g_{\text{BB}} = \frac{4\pi a_{\text{BB}}\hbar^2}{m}. \tag{2.5}$$

Note that the isotropic contact interaction (2.4) is modified for atoms with a magnetic dipole moment or heteronuclear molecules with an electric dipole moment, which interact over many lattice sites due to the long-range and anisotropic dipole-dipole interaction [41].

For the external potential $V_{\text{ext}}(\mathbf{x})$ we only assume the optical lattice and neglect the finite width of the laser beams. Typically such optical lattices are described by the form

$$V_{\text{ext}}(\mathbf{x}) = V_0 \left[\sin^2\left(\frac{\pi}{a}x\right) + \sin^2\left(\frac{\pi}{b}y\right) + \sin^2\left(\frac{\pi}{c}z\right)\right], \tag{2.6}$$

where a, b, and c are the lattice constants in the three different directions x, y, and z. The optical lattice potential is thus periodic. Therefore an appropriate decomposition of the field operators $\hat{\psi}$ in (2.1) is given in the basis of the Wannier functions known from solid-state physics. Although these functions are not eigenfunctions of the Hamiltonian, they are localized on one point x_i as well as complete

$$\sum_i w^\star(\mathbf{x} - \mathbf{x}_i)\; w(\mathbf{x}' - \mathbf{x}_i) = \delta(\mathbf{x} - \mathbf{x}') \tag{2.7}$$

and orthonormal

$$\int_{-\infty}^{\infty} d^3x\; w^\star(\mathbf{x} - \mathbf{x}_i)\; w(\mathbf{x} - \mathbf{x}_j) = \delta(\mathbf{x}_i - \mathbf{x}_j), \tag{2.8}$$

thus they form a basis. Due to the completeness (2.7) we expand the field operators in terms of the bosonic creation and annihilation operators $\hat{a}_i^\dagger$ and $\hat{a}_i$ for the lattice site i, thus we get

$$\hat{\psi}(\mathbf{x}) = \sum_i w(\mathbf{x} - \mathbf{x}_i)\hat{a}_i, \quad \hat{\psi}^\dagger(\mathbf{x}) = \sum_i w^\star(\mathbf{x} - \mathbf{x}_i)\hat{a}_i^\dagger, \tag{2.9}$$

where $\hat{a}_i^\dagger$ and $\hat{a}_i$ fulfill according to (2.2) the commutator relations

$$[\hat{a}_i, \hat{a}_j]_- = 0, \quad [\hat{a}_i^\dagger, \hat{a}_j^\dagger]_- = 0, \quad [\hat{a}_i, \hat{a}_j^\dagger]_- = \delta_{ij}. \tag{2.10}$$

Inserting (2.9) in (2.1) we get

$$\begin{aligned}\hat{H} = &\sum_{i \neq j} \int d^3x \; w^\star(\mathbf{x} - \mathbf{x}_i) \left[-\frac{\hbar^2}{2m}\Delta + V_{\text{ext}}(\mathbf{x}) - \mu' \right] w(\mathbf{x} - \mathbf{x}_j) \hat{a}_i^\dagger \hat{a}_j \\ &+ \sum_i \int d^3x \; w^\star(\mathbf{x} - \mathbf{x}_i) \left[-\frac{\hbar^2}{2m}\Delta + V_{\text{ext}}(\mathbf{x}) - \mu' \right] w(\mathbf{x} - \mathbf{x}_i) \hat{a}_i^\dagger \hat{a}_i \\ &+ \frac{g_{\text{BB}}}{2} \sum_{i,j,k,l} \int d^3x \; w^\star(\mathbf{x} - \mathbf{x}_i) w^\star(\mathbf{x} - \mathbf{x}_j) w(\mathbf{x} - \mathbf{x}_k) w(\mathbf{x} - \mathbf{x}_l) \hat{a}_i^\dagger \hat{a}_j^\dagger \hat{a}_k \hat{a}_l. \end{aligned} \tag{2.11}$$

The first term describes the hopping between two different lattice sites i and j, therefore this term is called hopping term. The second term gives the energy on one site i, while the third one represents the interaction between the bosons. Due to the localization of the Wannier function only those terms survive, where all summation indices coincide, i.e. $i = j = k = l$.

With the following definitions

$$J_{ij} = -\int d^3x \; w^\star(\mathbf{x} - \mathbf{x}_i) \left[-\frac{\hbar^2}{2m}\Delta + V_{\text{ext}}(\mathbf{x}) - \mu' \right] w(\mathbf{x} - \mathbf{x}_j), \tag{2.12a}$$

$$\epsilon_i = \int d^3x \; w^\star(\mathbf{x} - \mathbf{x}_i) \left[-\frac{\hbar^2}{2m}\Delta + V_{\text{ext}}(\mathbf{x}) - \mu' \right] w(\mathbf{x} - \mathbf{x}_i), \tag{2.12b}$$

$$U_i = g_{\text{BB}} \int d^3x \; |w(\mathbf{x} - \mathbf{x}_i)|^4 \tag{2.12c}$$

and an effective chemical potential $\mu_i = \mu' - \epsilon_i$ we get the Bose-Hubbard Hamiltonian for a discrete lattice

$$\hat{H}_{\text{BHM}} = -\sum_{i \neq j} J_{ij} \hat{a}_i^\dagger \hat{a}_j - \sum_i \mu_i \hat{a}_i^\dagger \hat{a}_i + \sum_i \frac{U_i}{2} \hat{a}_i^\dagger \hat{a}_i^\dagger \hat{a}_i \hat{a}_i, \tag{2.13}$$

where i enumerates the lattice sites. The hopping parameter J_{ij} describes the ability that a particle can hop from one lattice site i to another j, μ_i denotes the effective chemical potential at site i, and U_i stands for the interaction energy between two bosons at the same lattice site i. Since only the nearest neighbor hopping is relevant, (2.13) reduces to the common Bose-Hubbard Hamiltonian mentioned in (1.1).

2.2. Method of continued fraction

We now follow Ref. [42] and introduce a numerical method to obtain the Wannier functions, which relies on the method of continued fractions.

In general the Hamiltonian of our system contains a kinetic part as well as an external potential $V_{\text{ext}}(x)$ which describes the optical lattice as well as possibly other external influences and an interaction potential $V_{\text{int}}(x)$ between two particles. In the following calculation we neglect the interaction term. Furthermore we assume $V_{\text{ext}}(x)$ to have the form (2.6). Due to the periodicity of the external potential we know from solid-state physics that the energy shows a typical band structure and that the wavefunctions are then Bloch functions $\phi_k(x)$ [43]. To determine these functions we have to solve the three-dimensional Schrödinger equation. This we can reduce to a one-dimensional Schrödinger equation using the fact that the potential (2.6) is spatially separable. Therefore we have to solve the one-dimensional Schrödinger equation

$$\left[-\frac{\hbar^2}{2m}\partial_x^2 + V_0 \sin^2\left(\frac{\pi}{a}x\right)\right]\phi_{n,k}(x) = E_n(k)\phi_{n,k}(x), \tag{2.14}$$

where n marks the number of the energy band and k the wave number. The possible values for the wave numbers are depending on the number of lattice sites as is further discussed in the next section.

Using the following transformation in dimensionless coordinates

$$\tilde{x} = \frac{\pi}{a}x, \qquad \partial_{\tilde{x}} = \frac{a}{\pi}\partial_x, \tag{2.15}$$

as well as the dimensionless wave number

$$\tilde{k} = \frac{a}{\pi}k, \tag{2.16}$$

and the trigonometric relation $\sin^2(x) = \frac{1}{2}[1 - \cos(2x)]$ we get from (2.14)

$$\left\{-\frac{\hbar^2\pi^2}{2ma^2}\partial_{\tilde{x}}^2 + \frac{V_0}{2}\Big[1 - \cos(2\tilde{x})\Big]\right\}\phi_{n,\tilde{k}}\left(\frac{a}{\pi}\tilde{x}\right) = E_n(\tilde{k})\phi_{n,\tilde{k}}\left(\frac{a}{\pi}\tilde{x}\right). \tag{2.17}$$

Here we define the recoil energy

$$E_{\text{R}} = \frac{\hbar^2\pi^2}{2ma^2} \tag{2.18}$$

as the underlying energy unit and use it to introduce the following dimensionless energies

$$\tilde{V}_0 = \frac{V_0}{E_\mathrm{R}}, \quad \tilde{E}_n(\tilde{k}) = \frac{E_n(\tilde{k})}{E_\mathrm{R}}. \tag{2.19}$$

Furthermore, we define the dimensionless Bloch function

$$\tilde{\phi}_{n,\tilde{k}}(\tilde{x}) = \phi_{n,\tilde{k}}\left(\frac{a}{\pi}\tilde{x}\right), \tag{2.20}$$

thus (2.17) reduces to

$$\left\{-\partial_{\tilde{x}}^2 + \frac{\tilde{V}_0}{2}\Big[1 - \cos(2\tilde{x})\Big]\right\}\tilde{\phi}_{n,\tilde{k}}(\tilde{x}) = \tilde{E}_n(\tilde{k})\tilde{\phi}_{n,\tilde{k}}(\tilde{x}) \tag{2.21}$$

This equation represents the dimensionless form of the Schrödinger equation (2.14).

At sufficiently low temperatures we can assume that only the lowest energy band is occupied. Therefore we simplify our problem by setting $n = 0$ and omit the band index in further calculations. As we have a periodic potential $V_\mathrm{ext}(x)$ with the lattice constant a as the period, thus $V_\mathrm{ext}(x) = V_\mathrm{ext}(x + a)$, we express due to the Bloch theorem the Bloch function as a lattice periodic function $u_k(x)$ and an exponential function

$$\phi_k(x) = \frac{1}{\sqrt{N_s}} u_k(x) e^{ikx} \tag{2.22}$$

with the number of lattice sites N_s and the lattice periodic function $u_k(x)$ fulfilling $u_k(x) = u_k(x + a)$. Using (2.22), we obtain from (2.21)

$$\left\{\tilde{k}^2 - 2i\tilde{k}\partial_{\tilde{x}} - \partial_{\tilde{x}}^2 + \frac{\tilde{V}_0}{2}\Big[1 - \cos(2\tilde{x})\Big]\right\}\tilde{u}_{\tilde{k}}(\tilde{x}) = \tilde{E}(\tilde{k})\tilde{u}_{\tilde{k}}(\tilde{x}). \tag{2.23}$$

The periodicity of the function $u_k(x)$ allows to expand it in a Fourier series

$$u_k(x) = \sum_{l=-\infty}^{\infty} A_l(k) e^{2il\tilde{x}}. \tag{2.24}$$

Inserting this and using the Euler formula $\cos(x) = \frac{1}{2}(e^{ix} + e^{-ix})$ we get

$$\sum_{l=-\infty}^{\infty} \left\{ \left[(\tilde{k} + 2l)^2 - \frac{\tilde{V}_0}{2} \right] A_l(\tilde{k}) + \frac{\tilde{V}_0}{4} \left[A_{l+1}(\tilde{k}) + A_{l-1}(\tilde{k}) \right] \right\} e^{2il\tilde{x}} = \sum_{l=-\infty}^{\infty} \tilde{E}(\tilde{k}) e^{2il\tilde{x}}. \tag{2.25}$$

This is the equation we actually use to calculate the components of the Fourier series $A_l(k)$. To this end we start with the definition

$$F(l) = \frac{\tilde{V}_0}{4\left[\tilde{E}(k) - (k + 2l)^2 - \frac{\tilde{V}_0}{2}\right]}. \tag{2.26}$$

Due to the linear independence of the exponential functions the prefactors in (2.25) have to be zero, thus we can simplify (2.25) to the tridiagonal recursion relation

$$F(l)A_{l+1} + A_l + F(l)A_{l-1} = 0. \tag{2.27}$$

Introducing the ladder operator

$$S_l^{(-)} = \frac{A_{l+1}}{A_l}, \tag{2.28}$$

Eq. (2.27) can be rewritten as

$$S_{l-1}^{(-)} = -\frac{F(l)}{1 + F(l)S_l^{(-)}}. \tag{2.29}$$

Changing the index allows to determine $S_l^{(-)}$ from $S_{l+1}^{(-)}$. An analogue iteration can be derived for

$$S_l^{(+)} = \frac{A_{l-1}}{A_l}, \tag{2.30}$$

which reads

$$S_{l+1}^{(+)} = -\frac{F(l)}{1 + F(l)S_l^{(+)}}, \tag{2.31}$$

so that $S_l^{(+)}$ can be determined from $S_{l-1}^{(+)}$. Combining both iterations, we get for the

starting point $l = 0$

$$\left(-\frac{F(1)}{1 - F(1)\frac{F(2)}{1-F(2)\frac{F(3)}{\cdots}}} + 1 - \frac{F(-1)}{1 - F(-1)\frac{F(-2)}{1-F(-2)\frac{F(-3)}{\cdots}}} \right) A_0 = 0. \tag{2.32}$$

This is an expression of infinite fractions, thus it is called method of continued fraction.

For the numerical calculation of the Bloch functions we use (2.25), where we define

$$G(l) = (\tilde{k} + 2l)^2 + \frac{\tilde{V}_0}{2}, \tag{2.33}$$

thus we can rewrite (2.25) as a matrix equation

$$\underline{M}\big(G(l)\big) \cdot \begin{pmatrix} \vdots \\ A_{-1}(\tilde{k}) \\ A_0(\tilde{k}) \\ A_{+1}(\tilde{k}) \\ \vdots \end{pmatrix} = \tilde{E}(\tilde{k}) \begin{pmatrix} \vdots \\ A_{-1}(\tilde{k}) \\ A_0(\tilde{k}) \\ A_{+1}(\tilde{k}) \\ \vdots \end{pmatrix} \tag{2.34}$$

with the tri-diagonal matrix

$$\underline{M}\big(G(l)\big) = \begin{pmatrix} \ddots & \ddots & \ddots & \ddots & \ddots & & & \\ & 0 & -\frac{\tilde{V}_0}{4} & G(-1) & -\frac{\tilde{V}_0}{4} & 0 & & \\ & & 0 & -\frac{\tilde{V}_0}{4} & G(0) & -\frac{\tilde{V}_0}{4} & 0 & \\ & & & 0 & -\frac{\tilde{V}_0}{4} & G(+1) & -\frac{\tilde{V}_0}{4} & 0 \\ & & & & \ddots & \ddots & \ddots & \ddots \end{pmatrix}. \tag{2.35}$$

To get the exact solution of this problem we have to consider an infinite amount of terms. In order to obtain a numerical approximation, we cut off the possible values for l. Equation (2.34) is then a typical eigenvalue problem with a matrix with dimension $2l_{\max} + 1$ as well as the eigenvector $\mathbf{A}(\tilde{k})$ and the eigenenergy $\tilde{E}(\tilde{k})$.

Due to the ladder operators (2.28) and (2.30) the values $A_{\pm1}(k), A_{\pm2}(k)$ can be expressed in terms proportional to $A_0(k)$. Thus the solution of (2.34) is only depending on the single entry $A_0(k)$ of the eigenvector. Due to the normalization freedom of an eigenvector, this number $A_0(k)$ can be set to one without loss of generality.

In the following we show and discuss the numerical results for the Bloch functions using this method as well as calculate the Wannier functions and the corresponding

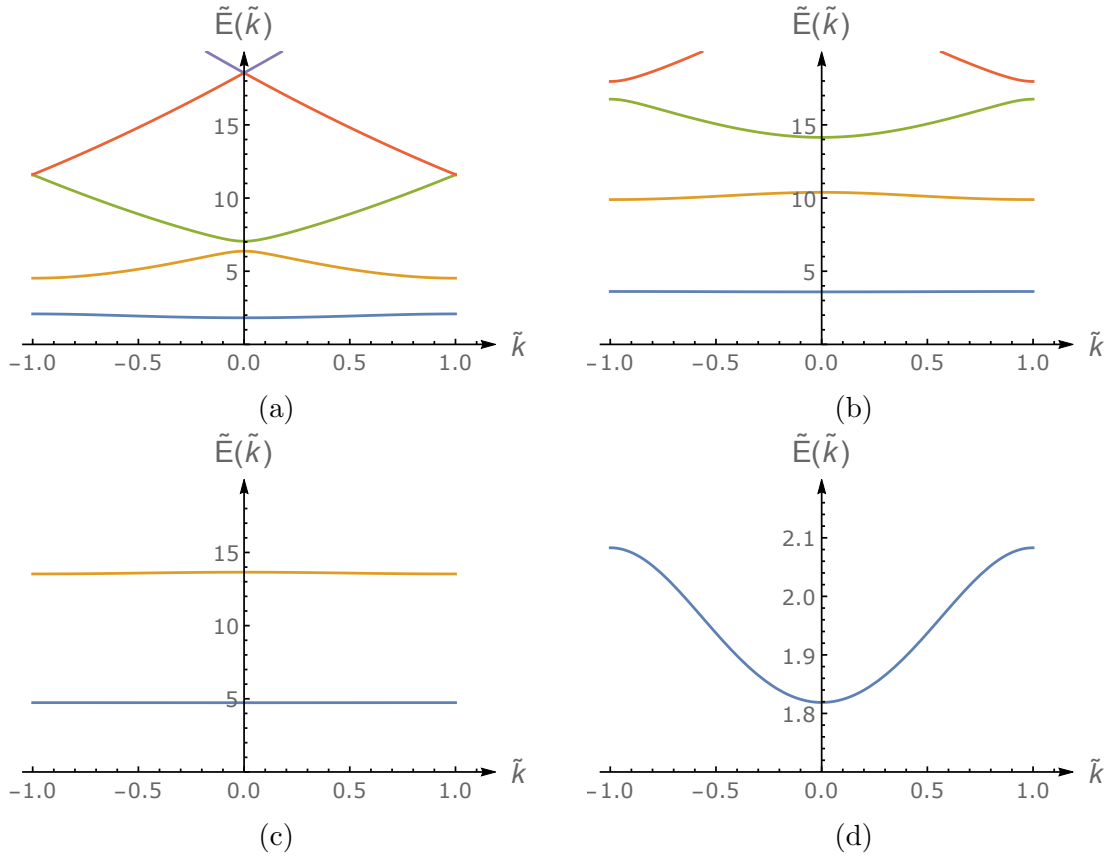

Figure 2.1.: Lowest energy bands for varying lattice depth: (a) $\tilde{V}_0 = 5$, (b) $\tilde{V}_0 = 15$, (c) $\tilde{V}_0 = 25$, (d) only the lowest band for $\tilde{V}_0 = 5$.

hopping parameter.

2.3. Bloch and Wannier functions

With the method of continued fraction discussed in the previous section we are now able to calculate numerically both the Bloch functions and the Wannier functions out of the eigenvectors of (2.34) as well as the energy bands in terms of the eigenvalues. For the following figures we use dimensionless units introduced in (2.15) unless otherwise noted.

First we look at the resulting energy bands. The eigenvalue $\tilde{E}_n(k)$ in (2.34) depends on the band index n, the wave number k, and the lattice depth $\tilde{V}_0$. In principle n can move up to infinity although we are interested in the lowest bands. The wave number k has in general discrete values within the first Brillouin zone $k \in [-\frac{\pi}{a}, \frac{\pi}{a}]$ or rather $\tilde{k} \in [-1, 1]$ in dimensionless units.

In Fig. 2.1 the lowest energy bands are shown for different lattice depths $\tilde{V}_0$. The

structure of the energy bands reminds of the bands in a crystal structure in solid-state physics which we are imitating with the optical lattice. We see that for increasing lattice depth the energy values as well as the band gaps increase and the bands get flater. As mentioned above, we are only interested in the lowest band $\tilde{E}_0(k)$ which is shown enlarged in Fig. 2.1d for a particular lattice depth.

The next step is to investigate the Bloch functions. To do so we use the entries of the eigenvectors $A(k)$ as well as the Fourier series of the lattice periodic function $u_k(x)$ in (2.24) and the Bloch theorem (2.22).

Because we are interested in the lowest energy band we determine the corresponding eigenvector. If this eigenvector is normalized, the lattice periodic functions fulfill

$$\int_{-\infty}^{\infty} \mathrm{d}x \; u_k^\star(x) u_{k'}(x) = \delta_{k,k'} \tag{2.36}$$

so they are orthonormal due to (2.24). In the following we omit the integration range unless otherwise noted. With the Bloch theorem (2.22) we can show that the Bloch functions are also orthonormal

$$\int \mathrm{d}x \; \phi_k^\star(x) \phi_{k'}(x) = \delta_{k,k'}. \tag{2.37}$$

We show now that the number of lattice sites N_s is related to the possible values of wave numbers k. If we assume periodic boundary conditions and set $N_s a$ as the length of the chain we know that

$$\phi_k(0) = \phi_k(N_s a). \tag{2.38}$$

Inserting the Bloch theorem (2.22) yields

$$\frac{1}{\sqrt{N_s a}} u_k(0) = \frac{1}{\sqrt{N_s a}} e^{ikN_s a} u_k(N_s a). \tag{2.39}$$

Using the periodicity $u_{n,k}(x) = u_{n,k}(x + a)$ gives us the condition

$$e^{ikN_s a} = 1, \tag{2.40}$$

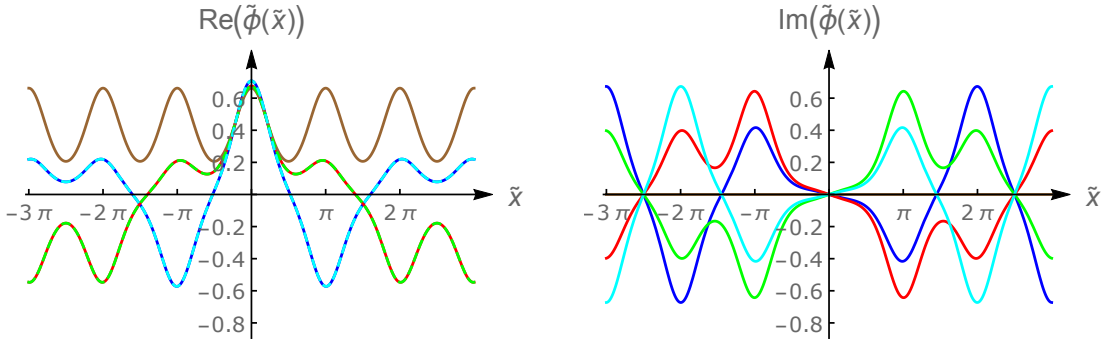

(a) (b)

Figure 2.2.: Real (a) and imaginary (b) part of Bloch functions for the lattice depth $\tilde{V}_0 = 5$. To have a better view we assume $N_s = 5$ so we have five different Bloch functions. Each line marks a different k or respectively according to (2.41) a different value for p: $p = -2$ (blue), $p = -1$ (red), $p = 0$ (brown), $p = 1$ (green), and $p = 2$ (cyan).

which is solved by the wave numbers

$$k_p = \frac{2\pi}{N_s a} p, \tag{2.41}$$

and the numbers

$$p = -\frac{N_s - 1}{2}, -\frac{N_s - 1}{2} + 1, ..., \frac{N_s - 1}{2}, \tag{2.42}$$

provided that N_s is odd. Here we see that for N_s lattice sites we get exactly N_s possible wave numbers k thus we have N_s different Bloch functions. We also know that the Bloch functions are in general complex wave functions so we have to look in general at both a real and an imaginary part.

The results of the numeric calculations are shown in Fig. 2.2. We see that the real parts are symmetric and the imaginary parts are antisymmetric with respect to both $x \to -x$ and $k \to -k$. Thus we get the symmetry relations

$$\mathrm{Re}[\phi_k(x)] = \mathrm{Re}[\phi_{-k}(x)] \quad = \mathrm{Re}[\phi_k(-x)] \quad = \mathrm{Re}[\phi_{-k}(-x)], \tag{2.43a}$$

$$\mathrm{Im}[\phi_k(x)] = -\mathrm{Im}[\phi_{-k}(x)] = -\mathrm{Im}[\phi_k(-x)] = \mathrm{Im}[\phi_{-k}(-x)]. \tag{2.43b}$$

Note that the peaks at 1π, 2π, ... mark the values of the Bloch functions at the nearest neighbor, next nearest neighbor, ... due to the dimensionless units

The Bloch functions $\phi_k(x)$ are extended over the whole lattice. By using the Fourier

transformation we get the localized Wannier functions

$$w(x - x_i) = \frac{1}{\sqrt{N_s}} \sum_{k \in 1.\mathrm{BZ}} \phi_k(x) e^{-ikx_i}, \tag{2.44}$$

where x_i marks the localization point of the function and the sum is performed over every values of k within the first Brillouin zone. We can show that these Wannier functions are real functions by directly calculating real and imaginary part via

$$\mathrm{Re}[w(x - x_i)] = \frac{1}{2}[w(x - x_i) + w^*(x - x_i)] \tag{2.45a}$$

$$\mathrm{Im}[w(x - x_i)] = \frac{1}{2i}[w(x - x_i) - w^*(x - x_i)]. \tag{2.45b}$$

Using the definition of the Wannier functions (2.44) and exploiting the symmetry relations of the Bloch functions (2.43a) and (2.43b) the imaginary part vanishes, while the real part stays unequal to zero. Note that we can also prove the orthonormalization (2.8) of the Wannier functions with (2.44) and the orthonormality of the Bloch functions (2.37).

Figure 2.3 shows the Wannier function for $x_i = 0$ and different values of l. For the plots we assume $N_s = 31$. We see that the functions hardly differ for $l = 2$ and $l = 4$, thus $l = 6$ is good enough for the following calculations in this work. The Wannier function is also depending on $\tilde{V}_0$ as is shown in Fig. 2.4a. More exactly the maximum value is increasing and the curve is getting narrower for increasing lattice depth $\tilde{V}_0$. The logarithmic plot shows in addition that the Wannier functions are oscillating with decreasing amplitude around the x-axis as described in Ref. [44]. Note that the dips in Fig. 2.4b are going down to zero since the Wannier functions have a root there. This behavior is typical for these functions. Thus there is a finite probability to find a particle at other lattice sites which is the reason why tunneling is possible in these lattice systems. By increasing the lattice depths, the probabilities shrink. Already here we can deduce that the nearest neighbor hopping approximation assumed in Section 2.1 is quite good by comparing the size of the first and second maxima and that the hopping parameter becomes quite small for deep lattices, as it depends on the Wannier function.

For deep lattices it is good enough to approximate the Wannier function with a Gaussian function. This has also been investigated in Refs. [42, 44]. Here in this work we only use the Wannier function calculated with the method of continued fraction.

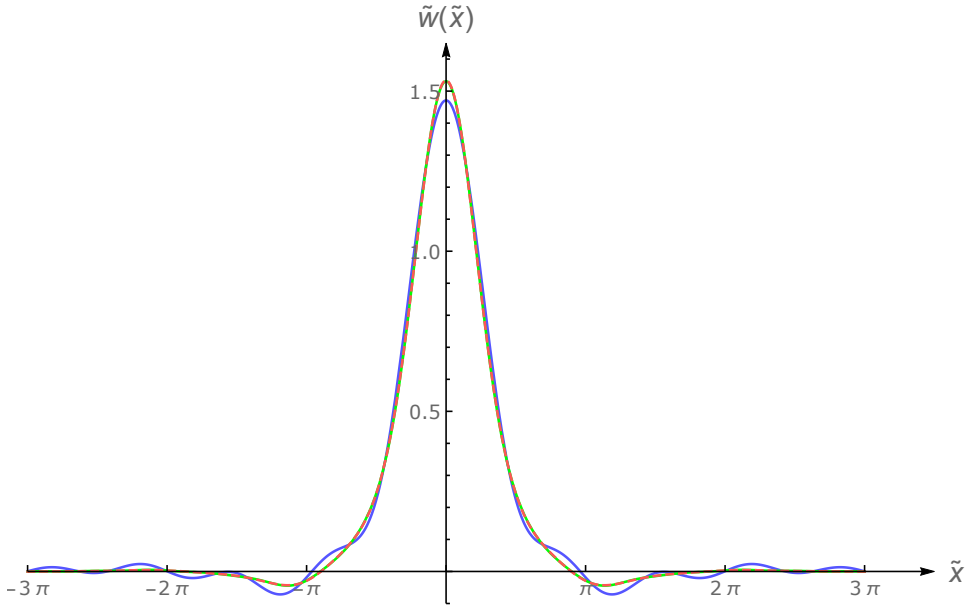

Figure 2.3.: Wannier function for $N_s = 31$ and different values of $l_{\max}$: $l_{\max} = 1$ (blue), $l_{\max} = 2$ (green), and $l_{\max} = 4$ (red dashed).

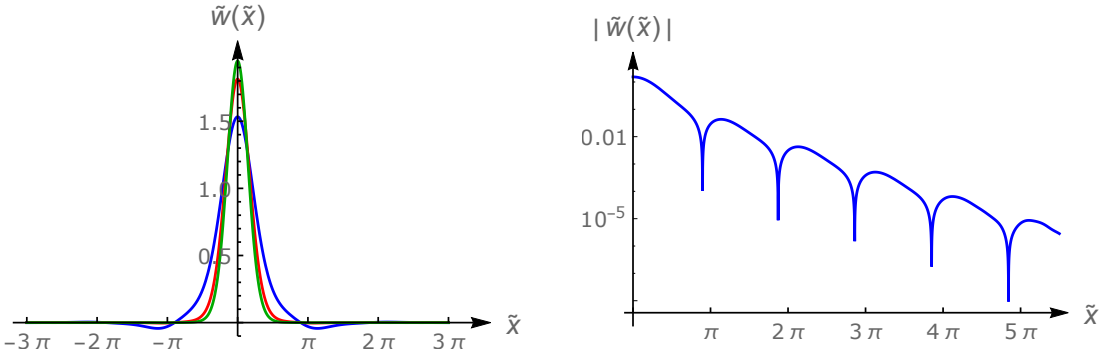

Figure 2.4.: Wannier function for (a) varying lattice depth $\tilde{V}_0 = 5$ (blue), $\tilde{V}_0 = 15$ (red), and $\tilde{V}_0 = 25$ (green) and (b) logarithmic plot of (a) for $\tilde{V}_0 = 5$.

2.4. Hopping parameter and onsite energy

Now we determine the hopping parameter J_{ij} and the onsite energy ϵ_i. Since we have calculated the Wannier function we just have to insert the results in the definitions (2.12a) and (2.12b). Another way to calculate the hopping parameter and the onsite energy via the energy bands is worked out in Ref. [45] and further extended in Appendix A.

The hopping parameter for three different hopping lengths $sa = x_j - x_i$ with an integer s is shown in Fig. 2.5. Here i is set to zero although for other points the results stay the same due to the homogenuity of the optical lattice, meaning $J_{i,i+s} = J_{0,s}$. The hopping parameter is exponentially decreasing for increasing lattice depth and the sign seems to alternate with the dimensionless hopping length s. The value of nearest neighbor hopping $J_{i,i+1}$ for an explicit $\tilde{V}_0$ is much larger than the others so that usually the approximation of only taking into account of the nearest neighbors is valid. Two logarithmic plots confirm the exponential decrease with increasing lattice depth $\tilde{V}_0$ in Fig. 2.6a as well as increasing dimensionless hopping distance s in Fig. 2.6b.

In the tight-binding limit $V_0 \gg E_\mathrm{R}$ an exact result for the nearest neighbor hopping parameter can be obtained as a result of the one-dimensional Mathieu-equation (2.21), see Ref. [46]

$$J_{0,1} = \frac{4}{\sqrt{\pi}} \tilde{V}_0^{\frac{3}{4}} e^{-2\sqrt{\tilde{V}_0}}. \tag{2.46}$$

This is a quite accurate approximation for $\tilde{V}_0 \geq 10$, as we can see in Fig. 2.5.

Although we are mostly interested in the hopping parameter, we show the numerical results for the oniste energy depending on the lattice depth $\tilde{V}_0$ in Figure 2.7, as well. We see that the energy is increasing for deeper lattices. The form approximately corresponds to a square root function which is the result of the Gaussian approximation for the Wannier functions, see Ref. [42]

$$\epsilon_i = \sqrt{\tilde{V}_0}. \tag{2.47}$$

2.5. Continuum limit

At the beginning of this chapter, we derived the Bose-Hubbard model for bosons on a lattice by using the Wannier functions. To this end we started with the Hamiltonian in second quantization (2.1) and expressed the field operators by the Wannier func-

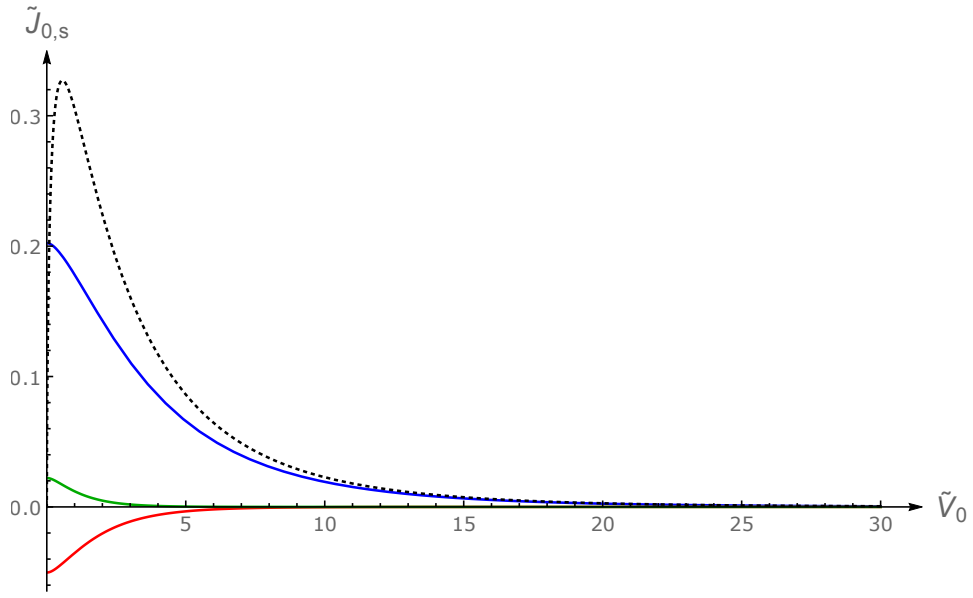

Figure 2.5.: Hopping parameter depending on the dimensionless lattice depth $\tilde{V}_0$. The three curves show the hopping parameter $J_{0,s}$ for $s = 1$ (blue), $s = 2$ (red), and $s = 3$ (green). The black dotted line shows the result for the tight-binding limit $V_0 \gg E_\mathrm{R}$ for nearest neighbor $s = 1$ (2.46).

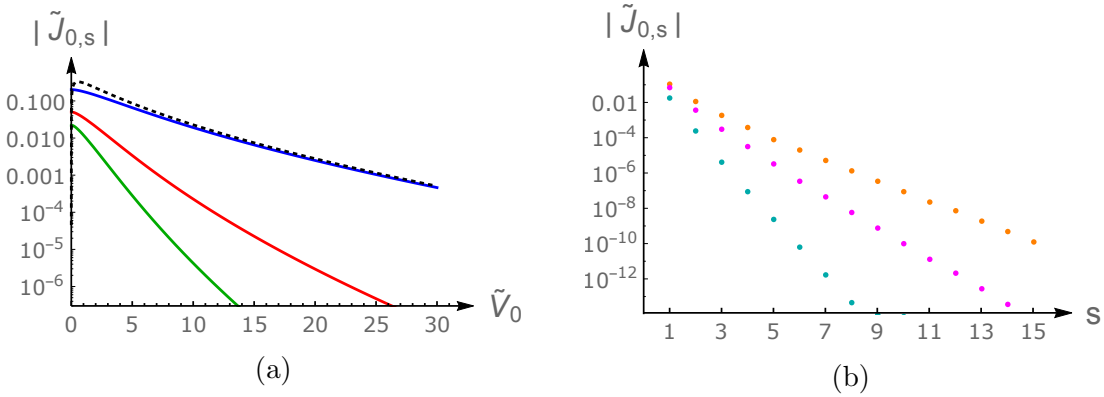

Figure 2.6.: (a) Fig. 2.5 in a logarithmic plot, (b) hopping parameter for $\tilde{V}_0 = 3$ (orange), $\tilde{V}_0 = 5$ (magenta) and $\tilde{V}_0 = 10$ (cyan) depending on the hopping distance s.

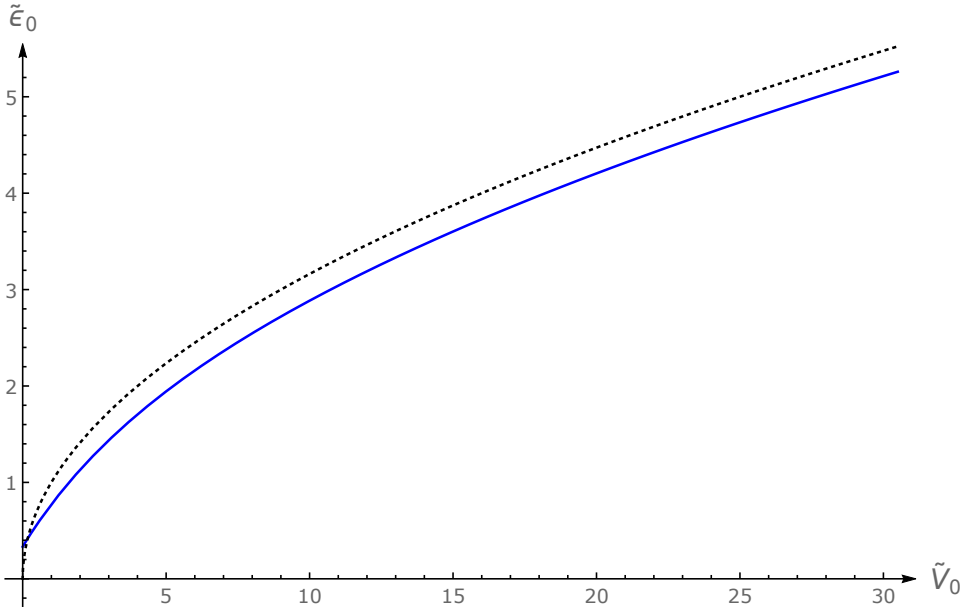

Figure 2.7.: Onsite energy depending on the lattice depth $\tilde{V}_0$ (blue). The black dotted line shows the square root function (2.47).

tions (2.9). The definitions of the hopping parameter (2.12a), the onsite energy (2.12b) and the interaction term (2.12c) led then to the Bose-Hubbard Hamiltonian (2.13).

Now in this section we proceed inversely and start with the lattice Hamiltonian and derive from this the initial Hamiltonian in (2.1) in the continuum. To this end we discuss in the following two continuum limits. Since the hopping parameter J_{ij} represents the kinetic energy, we have to determine an expression for it in the respective limit.

For the first one we perform in Section 2.5.1 the limit of vanishing lattice constant $a \to 0$ for the hopping parameter J_{ij} derived from the Bloch functions. The hopping parameter J_{ij} is in general a function of both the lattice depth V_0 and the lattice constant a. We express the potential depth by the dimensionless lattice depth $\tilde{V}_0$ due to (2.19), thus we get a function $J_{ij}(\tilde{V}_0, a)$. However, the recoil energy (2.18) occurring in $\tilde{V}_0$ is proportional to $1/a^2$ and becomes infinite in the limit of vanishing lattice constant. To this end the dimensionless lattice depth $\tilde{V}_0$ becomes zero. Therefore we first have to determine the hopping parameter for vanishing lattice depth as an intermediate step.

The second continuum limit treated in Section 2.5.2 is based on the long wave lengths approximation of the lowest energy band dispersion. Thus, for small wave numbers k we get a free dispersion, which allows to relate the hopping parameter with the effective particle mass. For vanishing lattice depth the effective mass can be identified with the real mass of a point particle.

In Section 2.5.3 we apply the expressions of the hopping parameter to the Bose-Hubbard Hamitlonian and by performing the limit of vanishing lattice constant a we derive the Hamiltonian in the continuum via both ways. In the end we briefly discuss the results.

2.5.1. Limit of vanishing lattice depth

In this part we investigate the limit of vanishing lattice depth $\tilde{V}_0 \to 0$ for the hopping parameter given by (2.12a). Starting point for this calculation are the Bloch functions. For vanishing lattice depth $\tilde{V}_0 \to 0$ the Bloch functions reduce to plane waves [47]

$$\phi_k(x) = \frac{1}{\sqrt{N_s a}} e^{ikx}. \tag{2.48}$$

Inserting this in (2.44) yields the Wannier functions

$$w(x - x_i) = \frac{1}{N_s \sqrt{a}} \sum_{k \in 1.\mathrm{BZ}} e^{-ik(x - x_i)}. \tag{2.49}$$

For the continuum we are interested in the limit of an infinitely large number of lattice sites $N_s \to \infty$. The wave number k becomes then a continuous variable according to (2.41) and we can substitute the sum as an integral

$$\sum_{k \in 1.\mathrm{BZ}} \to \frac{N_s a}{2\pi} \int_{-\frac{\pi}{a}}^{\frac{\pi}{a}} \mathrm{d}k. \tag{2.50}$$

For the exponential function we use the Euler formula $e^{ix} = \frac{1}{2}(\cos x + i \sin x)$ and get

$$w(x - x_i) = \frac{1}{\sqrt{a}} \frac{a}{2\pi} \int_{-\frac{\pi}{a}}^{\frac{\pi}{a}} \mathrm{d}k \left\{ \cos\left[k(x - x_i)\right] + i \sin\left[k(x - x_i)\right] \right\}. \tag{2.51}$$

The sine term cancels due to symmetry and the rest is an elementary integral. As result we get the Wannier function for $\tilde{V}_0 \to 0$ as given in Refs. [44, 47]:

$$w(x - x_i) = \frac{1}{\sqrt{a}} \frac{\sin\left[\frac{\pi}{a}(x - x_i)\right]}{\frac{\pi}{a}(x - x_i)}. \tag{2.52}$$

This sort of functions is well known in optics as the diffraction function of a single slit [48]. Note that we are able to show that the diffraction functions (2.52) still fulfill the orthonormality relation of the Wannier functions (2.8).

With the diffraction functions as the Wannier functions we investigate now the value of the hopping parameter for $\tilde{V}_0 \to 0$. We start with the definition of the hopping parameter (2.12a)

$$J_{ij} = -\int_{-\frac{N_s a}{2}}^{\frac{N_s a}{2}} \mathrm{d}x\; w(x - x_i) \left[-\frac{\hbar^2}{2m}\partial_x^2 + V_0 \sin\left(\frac{\pi}{a}x\right)\right] w(x - x_j). \tag{2.53}$$

Using the dimensionless units and the limit of an infinitely large number of lattice sites $N_s \to \infty$ we get

$$\tilde{J}_{ij} = -\int_{-\infty}^{\infty} \mathrm{d}\tilde{x}\; \frac{a}{\pi}\; w\left(\frac{a}{\pi}(\tilde{x} - \tilde{x}_i)\right) \left[-\partial_{\tilde{x}}^2 + \tilde{V}_0 \sin^2(\tilde{x})\right] w\left(\frac{a}{\pi}(\tilde{x} - \tilde{x}_j)\right). \tag{2.54}$$

We are interested in the limit $\tilde{V}_0 \to 0$, thus the second part within the integral vanishes and we insert (2.52) for the Wannier function

$$\tilde{J}_{ij} = \int_{-\infty}^{\infty} \mathrm{d}\tilde{x}\; \frac{a}{\pi}\; \frac{1}{\sqrt{a}} \frac{\sin(\tilde{x} - \tilde{x}_i)}{\tilde{x} - \tilde{x}_i}\; \partial_{\tilde{x}}^2 \left(\frac{1}{\sqrt{a}} \frac{\sin(\tilde{x} - \tilde{x}_j)}{\tilde{x} - \tilde{x}_j} \right). \tag{2.55}$$

The substitution $\tilde{x}' = \tilde{x} - \tilde{x}_i$ and an arbitrary hopping distance $\tilde{x}_j - \tilde{x}_i = s\pi$, where s is an integer, leads to

$$\tilde{J}_{i,i+s} = \frac{1}{\pi} \int_{-\infty}^{\infty} \mathrm{d}\tilde{x}'\; \frac{\sin \tilde{x}'}{\tilde{x}'}\; \partial_{\tilde{x}'}^2 \left(\frac{\sin(\tilde{x}' - s\pi)}{\tilde{x}' - s\pi} \right). \tag{2.56}$$

Here we use the formula $\sin(x - s\pi) = (-1)^s\; \sin x$ and rewrite the appearing integral via partial fraction expansion. The only remaining part is solvable and yields

$$\tilde{J}_{i,i+s} = (-1)^{s+1} \frac{2}{s^2\pi^2}. \tag{2.57}$$

We compare this result with Fig. 2.5 at the point $\tilde{V}_0 = 0$. To this end we have to calculate $\tilde{J}_{i,i+s}$ for $s = 1,\ 2,\ 3$ and get, indeed, the correct values as in Fig. 2.5. Especially the prefactor $(-1)^{s+1}$ explains the alternating sign behavior. Thus the analytic result here agrees with the numerics in Section 2.4.

In most of the literature only the dimensionless hopping parameter for nearest neighbors appears. Therefore we just have to set $s = 1$ in (2.57) and get

$$\tilde{J}_{i,i+1} = \frac{2}{\pi^2}. \tag{2.58}$$

With the recoil energy (2.18) the hopping parameter is then given by

$$J_{i,i+1} = \tilde{J}_{i,i+1} E_{\mathrm{R}} = \frac{\hbar^2}{ma^2}. \tag{2.59}$$

Due to the homogeneity of the optical lattice the hopping parameter is independent of the lattice site i, thus we define

$$J^{\mathrm{Bloch}} = J_{i,i+1} = \frac{\hbar^2}{ma^2}. \tag{2.60}$$

Note that the hopping parameter is proportional to $1/a^2$. With this result we have finished the preparations for performing the continuum limit.

2.5.2. Limit of long wave lengths

Another way to calculate the continuum limit is the effective mass approximation treated in Ref. [47]. To this end we suppose the lattice depth $V_0 > 0$ to be fixed, thus in one dimension and due to the homogeneity of the lattice the lowest energy band can be expressed as implied in Fig. 2.1d by

$$E(k) = -2J\cos(ka) + 2J, \tag{2.61}$$

where we shift the energy by $2J$ to avoid negative values. This additional term is interpreted as a part of the chemical potential.

For the effective mass approximation we are interested in energies for long wave lengths, thus the wave number k becomes small. In this case we expand the cosine in a Taylor series up to the first order, so that the energy yields

$$E(k) = Jk^2a^2, \tag{2.62}$$

which is similar to the dispersion relation of a free particle with respect to k

$$E_{\mathrm{free}}(k) = \frac{\hbar^2 k^2}{2m}. \tag{2.63}$$

Thus we identify the hopping parameter with

$$J = \frac{\hbar^2}{2m^\star a^2}, \tag{2.64}$$

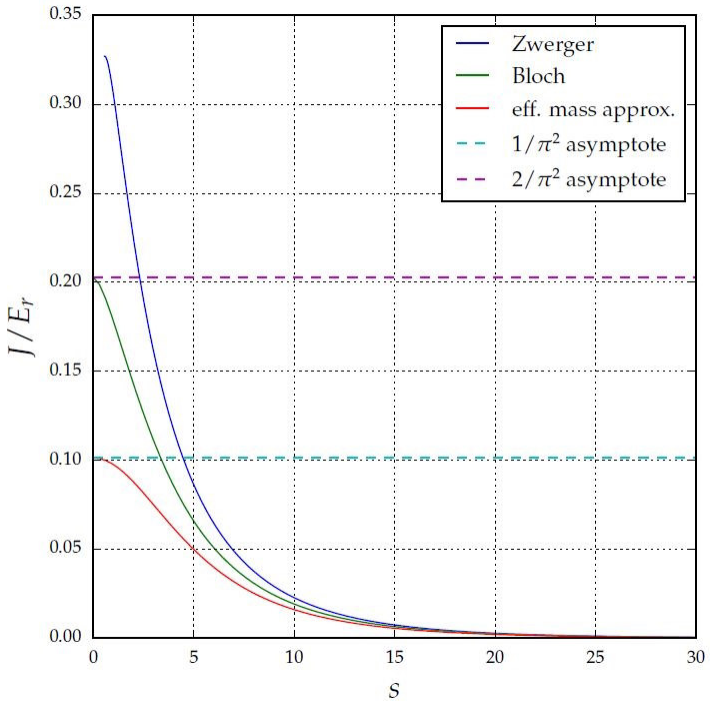

Figure 2.8.: Nearest neighbor hopping parameters calculated via different methods adapted from Ref. [47]: Green line denotes the hopping parameter derived by the Bloch functions, red line is the hopping parameter via the effective mass approximation, and blue line stands for the tight-binding approximation of (2.46). The abscissae s is equal to $\tilde{V}_0$, which is used in this thesis for the dimensionless lattice depth.

where we introduce the effective mass $m^\star$, which depends in general on the direction of the hopping. This quantity is often used in solid-state physics and describes the mass of a particle within a lattice as if it is a free particle with an effective mass.

In the limit of vanishing lattice depth $V_0 \to 0$ the effective mass becomes the real mass of a free particle $m^\star \to m$, thus the hopping parameter is given by

$$J^{\text{mass}} = \frac{\hbar^2}{2ma^2}. \tag{2.65}$$

A comparison between both hopping parameters J^{Bloch} of (2.60) and J^{mass} of (2.65) for vanishing lattice depth V_0 yields a difference of a factor 2. This difference is shown in Fig. 2.8 at the point $V_0 = 0$ indicated by the two asymptotic lines. However, in the following we continue our derivation of the Hamiltonian in the continuum.

2.5.3. Continuous Hamiltonian

In order to derive the continuous Hamiltonian, we now start with the Bose-Hubbard model (2.13) in the discrete lattice without the interaction term:

$$\hat{H}_{\mathrm{BHM}} = -\sum_{<i,j>} J_{ij}\hat{a}_i^\dagger \hat{a}_j + \sum_i \epsilon_i \hat{a}_i^\dagger \hat{a}_i. \tag{2.66}$$

We rewrite down explicitly the sum over the nearest neighbors

$$\hat{H}_{\mathrm{BHM}} = -\sum_i \Big(J_{i,i+1}\ \hat{a}_i^\dagger\ \hat{a}_{i+1} + J_{i,i-1}\ \hat{a}_i^\dagger\ \hat{a}_{i-1} \Big) + \sum_i \epsilon_i \hat{a}_i^\dagger \hat{a}_i. \tag{2.67}$$

Due to the homogeneity of the optical lattice the hopping parameter $J_{i,i\pm1}$ is independent of the lattice site i, therefore we can omit the index.

In the limit of vanishing lattice constant a the number of lattice sites i becomes infinitely large, so that the sum over i becomes an integral over x and the creation and annihilation operator a_i and $a_i^\dagger$ turn into the field operator $\psi(x)$ and $\psi^\dagger(x)$ according to

$$\hat{a}_i = \sqrt{a}\hat{\psi}(x), \quad \hat{a}_{i\pm1} = \sqrt{a}\hat{\psi}(x \pm a), \tag{2.68a}$$
$$\hat{a}_i^\dagger = \sqrt{a}\hat{\psi}^\dagger(x), \quad \hat{a}_{i\pm1}^\dagger = \sqrt{a}\hat{\psi}^\dagger(x \pm a). \tag{2.68b}$$

The onsite energy ϵ_i goes then over to $\epsilon(x)$, which is equal to a constant ϵ due to the homogeneity. By inserting (2.68a), and (2.68b) in (2.67) we get

$$\hat{H} = \int dx\ \frac{1}{a}(-J)\sqrt{a}\hat{\psi}^\dagger(x)\Big[\sqrt{a}\hat{\psi}(x+a) + \sqrt{a}\hat{\psi}(x-a)\Big] + \int dx\ \epsilon\hat{\psi}^\dagger(x)\psi(x). \tag{2.69}$$

Since the lattice constant a is small with respect to the continuum limit we perform a Taylor expansion for $\psi(x \pm a)$ and obtain

$$\hat{H} = \int dx\ \Big[-Ja^2\hat{\psi}^\dagger(x)\partial_x^2\hat{\psi}(x) + (\epsilon - J)\hat{\psi}^\dagger(x)\hat{\psi}(x)\Big]. \tag{2.70}$$

The second term can be absorbed in the potential term or the chemical potential. More interesting is the kinetic part. If we compare this with the first part of the Hamiltonian

(2.3) in second quantization

$$\hat{H} = \int \mathrm{d}x\ \hat{\psi}^\dagger(x) \left[-\frac{\hbar^2}{2m} \partial_x^2 \right] \hat{\psi}(x), \tag{2.71}$$

we identify

$$-Ja^2 \stackrel{!}{=} -\frac{\hbar^2}{2m}. \tag{2.72}$$

The hopping parameter J^{mass} of the long wave length limit fulfills Eq. (2.72), thus we obtain with this approximation the correct continuum limit of the Hamiltonian.

On the other hand, inserting J^{Bloch} of (2.60) leads to an error of a factor 2. Although this limit is based on an analytically exact method, it is surprising to get the wrong continuum limit. A possible explanation of this error is the following: Within the limit of vanishing lattice depth $V_0 \to 0$ the Wannier functions represent not any longer a proper basis because we have to take into account all higher energy bands as well as hoppings over larger distances than just the nearest neighbors. At least the last part we are able to calculate by using the formula for the hopping parameter for arbitrary hopping distances (2.57). The sum over all possible values s gives then the total hopping parameter at vanishing lattice depth

$$\tilde{J}^{\mathrm{total}} = \frac{2}{\pi^2} \sum_{s=1}^{\infty} \frac{(-1)^{s+1}}{s^2}. \tag{2.73}$$

The sum converges and has the value $\pi^2/12$, thus it yields for the dimensionless hopping parameter

$$\tilde{J}^{\mathrm{total}} = \frac{1}{6} \tag{2.74}$$

and with the recoil energy we get

$$J^{\mathrm{total}} = \frac{\hbar^2}{2ma^2} \frac{\pi^2}{6} = 1.64 \frac{\hbar^2}{2ma^2}. \tag{2.75}$$

We see that there is still an error but it is at least smaller than 2.

Nevertheless, the continuum limit shows that we are able to reconstruct the Hamiltonian in the continuum out of the discrete Hamiltonian of the Bose-Hubbard model. This will be a very useful tool to test the results of the one-dimensional Bose-Hubbard

model for a curved lattice treated in Section 5. Before that we have to introduce some fundamentals as well as some important relations of differential geometry in Section 3 and perturbation theory in Section 4.

3. Curved manifolds

Since the aim of this work is to investigate the behavior of quantum particles in curved lattices, we now investigate how to describe curvature within the realm of the Riemann differential geometry. To this end we introduce in Section 3.1 at first the metric tensor and the covariant derivative. Afterwards, we derive in Section 3.2 the Laplace-Beltrami operator, which extends the Laplace operator to curved manifolds, and the general volume element, as well. With this we determine expressions for the single-particle Hamiltonian and the scalar product on curved manifolds. Furthermore, we discuss the properties of the single-particle Hamiltonian and the scalar product as well as the second quantized Hamiltonian for the special case of one dimension.

3.1. Differential geometry

In this section we introduce the differential geometry following Refs. [49, 50] to be able to describe curvature in general. In Section 3.1.1 we first explain the notion of manifolds and then we define the metric in Section 3.1.2 as well as the affine connection in Section 3.1.3, which leads us to tensors and their covariant derivative. Since any form of torsion will go beyond the scope of this diploma thesis, we specialize in Section 3.1.4 to the Riemannian differential geometry, where we also give an approximation for the metric tensor in the case of small curvature.

3.1.1. Manifolds

A d-dimensional manifold is a topological space, which is locally equal to the d-dimensional Euclidean space at each point. The points of such a manifold are given by the coordinates x^i, where $i = 1, ..., d$, although the manifold itself is not depending on them. If we rename the coordinates as x'^μ, where $\mu = 1, ..., d$ with the coordinate transformation

$$x^i = x^i(x'), \qquad x'^\mu = x'^\mu(x), \tag{3.1}$$

we get for the coordinate differentials

$$dx^i = \frac{\partial x^i}{\partial x'^\mu} dx'^\mu = e^i{}_\mu(x') dx'^\mu \tag{3.2}$$

$$dx'^\mu = \frac{\partial x'^\mu}{\partial x^i} dx^i = e_i{}^\mu(x') dx^i, \tag{3.3}$$

where we use the Einstein sum convention. The transformation matrices or d-beins $e^i{}_\mu$ and $e_i{}^\mu$ fulfill the orthonormality and completeness relation

$$e^i{}_\mu(x') e_i{}^\nu(x') = \delta_\mu{}^\nu \tag{3.4}$$

$$e^i{}_\mu(x') e_j{}^\mu(x') = \delta^i{}_j. \tag{3.5}$$

The gradients of the old and new coordinates transform contragredient according to

$$\partial_i = e_i{}^\mu \partial_\mu, \qquad \partial_\mu = e^i{}_\mu \partial_i. \tag{3.6}$$

We can now define on the manifold tensors of different ranks due to their properties after a coordinate transformation (3.1). If a quantity is invariant under coordinate transformation, we call it a scalar

$$S(x) = S\big(x'(x)\big), \qquad S(x') = S\big(x(x')\big). \tag{3.7}$$

A contravariant vector, i.e. a tensor of first rank, transforms like the coordinate differential (3.2), thus

$$A^i(x) = e^i{}_\mu\big(x'(x)\big) A^\mu\big(x'(x)\big), \qquad A^\mu(x') = e_i{}^\mu(x') A^i\big(x(x')\big), \tag{3.8}$$

and it follows for a covariant vector

$$A_i(x) = e_i{}^\mu\big(x'(x)\big) A_\mu\big(x'(x)\big), \qquad A_\mu(x') = e^i{}_\mu(x') A_i\big(x(x')\big). \tag{3.9}$$

In general, a tensor of the rank r is a quantity with r indices, which transforms like a

vector in every single index. For example a tensor of rank two transforms like

$$T^{ij}(x) = e^{i}{}_{\mu}\big(x'(x)\big)e^{j}{}_{\nu}\big(x'(x)\big)T^{\mu\nu}\big(x'(x)\big), \tag{3.10a}$$
$$T^{i}{}_{j}(x) = e^{i}{}_{\mu}\big(x'(x)\big)e_{j}{}^{\nu}\big(x'(x)\big)T^{\mu}{}_{\nu}\big(x'(x)\big), \tag{3.10b}$$
$$T_{i}{}^{j}(x) = e_{i}{}^{\mu}\big(x'(x)\big)e^{j}{}_{\nu}\big(x'(x)\big)T_{\mu}{}^{\nu}\big(x'(x)\big), \tag{3.10c}$$
$$T_{ij}(x) = e_{i}{}^{\mu}\big(x'(x)\big)e_{j}{}^{\nu}\big(x'(x)\big)T_{\mu\nu}\big(x'(x)\big), \tag{3.10d}$$

where every single index can be contra- or covariant. The transformation from the new coordinates x' to the old coordinates x is given in an analogue way to (3.8) and (3.9).

3.1.2. Metric

As a structure element of the manifold we introduce now the contravariant metric

$$g^{ij}(x) = g^{ji}(x) \tag{3.11}$$

and the covariant metric

$$g_{ij}(x) = g_{ji}(x) \tag{3.12}$$

with the condition

$$g^{ij}(x)g_{jk}(x) = \delta^{i}{}_{k}. \tag{3.13}$$

If each metric transforms like a tensor second rank (3.10a) and (3.10d), we can rewrite a contravariant vector A^i as a covariant vector A_i and vice versa

$$A^{i}(x) = g^{ij}(x)A_{j}(x), \tag{3.14}$$
$$A_{i}(x) = g_{ij}(x)A^{j}(x). \tag{3.15}$$

These relations are also valid for the new coordinates x' as well as with tensors of higher rank for every single component.

3.1.3. Affine connection

Since the partial derivative of a tensor turns out to be in general no longer a tensor, we now generalize the partial derivative on manifolds. The so called covariant derivative is

defined such that, applied to a tensor with rank r, the result is a tensor of rank $r+1$. For a scalar $S(x)$ it follows that

$$D_i S(x) = \partial_i S(x), \tag{3.16}$$

which is a covariant vector in agreement to (3.6) and thus fulfills this condition. The covariant derivative of a contravariant vector should then lead to a tensor of second rank, which transforms analogue to (3.10c) like

$$D_\nu A^\mu(x') = e_i{}^\mu(x') e^j{}_\nu(x') D_j A^i\big(x(x')\big). \tag{3.17}$$

It turns out that the partial derivative cannot fulfill this condition and we have to introduce the affine connection $\gamma_{jk}{}^i(x)$ as another structure element of the manifold. The covariant derivative of a contravariant vector yields then

$$D_j A^i(x) = \partial_j A^i(x) + \gamma_{jk}{}^i(x) A^k(x), \tag{3.18}$$

which should be invariant under coordinate transformation, thus

$$D_\nu A^\mu(x') = \partial_\nu A^\mu(x') + \gamma_{\nu\lambda}{}^\mu(x') A^\lambda\big(x(x')\big). \tag{3.19}$$

With (3.6) and (3.8) we obtain the transformation rule for the affine connection

$$\gamma_{\nu\lambda}{}^\mu(x') = e_i{}^\mu(x') e^j{}_\nu(x') e^k{}_\lambda(x') \gamma_{jk}{}^i\big(x(x')\big) + e_i{}^\mu(x') \partial_\nu e^i{}_\lambda(x'), \tag{3.20}$$

thus the affine connection is not a tensor of rank three.

We can also define the covariant derivative D_i of a covariant vector A_j by assuming the product rule

$$D_i \left[A_j(x) B^j(x)\right] = A_j(x) D_i B^j(x) + B^j(x) D_i A_j(x). \tag{3.21}$$

On the left hand-side we have the covariant derivative of a scalar, which is given by (3.16), and the first part of the left hand-side is given by (3.18), thus we conclude

$$D_i A_j(x) = \partial_i A_j(x) - \gamma_{ij}{}^k(x) A_k(x). \tag{3.22}$$

The covariant derivative of a tensor of higher rank is then defined by applying (3.18)

and (3.22) for each component, for instance we have

$$D_i T^j{}_k(x) = \partial_i T^j{}_k(x) - \gamma_{il}{}^j(x) T^l{}_k(x) + \gamma_{ik}{}^l(x) T^j{}_l(x). \tag{3.23}$$

3.1.4. Riemannian differential geometry

If we assume a connection between both the metric and the affine connection, we can define certain manifolds. For instance, the Riemann-Cartan manifold is defined by the condition that the covariant derivative and the metric commutate. For the example of a vector this condition yields

$$D_k \left[g^{ij}(x) A_j(x) \right] = g^{ij}(x) D_k A_j(x), \tag{3.24}$$
$$D_k \left[g_{ij}(x) A^j(x) \right] = g_{ij}(x) D_k A^j(x). \tag{3.25}$$

The covariant derivative of the metric then has to vanish, thus for the covariant metric we obtain

$$0 = D_i g_{jk}(x) = \partial_i g_{jk}(x) - \gamma_{ij}{}^l(x) g_{lk}(x) - \gamma_{ik}{}^l(x) g_{jl}(x). \tag{3.26}$$

With a cyclic permutation in the indices i, j, and k we get the following decomposition for the affine connection:

$$\gamma_{jk}{}^i(x) = \Gamma_{jk}{}^i(x) + K_{jk}{}^i(x). \tag{3.27}$$

The Christoffel symbol of the second kind $\Gamma_{jk}{}^i(x)$ is given by the metric

$$\Gamma_{jk}{}^i(x) = \frac{1}{2} g^{il}(x) \Big[\partial_j g_{kl}(x) + \partial_k g_{lj}(x) - \partial_l g_{jk}(x) \Big] \tag{3.28}$$

and is due to (3.12) symmetric with respect to the two lower indices

$$\Gamma_{jk}{}^i(x) = \Gamma_{kj}{}^i(x). \tag{3.29}$$

The second part on the right hand-side of (3.27) denotes the contortion tensor $K_{jk}{}^i(x)$, which can be written as

$$\begin{aligned} K_{jk}{}^i(x) &= g^{il}(x) K_{jkl}(x) \\ &= S_{jkl}(x) + S_{ljk}(x) - S_{klj}(x), \end{aligned} \tag{3.30}$$

where $S_{jk}{}^{i}(x) = g^{il}(x)S_{jkl}(x)$ is called the torsion tensor. This quantity is given by the antisymmetric part of the affine connection

$$S_{jk}{}^{i}(x) = \frac{1}{2}\Big[\Gamma_{jk}{}^{i}(x) - \Gamma_{kl}{}^{i}(x)\Big] \tag{3.31}$$

and describes possible torsions within the manifold.

Additionally to the condition (3.24) we can assume that the lower two indices of the affine connection are symmetric

$$\gamma_{jk}{}^{i}(x) = \gamma_{kj}{}^{i}(x). \tag{3.32}$$

In that case we restrict the Riemann-Cartan manifold to the Riemann manifold as a special case. With the assumption (3.32) the torsion tensor (3.31) vanishes, thus we get for the contortion tensor

$$K_{jk}{}^{i}(x) = 0. \tag{3.33}$$

Due to (3.27) the affine connection is then only determined by the Christoffel symbol

$$\gamma_{jk}{}^{i}(x) = \Gamma_{jk}{}^{i}(x). \tag{3.34}$$

The Riemannian manifold is the mathematical basis of the General Relativity Theory [51, 52]. In this theory the metric tensor

$$(g_{\mu\nu}(x)) = \begin{pmatrix} g_{00}(x) & \dots & g_{03}(x) \\ \vdots & \ddots & \vdots \\ g_{30}(x) & \dots & g_{33}(x) \end{pmatrix} \tag{3.35}$$

describes the curvature of the space-time. In the limit of vanishing curvature of space-time the metric tensor $g_{\mu\nu}$ becomes the Minkowski metric

$$(\eta_{\mu\nu}) = \begin{pmatrix} -1 & 0 & 0 & 0 \\ 0 & 1 & 0 & 0 \\ 0 & 0 & 1 & 0 \\ 0 & 0 & 0 & 1 \end{pmatrix}, \tag{3.36}$$

which is used in Special Relativity. In the case of a small curvature the metric tensor

differs slightly from the Minkowski tensor (3.36) so we can assume that the metric tensor has the following form

$$g_{\mu\nu} = \eta_{\mu\nu} + h_{\mu\nu}, \tag{3.37}$$

$$g^{\mu\nu} = \eta^{\mu\nu} - h^{\mu\nu}, \tag{3.38}$$

where $|h_{\mu\nu}| \ll 1$. This approximation is used, for instance, to derive gravitational waves [53].

3.2. Laplace-Beltrami operator and volume element

In this section we investigate the Laplace-Beltrami operator and the volume element on Riemannian manifolds. We start in the Section 3.2.1 with the derivation of the Laplace-Beltrami operator as a generalization of the Laplace operator on manifolds and determine the single-particle Hamiltonian by replacing the Laplace operator by the Laplace-Beltrami operator. Since we are interested in the second quantized Hamiltonian, we have to discuss the scalar product on manifolds. To this end we derive the general volume element on manifolds in Section 3.2.2. With this we obtain an expression for the Hamiltonian in second quantization. In Section 3.2.3 we restrict ourselves to a one-dimensional system. We show that under a proper coordinate transformation the Laplace-Beltrami operator becomes the Laplace operator. Furthermore, we find out that under the same transformation the Riemannian scalar product goes over to the Euclidean scalar product. Combining both the Laplace-Beltrami operator and the scalar product we get as result a one-dimensional Euclidean Hamiltonian in second quantization, which contains an effective potential.

3.2.1. Derivation of Laplace-Beltrami operator

The Laplace operator utilized on an arbitrary scalar field S can be written as

$$\Delta S = \mathrm{div}(\mathrm{grad}\ S). \tag{3.39}$$

On a d-dimensional Riemannian manifold we use the covariant derivative introduced in the previous section, thus we obtain

$$\Delta_{\mathrm{LB}} S = D_\mu (D^\mu S), \tag{3.40}$$

Now we derive an expression for the Laplace-Beltrami operator following Ref. [54]. To this end we insert the covariant derivative of a scalar (3.16) and of a vector (3.18), so we get

$$\begin{aligned}\Delta_{\mathrm{LB}} S &= D_\mu(\partial^\mu S) \\ &= \partial_\mu(\partial^\mu S) + \Gamma_{\mu\nu}{}^{\mu}(\partial^\nu S).\end{aligned} \tag{3.41}$$

Here we rewrite the Christoffel symbol $\Gamma_{\mu\nu}{}^{\mu}$ with (3.28) in terms of the metric tensor, where the last two terms cancel each other because of the contraction of μ, thus we get

$$\Gamma_{\mu\nu}{}^{\mu} = \frac{1}{2} g^{\mu\lambda}\, \partial_\nu g_{\lambda\mu}. \tag{3.42}$$

In order to obtain a more concise expression for (3.42), we verify at first the following equation for an arbitrary matrix $M(x)$ depending on a coordinate x

$$\partial_x \det M(x) = \mathrm{Tr}\left[M^{-1}(x)\, \partial_x M(x)\right], \tag{3.43}$$

where $\det M(x)$ denotes the determinant of $M(x)$ and $M^{-1}(x)$ stands for the inverse of the matrix. To proof this relation we assume an infinitesimal change from x to $x + dx$

$$\begin{aligned}\det M(x+dx) &= \det\left[M(x) + \partial_x M(x) dx\right] \\ &= \det\left[M(x)\Big(\mathbb{1} + M^{-1}(x)\, \partial_x M(x) dx\Big)\right] \\ &= \det M(x)\, \det\left[\mathbb{1} + M^{-1}(x)\, \partial_x M(x) dx\right].\end{aligned} \tag{3.44}$$

According to the Laplace formula for determinants, the only remaining part of the second determinant on the right hand-side of (3.44) in first-order approximation in dx is the sum of the diagonal terms, other terms are at least of second order in dx. Thus we get

$$\det\left[\mathbb{1} + M^{-1}(x)\, \partial_x M(x) dx\right] = 1 + \mathrm{Tr}\left[M^{-1}(x)\, \partial_x M(x)\right] dx + \mathcal{O}(dx^2). \tag{3.45}$$

Inserting (3.45) in (3.44) and defining the derivative as the limit of the difference quotient leads us to the relation (3.43). If the matrix is depending on multiple variables we have to replace ∂_x by ∂_μ.

After this digression we return to our initial problem (3.42) and assume that the matrix $M(x^\lambda)$ is given by the covariant metric tensor $g_{\lambda\mu}$. The inverse matrix is then

according to (3.13) the contravariant metric tensor and we identify

$$M(x^\lambda) = g_{\lambda\mu} \ , \quad M^{-1}(x^\lambda) = g^{\lambda\mu}. \tag{3.46}$$

With the definition

$$g = \det\left(g_{\lambda\mu}\right) \tag{3.47}$$

we get from (3.43) the useful identity

$$\partial_\nu g = g \ g^{\mu\lambda}\partial_\nu g_{\lambda\mu}. \tag{3.48}$$

Applying the chain rule on $\partial_\nu\sqrt{|g|}$ the result (3.48) leads to

$$\partial_\nu\sqrt{g} = \frac{\sqrt{g}}{2}g^{\mu\lambda}\partial_\nu g_{\lambda\mu}, \tag{3.49}$$

so we can rewrite the contraction of the Christoffel symbol (3.42) according to

$$\Gamma_{\mu\nu}{}^{\mu} = \frac{1}{\sqrt{g}}\partial_\nu\sqrt{g}. \tag{3.50}$$

This result we need in (3.41) to obtain the following useful representation of the Laplace-Beltrami operator

$$\Delta_{\mathrm{LB}}S = \partial_\mu(\partial^\mu S) + \frac{1}{\sqrt{g}}\Big(\partial_\nu\sqrt{g}\Big) \ (\partial^\nu S). \tag{3.51}$$

We rename the indices in the second part and apply the product rule

$$\Delta_{\mathrm{LB}}S = \frac{1}{\sqrt{g}}\partial_\mu\Big[\sqrt{g} \ (\partial^\mu S)\Big] \tag{3.52}$$

as well as (3.14) to get

$$\Delta_{\mathrm{LB}}S = \frac{1}{\sqrt{g}}\partial_\mu\left(\sqrt{g} \ g^{\mu\nu}\partial_\nu S\right) \tag{3.53}$$

Thus the Laplace-Beltrami operator as the generalization of the Laplace operator on a

Riemannian manifold can be represented by

$$\Delta_{\mathrm{LB}} = \frac{1}{\sqrt{g}} \partial_\mu \left(\sqrt{g}\, g^{\mu\nu} \partial_\nu \right). \tag{3.54}$$

Since we derived the Laplace-Beltrami operator by applying the covariant derivative, the operator is manifestly invariant under a general coordinate transformation.

With the Laplace-Beltrami operator (3.54), the single-particle Hamiltonian with an arbitrary potential $V(x^\mu)$ is then given by

$$H_{\mathrm{free}} = -\frac{\hbar^2}{2m} \Delta_{\mathrm{LB}} + V(x^\mu). \tag{3.55}$$

With (3.54) we obtain explicitly

$$H_{\mathrm{free}} = -\frac{\hbar^2}{2m} \frac{1}{\sqrt{g}} \partial_\mu \left(\sqrt{g}\, g^{\mu\nu} \partial_\nu \right) + V(x^\mu). \tag{3.56}$$

3.2.2. Volume element on manifolds

If one applies a coordinate transformation to an Euclidean space, the volume element in d dimensions is given by the Jacobian matrix

$$dV = |\det(J)\,| dx_1 dx_2 ... dx_d. \tag{3.57}$$

We now have to find a connection between the Jacobian matrix and the metric tensor g_{ij}, so that the volume element can be expressed in dependence of the metric.

The metric tensor g_{ij} transforms like a tensor of rank two (3.10d)

$$g_{\mu\nu} = e^i{}_\mu(x') e^j{}_\nu(x') g_{ij}, \tag{3.58}$$

where the transformation matrices $e^i{}_\mu(x')$ are given by the first derivatives of the coordinates according to (3.2). Thus the metric tensor can be expressed as the product of the transposed Jacobian matrix and the Jacobian matrix. In the definition of the determinant of the covariant metric (3.47) we replace the metric tensor by the Jacobian matrices and use the product rule for determinants

$$g = \det\left(J^T\right) \det(J). \tag{3.59}$$

The determinant of a transposed matrix is equal to the determinant of the matrix itself,

thus we get

$$\det(J) = \sqrt{g}. \tag{3.60}$$

Inserting (3.60) in (3.57) yields then

$$dV = \sqrt{g}\, dx_1 dx_2 ... dx_d. \tag{3.61}$$

By using the volume element (3.61), we obtain an expression for the standard scalar product of two arbitrary wave functions ψ and φ on a d-dimensional Riemannian manifold

$$\langle \psi | \varphi \rangle = \int \mathrm{d}^d x\, \sqrt{g}\, \psi^\star(x) \varphi(x). \tag{3.62}$$

Another important application of the volume element (3.61) is to generalize the Gauss's theorem on an Euclidean manifold for an arbitrary vector $\mathbf{A}$

$$\int_V \mathrm{d}V\, \mathrm{div}\mathbf{A} = \oint_{\partial V} \mathrm{d}\mathbf{F} \cdot \mathbf{A}, \tag{3.63}$$

where ∂V is the complete surface of a volume V and $d\mathbf{F}$ an infinitesimal surface element. On a Riemannian manifold the divergence is replaced by the covariant derivative (3.18), thus we have

$$D_\mu A^\mu = \partial_\mu A^\mu + \Gamma_{\mu\nu}{}^{\mu} A^\nu. \tag{3.64}$$

The contracted Christoffel symbol can be expressed by (3.50) and with the product rule it follows

$$D_\mu A^\mu = \frac{1}{\sqrt{g}} \partial_\mu \left(\sqrt{g} A^\mu \right). \tag{3.65}$$

Due to (3.61) and (3.65) we obtain

$$\int_V \mathrm{d}^d x\, \sqrt{g}\, D_\mu A^\mu = \int_V d^d x\, \partial_\mu \left(\sqrt{g} A^\mu \right), \tag{3.66}$$

where the factor $\sqrt{g}$ in the volume element is canceled by the prefactor of the covariant derivative. On the right hand-side of (3.66) we can now apply (3.63) to generalize the

Gauss's theorem on curved manifolds which is then given by

$$\int_V \mathrm{d}^d x \, \sqrt{g} \, D_\mu A^\mu = \oint_{\partial V} \mathrm{d}F_\mu \, \sqrt{g} \, A^\mu. \tag{3.67}$$

This relation is very important in physics, i.e. for showing that the number of particles in a system is conserved. Therefore we need the continuity equation, which we also expand on curved manifolds. In order to derive the continuity equation we start with the Schrödinger equation

$$i\hbar \frac{\partial}{\partial t}\psi = \left[-\frac{\hbar^2}{2m} \Delta_{\mathrm{LB}} + V \right] \psi, \tag{3.68}$$

where we replace the Laplace operator by the Laplace-Beltrami operator. The complex conjugation of (3.68) and the sum over both equations leads to

$$\psi^\star \left(\frac{\partial}{\partial t} \psi \right) + \left(\frac{\partial}{\partial t} \psi^\star \right) \psi = -\frac{\hbar}{2mi} \left[\psi^\star \left(\Delta_{\mathrm{LB}} \psi \right) - \left(\Delta_{\mathrm{LB}} \psi^\star \right) \psi \right]. \tag{3.69}$$

With the product rule and the expression for the Laplace-Beltrami operator (3.54) it follows the continuity equation

$$\frac{\partial}{\partial t} \rho + D_\mu j^\mu = 0, \tag{3.70}$$

where we define the probability density ρ and the probability flux j^μ as

$$\rho = \psi^\star \psi, \tag{3.71}$$

$$j^\mu = \frac{\hbar}{2mi} \left[\psi^\star \left(\partial^\mu \psi \right) - \left(\partial^\mu \psi^\star \right) \psi \right]. \tag{3.72}$$

Integrating the continuity equation (3.70) over the volume and applying the Gauss's theorem (3.67) leads to the conservation of the particle number.

3.2.3. Hamiltonian and scalar product in one dimension

The single-particle Hamiltonian on a Riemannian manifold given by (3.56) reduces for one dimension to

$$H_{\mathrm{free}} = -\frac{\hbar^2}{2m} \frac{1}{\sqrt{g}} \, \partial_x \left(g^{xx} \sqrt{g} \, \partial_x \right) + V(x). \tag{3.73}$$

For the one-dimensional metric tensor we can assume a function depending on one coordinate

$$g^{xx} = g(x) \tag{3.74}$$

and thus

$$g = \det(g_{xx}) = \frac{1}{g(x)}. \tag{3.75}$$

Inserting (3.74) and (3.75) in (3.73) as well as performing a coordinate transformation

$$x = x(u), \qquad dx = x'(u)du, \qquad \partial_x = \frac{1}{x'(u)}\,\partial_u, \tag{3.76}$$

where $x'(u)$ denotes the first derivative of $x(u)$ with respect to u, leads to

$$H_{\text{free}} = -\frac{\hbar^2}{2m}\sqrt{g\big(x(u)\big)}\;\frac{1}{x'(u)}\partial_u\left(\sqrt{g\big(x(u)\big)}\;\frac{1}{x'(u)}\partial_u\right) + V\big(x(u)\big). \tag{3.77}$$

If we choose $x'(u) = \sqrt{g\big(x(u)\big)}$ the Hamiltonian (3.77) simplifies to

$$H_{\text{free}} = -\frac{\hbar^2}{2m}\,\partial_u^2 + V\big(x(u)\big), \tag{3.78}$$

which is equal to a Hamiltonian in an Euclidean space with an effective potential depending on the coordinate transformation. Thus the Laplace-Beltrami operator becomes for one dimension the Laplace operator, where we have to pay attention to a change of the potential. Physically this means that in one dimension we cannot observe a real curvature.

We assume now two arbitrary wave functions ψ and φ. The scalar product of these two functions is then given by (3.62), thus we get for one dimension

$$\langle\psi|\varphi\rangle = \int \mathrm{d}x\;\sqrt{g}\psi^\star(x)\varphi(x). \tag{3.79}$$

With the same coordinate transformation (3.76) it follows

$$\langle\psi|\varphi\rangle = \int \mathrm{d}u\;x'(u)\frac{1}{\sqrt{g\big(x(u)\big)}}\psi^\star\big(x(u)\big)\varphi\big(x(u)\big). \tag{3.80}$$

Here we set again $x'(u) = \sqrt{g\big(x(u)\big)}$, so that (3.80) reduces to

$$\langle\psi|\varphi\rangle = \int \mathrm{d}u\ \psi^\star\big(x(u)\big)\varphi\big(x(u)\big), \tag{3.81}$$

which is equal to the Euclidean scalar product. Thus we get the same result as above that in one dimension no physical curvature appears.

To investigate problems of many-body physics on curved manifolds, we have to introduce the second quantized Hamiltonian

$$\hat{H} = \int \mathrm{d}^d x\ \sqrt{g}\ \hat{\psi}^\dagger(x^\mu) H_{\text{free}} \hat{\psi}(x^\mu), \tag{3.82}$$

where we use the single-particle Hamiltonian H_{free} (3.56) on manifolds. In one dimension we can simplify both the scalar product and the Hamiltonian due to (3.79) and (3.73). The second quantized Hamiltonian in one dimension is thus given by

$$\hat{H} = \int \mathrm{d}x\ \sqrt{g}\ \hat{\psi}^\dagger(x) \left[-\frac{\hbar^2}{2m}\frac{1}{\sqrt{g}}\ \partial_x \left(g^{xx}\sqrt{g}\,\partial_x\right) + V(x)\right] \hat{\psi}(x). \tag{3.83}$$

The coordinate transformation (3.76) yields in an analogue calculation

$$\hat{H} = \int \mathrm{d}u\ \hat{\psi}^\dagger\big(x(u)\big) \left[-\frac{\hbar^2}{2m}\ \partial_u^2 + V\big(x(u)\big)\right] \hat{\psi}\big(x(u)\big), \tag{3.84}$$

which is equal to the second quantized Hamiltonian on an Euclidean manifold according to (2.1) without an interaction term. Like in (3.78) we obtain an effective potential $V_{\text{eff}} = V\big(x(u)\big)$ depending on the coordinate transformation.

In order to derive a one-dimensional model for quantum particles in weakly curved optical lattices based on the Bose-Hubbard model, we have to use the formalism developed in this chapter. Due to the aim of describing weakly curved surfaces the next step is now investigating a perturbation theory. Perturbing the metric itself leads to perturbations of the Hamiltonian as well as the scalar product, thus we cannot apply the common Rayleigh-Schrödinger perturbation theory. Therefore we have to extend in the following chapter this theory on curved manifolds.

4. Perturbation theory on curved manifolds

After having provided an introduction to the Riemannian differential geometry we now investigate the perturbation theory on curved manifolds. To this end, we start in Section 4.1 with a small perturbation within the metric. It turns out that this sort of perturbation influences the Hamiltonian as well as the scalar product, where both can be expressed as the sum over an unperturbed part and a correction. The common Rayleigh-Schrödinger theory cannot be applied due to the perturbed scalar product. Therefore we have to formulate an extended form of the perturbation theory in Section 4.2 starting with the Schrödinger equation in Section 4.2.1. Analogue to the Rayleigh-Schrödinger perturbation theory we derive recursion formulas for the corrections for both the eigenenergy in Section 4.2.2 and the eigenstates in Section 4.2.3 and Section 4.2.4, where we have to take account of two different contributions treated. Additionally we compare the results of this chapter to the common Rayleigh-Schrödinger perturbation theory.

4.1. Small deformation of the metric

In this section we formulate the consequences if the metric itself is perturbed. In the sense of the perturbation theory we utilize the approximation (3.38), where we assume that the Riemannian metric slightly differs from the Minkowski metric $\eta^{\mu\nu}$ (3.36). Since we are interested in a time independent problem, we neglect the time coordinate within the Minkowski metric, which thus simplifies to the Euclidean metric $\delta^{\mu\nu}$. The metric can then be approximated with

$$g^{\mu\nu} = \delta^{\mu\nu} - h^{\mu\nu}, \tag{4.1}$$

$$g_{\mu\nu} = \delta_{\mu\nu} + h_{\mu\nu}, \tag{4.2}$$

with $|h_{\mu\nu}| \ll 1$. Applying the determinant on the covariant metric tensor in (4.2) leads to

$$g = \det\left(\mathbb{1}_d + h_{\mu\nu}\right). \tag{4.3}$$

Due to the assumption that $h_{\mu\nu}$ is small, it follows with the Laplace formula for determinants that

$$\det\left(\mathbb{1}_d + h_{\mu\nu}\right) = 1 + \mathrm{Tr}\left(h_{\mu\nu}\right)\mathcal{O}(h^2), \tag{4.4}$$

thus we get with (4.4) in (4.3) and a Taylor expansion

$$\sqrt{g} = 1 + \frac{1}{2}\mathrm{Tr}\left(h_{\mu\nu}\right), \tag{4.5}$$

$$\frac{1}{\sqrt{g}} = 1 - \frac{1}{2}\mathrm{Tr}\left(h_{\mu\nu}\right). \tag{4.6}$$

Now we derive the corrections of the Laplace-Beltrami operator for a perturbed metric. Inserting (4.5) and (4.6) in the general form of the Laplace-Beltrami operator (3.54) yields

$$\Delta_{\mathrm{LB}} = \partial_\mu\left[\delta^{\mu\nu}\partial_\nu - h^{\mu\nu}\partial_\nu + \frac{1}{2}\mathrm{Tr}\left(h_{\lambda\sigma}\right)\delta^{\mu\nu}\partial_\nu\right] - \frac{1}{2}\mathrm{Tr}\left(h_{\rho\kappa}\right)\partial_\mu\big(\delta^{\mu\nu}\partial_\nu\big), \tag{4.7}$$

where we neglect terms of higher than first order in the perturbation $h^{\mu\nu}$. With the product rule we obtain

$$\Delta_{LB} = \Delta^{(0)} + \Delta^{(1)}, \tag{4.8}$$

where

$$\Delta^{(0)} = \delta^{\mu\nu}\partial_\mu\partial_\nu \tag{4.9}$$

denotes the common Laplace operator and

$$\Delta^{(1)} = -\left[h^{\mu\nu}\partial_\mu\partial_\nu + \big(\partial_\mu h^{\mu\nu}\big)\partial_\nu - \frac{1}{2}\big(\partial_\mu \mathrm{Tr}\left(h_{\lambda\sigma}\right)\big)\delta^{\mu\nu}\partial_\nu\right] \tag{4.10}$$

is the first-order correction with respect to the perturbed metric.

The perturbed Laplace-Beltrami operator (4.8) can now be applied to the general

form of the Hamiltonian (3.55) on manifolds, so we get

$$H = H_0 + H_1 \tag{4.11}$$

with the unperturbed Hamiltonian

$$H_0 = -\frac{\hbar^2}{2m}\delta^{\mu\nu}\partial_\mu\partial_\nu + V\left(x^\mu\right). \tag{4.12}$$

We note that the correction

$$H_1 = +\frac{\hbar^2}{2m}\left[h^{\mu\nu}\partial_\mu\partial_\nu + \left(\partial_\mu h^{\mu\nu}\right)\partial_\nu - \frac{1}{2}\left(\partial_\mu \mathrm{Tr}(h_{\lambda\sigma})\right)\delta^{\mu\nu}\partial_\nu\right] \tag{4.13}$$

contains an additional part with the second spatial derivative and two terms with the first spatial derivative.

On the other hand, we know from (3.62) that the scalar product of two arbitrary wave functions ψ and φ depends on the metric tensor due to the volume element (3.61). A perturbation of the metric leads then to a correction of the factor $\sqrt{g}$ approximated by (4.5). Thus we get for the scalar product

$$\langle\psi|\varphi\rangle = \langle\psi|\varphi\rangle_0 + \langle\psi|\varphi\rangle_1 \tag{4.14}$$

with the unperturbed part

$$\langle\psi|\varphi\rangle_0 = \int \mathrm{d}^d x\ \psi^\star(x)\varphi(x) \tag{4.15}$$

and the correction

$$\langle\psi|\varphi\rangle_1 = +\frac{1}{2}\int \mathrm{d}^d x\ \mathrm{Tr}(h_{\mu\nu})\psi^\star(x)\varphi(x). \tag{4.16}$$

This means that we have to take account of an additional perturbation of the scalar product besides the perturbation of the Hamiltonian in (4.11). To handle this we have to develop a new form of Rayleigh-Schrödinger perturbation theory for quantum theory on curved manifolds, which contains both a perturbation of the Hamiltonian and a perturbation of the scalar product.

4.2. Perturbation theory on manifolds

In the last section we found out that a small deformation of the metric given by (4.1) leads to two different perturbations: a perturbed Hamiltonian and a perturbed scalar product according to (4.11) and (4.14). After clarifying the conditions and the Schödinger equation in Section 4.2.1, we investigate in Section 4.2.2 a recursion formula for the corrections of the eigenenergy due to both perturbations in a way, which is analogue to the common Rayleigh-Schrödinger perturbation theory [55, 56]. Due to an expansion of the corrections of the eigenstates we have to distinguish between two contributions to the corrections: the off-diagonal and the diagonal. The first one is treated in Section 4.2.3 and the second one in Section 4.2.4. Afterwards we are able to give a recursion formula for the correction of the eigenstates. A comparison to the common perturbation theory shows that the Rayleigh-Schrödinger perturbation is the special case of the theory developed in this chapter.

4.2.1. Schrödinger equation

The aim of the perturbation theory is in general to find an approximation as good as possible for the Schrödinger equation

$$H\left|\psi_n\right\rangle = E_n\left|\psi_n\right\rangle, \tag{4.17}$$

where the eigenvalue problem for H_0 is exactly solvable with

$$H_0\left|\psi_n^{(0)}\right\rangle = E_n^{(0)}\left|\psi_n^{(0)}\right\rangle \tag{4.18}$$

and the eigenenergies $E_n^{(0)}$ are not degenerate

$$E_n^{(0)} \neq E_m^{(0)} \quad \forall n, m \quad . \tag{4.19}$$

The unperturbed eigenstates $|\psi_n^{(0)}\rangle$ are supposed to fulfill the orthonormality and completeness relations with respect to the unperturbed scalar product

$$\langle\psi_n^{(0)}|\psi_m^{(0)}\rangle_0 = \delta_{n,m}, \tag{4.20}$$

$$\sum_n \left|\psi_n^{(0)}\right\rangle\left\langle\psi_n^{(0)}\right| = \mathbb{1}. \tag{4.21}$$

In order to solve (4.17) perturbatively we expand the eigenvalues and eigenstates in

power series of the correction order p

$$E_n = \sum_{p=0}^{\infty} E_n^{(p)}, \tag{4.22}$$

$$|\psi_n\rangle = \sum_{p=0}^{\infty} |\psi_n^{(p)}\rangle \,. \tag{4.23}$$

Inserting (4.22) and (4.23) in the Schrödinger equation (4.17) leads to

$$H_0 \,|\psi_n^{(0)}\rangle + \sum_{p=1}^{\infty} \Big(H_0 \,|\psi_n^{(p)}\rangle + H_1 \,|\psi_n^{(p-1)}\rangle \Big) = E_n^{(0)} \,|\psi_n^{(0)}\rangle + \sum_{p=1}^{\infty} \sum_{j=0}^{p} E_n^{(j)} \,|\psi_n^{(p-j)}\rangle \,, \tag{4.24}$$

which can be simplified by the unperturbed Schrödinger equation (4.18) to

$$\sum_{p=1}^{\infty} \Big(H_0 \,|\psi_n^{(p)}\rangle + H_1 \,|\psi_n^{(p-1)}\rangle \Big) = \sum_{p=1}^{\infty} \sum_{j=0}^{p} E_n^{(j)} \,|\psi_n^{(p-j)}\rangle \,. \tag{4.25}$$

This equation is the starting point for calculating the corrections of both the eigenenergy and the eigenstates. In the common perturbation theory we would restrict Eq. (4.25) to an arbitrary order of p, so that we can neglect the sum over p and multiply the equation with $\langle\psi_n^{(0)}|$ or $\langle\psi_m^{(0)}|$, where $m \neq n$. In our case of a perturbed scalar product we can not do this because within the scalar product (4.14) there are two different orders p and $p+1$.

4.2.2. Energy correction

First we derive the corrections of the eigenenergy E_n. To this end we multiply (4.25) with $\langle\psi_n^{(0)}|$ and get

$$\sum_{p=1}^{\infty} \langle\psi_n^{(0)}|H_0|\psi_n^{(p)}\rangle + \sum_{p=1}^{\infty} \langle\psi_n^{(0)}|H_1|\psi_n^{(p-1)}\rangle = \sum_{p=1}^{\infty} \sum_{j=0}^{p} E_n^{(j)} \,\langle\psi_n^{(0)}|\psi_n^{(p-j)}\rangle \,. \tag{4.26}$$

In order to apply the orthonormality relation of the eigenstates (4.20) we have to insert (4.14) into (4.26). To have a better view we treat the three appearing sums separately. For the first sum in (4.26) we get

$$\sum_{p=1}^{\infty} \langle\psi_n^{(0)}|H_0|\psi_n^{(p)}\rangle = \sum_{p=1}^{\infty} \Big(\langle\psi_n^{(0)}|H_0|\psi_n^{(p)}\rangle_0 + \langle\psi_n^{(0)}|H_0|\psi_n^{(p)}\rangle_1 \Big). \tag{4.27}$$

The first part has the order p while the second is of the order $p+1$ due to the additional order of the correction of the scalar product. The next step is splitting the first sum into one part with $p = 1$ and $p \geq 2$ as well as changing the summation index in the second sum into $p \to p + 1$

$$\sum_{p=1}^{\infty} \langle \psi_n^{(0)} | H_0 | \psi_n^{(p)} \rangle = \langle \psi_n^{(0)} | H_0 | \psi_n^{(1)} \rangle_0 + \sum_{p=2}^{\infty} \langle \psi_n^{(0)} | H_0 | \psi_n^{(p)} \rangle_0 + \sum_{p=2}^{\infty} \langle \psi_n^{(0)} | H_0 | \psi_n^{(p-1)} \rangle_1 \,. \tag{4.28}$$

In an analogue way we rewrite the other sum on the left hand-side of (4.26)

$$\sum_{p=1}^{\infty} \langle \psi_n^{(0)} | H_1 | \psi_n^{(p-1)} \rangle = \langle \psi_n^{(0)} | H_1 | \psi_n^{(0)} \rangle_0 + \sum_{p=2}^{\infty} \langle \psi_n^{(0)} | H_1 | \psi_n^{(p-1)} \rangle_0 + \sum_{p=2}^{\infty} \langle \psi_n^{(0)} | H_1 | \psi_n^{(p-2)} \rangle_1 \,. \tag{4.29}$$

On the right hand-side of (4.26) we also insert the perturbed scalar product (4.14)

$$\sum_{p=1}^{\infty} \sum_{j=0}^{p} E_n^{(j)} \, \langle \psi_n^{(0)} | \psi_n^{(p-j)} \rangle = \sum_{p=1}^{\infty} \sum_{j=0}^{p} \Big(E_n^{(j)} \, \langle \psi_n^{(0)} | \psi_n^{(p-j)} \rangle_0 + E_n^{(j)} \, \langle \psi_n^{(0)} | \psi_n^{(p-j)} \rangle_1 \Big). \tag{4.30}$$

Here we obtain the different orders p and $p + 1$ of the two parts like in (4.27), as well. We split the first sum in the parts $p = 1$, thus $j = 0$ and $j = 1$, and $p \geq 2$. In the second sum we change the summation index analogue to (4.28) to $p \to p + 1$, thus we get

$$\begin{aligned} \sum_{p=1}^{\infty} \sum_{j=0}^{p} E_n^{(j)} \, \langle \psi_n^{(0)} | \psi_n^{(p-j)} \rangle_0 &= E_n^{(0)} \, \langle \psi_n^{(0)} | \psi_n^{(1)} \rangle_0 + E_n^{(1)} \, \langle \psi_n^{(0)} | \psi_n^{(0)} \rangle_0 \\ &\quad + \sum_{p=2}^{\infty} \sum_{j=0}^{p} E_n^{(j)} \, \langle \psi_n^{(0)} | \psi_n^{(p-j)} \rangle_0 + \sum_{p=2}^{\infty} \sum_{j=0}^{p-1} E_n^{(j)} \, \langle \psi_n^{(0)} | \psi_n^{(p-1-j)} \rangle_1 \,. \end{aligned} \tag{4.31}$$

The aim of this calculation is to determine the correction of the eigenenergy $E_n^{(p)}$, which is part of the first sum over j. To this end, we split this sum in the parts $j = 0$, $j = p$, and the rest. The second sum over j we adapt by changing the summation index to

$j \to j-1$. The total expression on the left hand-side of (4.26) reads then

$$\begin{aligned}\sum_{p=1}^{\infty}\sum_{j=0}^{p} E_n^{(j)} \langle\psi_n^{(0)}|\psi_n^{(p-j)}\rangle &= E_n^{(0)} \langle\psi_n^{(0)}|\psi_n^{(1)}\rangle_0 + E_n^{(1)} \langle\psi_n^{(0)}|\psi_n^{(0)}\rangle_0 \\ &+ \sum_{p=2}^{\infty} E_n^{(0)} \langle\psi_n^{(0)}|\psi_n^{(p)}\rangle_0 + \sum_{p=2}^{\infty} E_n^{(p)} \langle\psi_n^{(0)}|\psi_n^{(0)}\rangle_0 \\ &+ \sum_{p=2}^{\infty}\sum_{j=1}^{p-1} E_n^{(j)} \langle\psi_n^{(0)}|\psi_n^{(p-j)}\rangle_0 + \sum_{p=2}^{\infty}\sum_{j=1}^{p-1} E_n^{(j-1)} \langle\psi_n^{(0)}|\psi_n^{(p-j)}\rangle_1 . \end{aligned} \tag{4.32}$$

The advantages of the Eqs. (4.28), (4.29), and (4.32) are the following: First of all, p gives now the correct order of perturbation because we have taken into account the additional order due to the correction of the scalar product $\langle\cdot|\cdot\rangle_1$ by changing the summation indices. The second advantage is that we can now apply the conditions (4.18) and (4.20) for the unperturbed Euclidean scalar products $\langle\cdot|\cdot\rangle_0$. To determine a formula for the energy correction $E_n^{(p)}$ we insert the Eqs. (4.28), (4.29), and (4.32) into (4.26) and order the parts in terms of the correction. For the first-order correction we get

$$E_n^{(1)} = \langle\psi_n^{(0)}|H_1|\psi_n^{(0)}\rangle_0 , \tag{4.33}$$

because all the other parts cancel or represent higher order corrections. For the order $p \geq 2$ we obtain the following recursion formula

$$\begin{aligned} E_n^{(p)} = &\langle\psi_n^{(0)}|H_1|\psi_n^{(p-1)}\rangle_0 + \langle\psi_n^{(0)}|H_0|\psi_n^{(p-1)}\rangle_1 + \langle\psi_n^{(0)}|H_1|\psi_n^{(p-2)}\rangle_1 \\ &- \sum_{j=1}^{p-1} E_n^{(j)} \langle\psi_n^{(0)}|\psi_n^{(p-j)}\rangle_0 - \sum_{j=1}^{p} E_n^{(j-1)} \langle\psi_n^{(0)}|\psi_n^{(p-j)}\rangle_1 . \end{aligned} \tag{4.34}$$

In comparison to the common Rayleigh-Schrödinger perturbation theory, see i.e. Refs. [55, 56], we obtain that the usual first-order correction of the energy [55, Eq.(7.39)] agrees with (4.33). However, for higher orders $p \geq 2$ in (4.34) additional corrections appear, which contain the correction of the scalar product $\langle\cdot|\cdot\rangle_1$. In the special case that this correction vanishes, i.e. $\langle\cdot|\cdot\rangle_1 = 0$, we reproduce the correct recursion formula in the Rayleigh-Schrödinger theory [55, Eq.(7.37)]. Note that the recursion (4.34) is only valid for $p \geq 2$ because it is explicitly depending on $|\psi_n^{(p-2)}\rangle$ in the third term. The first-order correction has to be calculated separately via (4.33) and represents the starting term for the recursion (4.34) on the right hand side.

4.2.3. Eigenstate correction: off-diagonal contribution

After the derivation of a formula for the correction of the eigenenergy $E_n^{(p)}$ we now compute the correction of the eigenstates $|\psi_n^{(p)}\rangle$. Due to the completeness relation (4.21) we expand

$$|\psi_n^{(p)}\rangle = \sum_m c_{mn}^{(p)} \, |\psi_m^{(0)}\rangle \,, \tag{4.35}$$

where we define $c_{mn}^{(p)} = \langle \psi_m^{(0)} | \psi_n^{(p)} \rangle_0$. In this section, we determine first the off-diagonal coefficients $c_{mn}^{(p)}$ for $m \neq n$ and afterwards in Section 4.2.4 the diagonal coefficients $c_{nn}^{(p)}$.

Analogue to the common perturbation theory we multiply (4.25) with $\langle \psi_m^{(0)}|$, where we assume $m \neq n$, thus we get

$$\sum_{p=1}^{\infty} \langle \psi_m^{(0)} | H_0 | \psi_n^{(p)} \rangle + \sum_{p=1}^{\infty} \langle \psi_m^{(0)} | H_1 | \psi_n^{(p-1)} \rangle = \sum_{p=1}^{\infty} \sum_{j=0}^{p} E_n^{(j)} \, \langle \psi_m^{(0)} | \psi_n^{(p-j)} \rangle \,. \tag{4.36}$$

As for the energy correction we also insert here the perturbed scalar product (4.14) and rewrite the respective sums. For the three terms in (4.36) we obtain then for the left hand-side

$$\sum_{p=1}^{\infty} \langle \psi_m^{(0)} | H_0 | \psi_n^{(p)} \rangle = \langle \psi_m^{(0)} | H_0 | \psi_n^{(1)} \rangle_0 + \sum_{p=2}^{\infty} \langle \psi_m^{(0)} | H_0 | \psi_n^{(p)} \rangle_0 + \sum_{p=2}^{\infty} \langle \psi_m^{(0)} | H_0 | \psi_n^{(p-1)} \rangle_1 \tag{4.37}$$

$$\sum_{p=1}^{\infty} \langle \psi_m^{(0)} | H_1 | \psi_n^{(p-1)} \rangle = \langle \psi_m^{(0)} | H_1 | \psi_n^{(0)} \rangle_0 + \sum_{p=2}^{\infty} \langle \psi_m^{(0)} | H_1 | \psi_n^{(p-1)} \rangle_0 + \sum_{p=2}^{\infty} \langle \psi_m^{(0)} | H_1 | \psi_n^{(p-2)} \rangle_1 \tag{4.38}$$

and for the right hand-side

$$\begin{aligned} \sum_{p=1}^{\infty} \sum_{j=0}^{p} E_n^{(j)} \, \langle \psi_m^{(0)} | \psi_n^{(p-j)} \rangle &= E_n^{(0)} \, \langle \psi_n^{(0)} | \psi_n^{(1)} \rangle_0 + E_n^{(1)} \, \langle \psi_m^{(0)} | \psi_n^{(0)} \rangle_0 \\ &+ \sum_{p=2}^{\infty} E_n^{(0)} \, \langle \psi_m^{(0)} | \psi_n^{(p)} \rangle_0 + \sum_{p=2}^{\infty} E_n^{(p)} \, \langle \psi_m^{(0)} | \psi_n^{(0)} \rangle_0 \\ &+ \sum_{p=2}^{\infty} \sum_{j=1}^{p-1} E_n^{(j)} \, \langle \psi_m^{(0)} | \psi_n^{(p-j)} \rangle_0 + \sum_{p=2}^{\infty} \sum_{j=1}^{p-1} E_n^{(j-1)} \, \langle \psi_m^{(0)} | \psi_n^{(p-j)} \rangle_1 \,. \end{aligned} \tag{4.39}$$

Thus we are now able to apply the conditions (4.18) and (4.20) to the Euclidean scalar product $\langle\cdot|\cdot\rangle_0$. Inserting (4.37)–(4.39) in (4.36) leads us to a long expression, which we sort with respect to the order of perturbation. Analogue to the energy correction we give the expression for the first order correction separately

$$\left(E_n^{(0)} - E_m^{(0)}\right) \langle\psi_m^{(0)}|\psi_n^{(1)}\rangle_0 = \langle\psi_m^{(0)}|H_1|\psi_n^{(0)}\rangle_0 \,. \tag{4.40}$$

Due to our assumption of non-degenerated energies (4.19) we are allowed to divide by the prefactor. Furthermore, we use again the completeness relation of the eigenstates (4.21) to get a formula for the first-order correction

$$|\psi_n^{(1)}\rangle = \sum_{m\neq n} |\psi_m^{(0)}\rangle \, \frac{1}{E_n^{(0)} - E_m^{(0)}} \, \langle\psi_m^{(0)}|H_1|\psi_n^{(0)}\rangle_0 \,, \tag{4.41}$$

thus we get the coefficient

$$c_{mn}^{(1)} = \frac{1}{E_n^{(0)} - E_m^{(0)}} \, \langle\psi_m^{(0)}|H_1|\psi_n^{(0)}\rangle_0 \,. \tag{4.42}$$

For the order $p \geq 2$ we obtain by the same procedure the recursion relation

$$\begin{aligned} |\psi_n^{(p)}\rangle = \sum_{m\neq n} \frac{|\psi_m^{(0)}\rangle}{E_n^{(0)} - E_m^{(0)}} \Big[& \langle\psi_m^{(0)}|H_1|\psi_n^{(p-1)}\rangle_0 + \langle\psi_m^{(0)}|H_0|\psi_n^{(p-1)}\rangle_1 + \langle\psi_m^{(0)}|H_1|\psi_n^{(p-2)}\rangle_1 \\ & - \sum_{j=1}^{p-1} E_n^{(j)} \, \langle\psi_m^{(0)}|\psi_n^{(p-j)}\rangle_0 - \sum_{j=1}^{p-1} E_n^{(j-1)} \, \langle\psi_m^{(0)}|\psi_n^{(p-j)}\rangle_1 \Big], \end{aligned} \tag{4.43}$$

where we used that in the first sum over j $\langle\psi_m^{(0)}|\psi_n^{(0)}\rangle_0 = 0$ due to the assumption $m \neq n$. Thus we obtain for $c_{mn}^{(p)}$ with $p \geq 2$ and $m \neq n$

$$\begin{aligned} c_{mn}^{(p)} = \frac{1}{E_n^{(0)} - E_m^{(0)}} \Bigg[& \langle\psi_m^{(0)}|H_1|\psi_n^{(p-1)}\rangle_0 + \langle\psi_m^{(0)}|H_0|\psi_n^{(p-1)}\rangle_1 + \langle\psi_m^{(0)}|H_1|\psi_n^{(p-2)}\rangle_1 \\ & - \sum_{j=1}^{p-1} E_n^{(j)} \, \langle\psi_m^{(0)}|\psi_n^{(p-j)}\rangle_0 - \sum_{j=1}^{p-1} E_n^{(j-1)} \, \langle\psi_m^{(0)}|\psi_n^{(p-j)}\rangle_1 \Bigg]. \end{aligned} \tag{4.44}$$

At the end of the next section after calculating the whole correction for the eigenstates we compare this result to the literature.

4.2.4. Eigenstate correction: diagonal contribution

In the last part we have to determine the diagonal coefficients $c_{nn}^{(p)}$. To this end we use the normalization of the perturbed eigenstates with respect to the perturbed scalar product

$$\langle \psi_m | \psi_n \rangle = \delta_{mn}. \tag{4.45}$$

If we insert the expansion of the eigenstate (4.23) we obtain in the case $m = n$

$$\langle \psi_n | \psi_n \rangle = \sum_{p=0}^{\infty} \langle \psi_n^{(p)} | \sum_{j=0}^{\infty} | \psi_n^{(j)} \rangle \,. \tag{4.46}$$

With the Cauchy resumation we can rewrite (4.46) by

$$\langle \psi_n | \psi_n \rangle = \sum_{p=0}^{\infty} \sum_{j=0}^{p} \langle \psi_n^{(j)} | \psi_n^{(p-j)} \rangle \tag{4.47}$$

and insert the scalar product (4.14)

$$\langle \psi_n | \psi_n \rangle = \langle \psi_n^{(0)} | \psi_n^{(0)} \rangle_0 + \langle \psi_n^{(0)} | \psi_n^{(0)} \rangle_1 + \sum_{p=1}^{\infty} \sum_{j=0}^{p} \Big(\langle \psi_n^{(j)} | \psi_n^{(p-j)} \rangle_0 + \langle \psi_n^{(j)} | \psi_n^{(p-j)} \rangle_1 \Big). \tag{4.48}$$

Now we simplify (4.48) by applying (4.20) and (4.45)

$$0 = \langle \psi_n^{(0)} | \psi_n^{(0)} \rangle_1 + \sum_{p=1}^{\infty} \sum_{j=0}^{p} \Big(\langle \psi_n^{(j)} | \psi_n^{(p-j)} \rangle_0 + \langle \psi_n^{(j)} | \psi_n^{(p-j)} \rangle_1 \Big). \tag{4.49}$$

The double sum is similar to the sum occurring in the energy correction (4.30), so that we repeat the calculations from (4.30) to (4.32). Splitting the sum into the part $p = 1$ and the rest leads to

$$\begin{aligned} - \langle \psi_n^{(0)} | \psi_n^{(0)} \rangle_1 = & \langle \psi_n^{(1)} | \psi_n^{(0)} \rangle_0 + \langle \psi_n^{(0)} | \psi_n^{(1)} \rangle_0 \\ & + \sum_{p=2}^{\infty} \sum_{j=0}^{p} \langle \psi_n^{(j)} | \psi_n^{(p-j)} \rangle_0 + \sum_{p=1}^{\infty} \sum_{j=0}^{p} \langle \psi_n^{(j)} | \psi_n^{(p-j)} \rangle_1 \end{aligned} \tag{4.50}$$

We split the first sum in the parts $j = 0$, $j = p$, and the rest and change both summation

indices $p \to p-1$ and $j \to j-1$ in the second sum. Thus we obtain

$$\begin{aligned} -\langle\psi_n^{(0)}|\psi_n^{(0)}\rangle_1 = &\langle\psi_n^{(1)}|\psi_n^{(0)}\rangle_0 + \langle\psi_n^{(0)}|\psi_n^{(1)}\rangle_0 \\ &+ \sum_{p=2}^{\infty}\Big(\langle\psi_n^{(0)}|\psi_n^{(p)}\rangle_0 + \langle\psi_n^{(p)}|\psi_n^{(0)}\rangle_0\Big) \\ &+ \sum_{p=2}^{\infty}\sum_{j=1}^{p-1}\langle\psi_n^{(j)}|\psi_n^{(p-j)}\rangle_0 + \sum_{p=2}^{\infty}\sum_{j=1}^{p}\langle\psi_n^{(j-1)}|\psi_n^{(p-j)}\rangle_1 . \end{aligned} \tag{4.51}$$

Assuming real wavefunctions $|\psi_n^{(0)}\rangle$ the first two parts are equal to $2c_{nn}^{(1)}$ and the following two parts can be rewritten as $2c_{nn}^{(p)}$, respectively, due to (4.35). Sorting with respect to the order of perturbation leads for the first order to the diagonal coefficient

$$c_{nn}^{(1)} = -\frac{1}{2}\langle\psi_n^{(0)}|\psi_n^{(0)}\rangle_1 \tag{4.52}$$

and for p-th order to the diagonal coefficient

$$c_{nn}^{(p)} = -\frac{1}{2}\left(\sum_{j=1}^{p-1}\langle\psi_n^{(j)}|\psi_n^{(p-j)}\rangle_0 + \sum_{j=1}^{p}\langle\psi_n^{(j-1)}|\psi_n^{(p-j)}\rangle_1\right). \tag{4.53}$$

Now we insert both the off-diagonal coefficients $c_{mn}^{(p)}$ and the diagonal coefficients $c_{nn}^{(p)}$ into the expansion of the eigenstates $|\psi_n^{(p)}\rangle$ (4.23). With the first-order coefficients (4.42) and (4.52) we get the first-order correction for the eigenstate

$$|\psi_n^{(1)}\rangle = \sum_{m\neq n}\frac{1}{E_n^{(0)} - E_m^{(0)}}\langle\psi_m^{(0)}|H_1|\psi_n^{(0)}\rangle_0\,|\psi_m^{(0)}\rangle - \frac{1}{2}\langle\psi_n^{(0)}|\psi_n^{(0)}\rangle_1\,|\psi_n^{(0)}\rangle . \tag{4.54}$$

In contrast to the first-order correction of the eigenenergy $E_n^{(1)}$ in (4.33) we obtain in (4.54) an additional term, which contains the correction of the scalar product. A short comparison to the usual Rayleigh-Schrödinger perturbation theory shows that we gain the correct result [55, Eq.(7.40)] in the special case that the correction of the scalar product $\langle\cdot|\cdot\rangle_1$ vanishes. Therefore, according to (4.52), it follows that $c_{nn}^{(1)} = 0$ in the common perturbation theory.

Furthermore, we obtain a recursion formula for the p-th order correction of the eigen-

states $|\psi_n^{(p)}\rangle$ by applying (4.44) and (4.53) to the expansion (4.23). This leads to

$$|\psi_n^{(p)}\rangle = \sum_{m\neq n} \frac{|\psi_m^{(0)}\rangle}{E_n^{(0)} - E_m^{(0)}} \Bigg[\langle\psi_m^{(0)}|H_1|\psi_n^{(p-1)}\rangle_0 + \langle\psi_m^{(0)}|H_0|\psi_n^{(p-1)}\rangle_1 + \langle\psi_m^{(0)}|H_1|\psi_n^{(p-2)}\rangle_1 - \sum_{j=1}^{p-1} E_n^{(j)} \langle\psi_m^{(0)}|\psi_n^{(p-j)}\rangle_0 - \sum_{j=1}^{p-1} E_n^{(j-1)} \langle\psi_m^{(0)}|\psi_n^{(p-j)}\rangle_1 \Bigg] - \frac{1}{2} \left(\sum_{j=1}^{p-1} \langle\psi_n^{(j)}|\psi_n^{(p-j)}\rangle_0 + \sum_{j=1}^{p} \langle\psi_n^{(j-1)}|\psi_n^{(p-j)}\rangle_1 \right) |\psi_n^{(0)}\rangle \,. \tag{4.55}$$

Analogue to the other corrections, we compare this with the Rayleigh-Schrödinger theory by assuming the special case of a vanishing correction of the scalar product. Note that (4.55) is only valid for $p \geq 2$, so that i.e. $c_{nn}^{(2)}$ does not vanish in agreement to [57, Ch. XI, Eq.(A-16)].

This perturbation theory is thus the extension of the Rayleigh-Schrödinger perturbation theory generalized on curved manifolds. The interesting point is that we have derived a recursion formula for both the correction of the eigenenergies (4.34) and the correction of the eigenstates (4.55), which are only valid for the order $p \geq 2$ in perturbation. The corresponding first-order correction is separately given by (4.33) and (4.54), where we obtain already in the first-order correction of the eigenstate a term depending on the perturbation of the scalar product $\langle\cdot|\cdot\rangle_1$.

In the next chapter we apply the perturbation theory on curved manifolds developed in this chapter to the Bose-Hubbard model for a curved optical lattice. To this end we restrict the perturbation theory to the first-order correction, in which the perturbation of the metric already occurs.

5. One-dimensional perturbed Bose-Hubbard model

In this chapter we analyze a one-dimensional Bose-Hubbard model for a curved optical lattice. Although we cannot have a real curvature in a one-dimensional chain, see Section 3.2, this toy model allows us to study a technical feature which goes beyond the flat case treated in Chapter 2. As we assume a small bending of the chain in form of a Lorentz function, we apply the perturbation theory on manifolds developed in Chapter 4.

In Section 5.1, we define the perturbed problem by its Hamiltonian and its corresponding scalar product. After that we determine in Section 5.2 the perturbed Bloch functions and the perturbed Wannier functions in Section 5.3. They are then used in Section 5.4 to calculate numerically the hopping parameter and in Section 5.5 the onsite energy for the slightly bent chain model. In Section 5.6 we perform the continuum limit analogue to the procedure for the flat case of Section 2.5.

Finally in Section 5.7 we suggest due to the special case of one dimension an alternative calculation with a flat Hamiltonian using the coordinate transformation and an effective potential derived in Section 3.2.3.

5.1. Perturbed problem

In this section we investigate the Hamiltonian and the corresponding perturbed scalar product for the Bose-Hubbard model of a weakly curved chain. To this end we start with the metric tensor, which we restrict to one dimension. According to (3.38) the contravariant metric for one dimension is given by

$$g(x) = 1 - h(x). \tag{5.1}$$

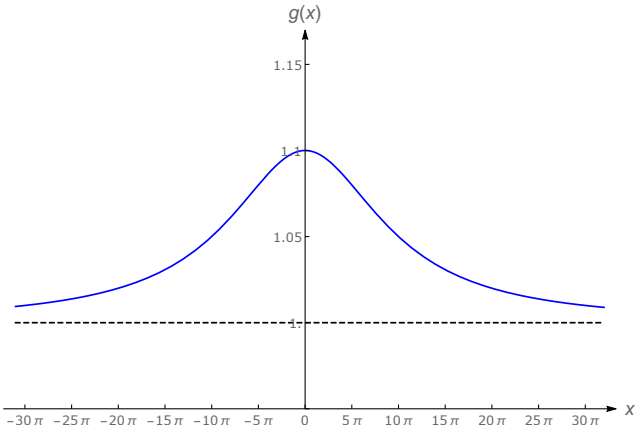

Figure 5.1.: Blue line denotes the contravariant metric (5.1) with the Lorentz correction (5.2) for the values $\alpha = 0.1$ and $\tilde{\rho} = 10\pi$. The black dashed line stands for the Euclidean metric. Note that we use here dimensionless units, which are introduced in (2.15).

For the perturbation $h(x)$ we now suppose a Lorentz function as an example

$$h(x) = -\alpha \frac{\rho^2}{x^2 + \rho^2}, \tag{5.2}$$

where the constant α describes the strength and ρ the width of the deviation of the contravariant metric (5.1) from the flat case, respectively. The function $h(x)$ represents a perturbation i.e. $|h(x)| \ll 1$, which implies $|\alpha| \ll 1$.

The resulting metric $g(x)$ is shown in Fig. 5.1. There we see that the perturbation is localized at the point $x = 0$ with the form of a Lorentz function and vanishes for large x, where the metric becomes Euclidean. Note that we use dimensionless units in the figure like in Chapter 2.

In order to determine the perturbed Hamiltonian we have to restrict the general form (4.11)–(4.13) on curved manifolds to one dimension. With $\delta^{\mu\nu} \to 1$ and $h^{\mu\nu} \to h(x)$ we obtain from (4.12) and (4.13)

$$H_0 = -\frac{\hbar^2}{2m}\partial_x^2 + V(x), \tag{5.3}$$

$$H_1 = +\frac{\hbar^2}{2m}\left[h(x)\partial_x^2 + \frac{1}{2}h'(x)\partial_x\right], \tag{5.4}$$

where $h'(x)$ denotes the first derivative of $h(x)$ with respect to x. With the perturbation

$h(x)$ of the metric given by (5.2) Eq. (5.4) reduces to

$$H_1 = -\frac{\hbar^2}{2m}\alpha\rho^2\left[\frac{1}{x^2+\rho^2}\partial_x^2 - \frac{x}{(x^2+\rho^2)^2}\partial_x\right]. \tag{5.5}$$

On the other side, we also need the perturbed scalar product on manifolds in order to apply the perturbation theory. The scalar product is given by (4.14)–(4.16), thus it follows for one dimension

$$\langle\psi|\varphi\rangle_0 = \int \mathrm{d}x\ \psi^\star(x)\varphi(x), \tag{5.6}$$

$$\langle\psi|\varphi\rangle_1 = +\frac{1}{2}\int \mathrm{d}x\ h(x)\psi^\star(x)\varphi(x), \tag{5.7}$$

where the latter reduces with (5.2) to

$$\langle\psi|\varphi\rangle_1 = -\frac{1}{2}\alpha\rho^2\int \mathrm{d}x\ \frac{1}{x^2+\rho^2}\psi^\star(x)\varphi(x). \tag{5.8}$$

In the following we apply the perturbation theory developed in Chapter 4 in order to determine the Bloch functions with respect to the corrections of both the Hamiltonian (5.5) and the scalar product (5.8).

5.2. Perturbed Bloch functions

According to the Schrödinger equation (2.14) the Bloch functions $\phi_k(x)$ are the eigenstates of the Hamiltonian H. We still assume that the temperature is low enough that only the lowest energy band is occupied, therefore we set $n = 0$ and drop the band index in the following. Using the perturbation theory then leads to an additional correction term for the Bloch functions

$$\phi_k(x) = \phi_k^{(0)}(x) + \phi_k^{(1)}(x). \tag{5.9}$$

We already know the unperturbed Bloch functions $\phi_k^{(0)}(x)$ from Section 2.3. From Fig. 2.1 we read off that the energy is degenerate for $k \neq 0$ with order two. Thus, in principle, we have to use for $k = 0$ the non-degenerated and for $k \neq 0$ the degenerated perturbation theory to determine the correction $\phi_k^{(1)}(x)$ of the Bloch functions. But here in our case we can simplify the problem by the following consideration.

First of all we assume the number of lattice sites N_s to be odd. According to (2.41)

and (2.42) we know then the possible values for k and for p, respectively, which have to be integers due to the periodic boundary condition (2.38).

In general we now have to find new eigenstates which diagonalize the Hamiltonian (5.5) but as in many cases we can exploit the symmetry of H_1 to simplify the whole perturbative calculation. Because both H_0 and H_1 are even functions in x, we suppose for the new eigenstates a superposition of the old eigenstates

$$\phi^{(0)}_{k,\pm}(x) = \frac{1}{\sqrt{2}}\left[\phi^{(0)}_k(x) \pm \phi^{(0)}_{-k}(x)\right]. \tag{5.10}$$

Here we have to restrict the values of the wave number. The superposition (5.10) is only valid for half of the initially possible values of the wave number k according to the order of degeneracy. We consider (5.10) for $k \geq 0$, thus $p = 0, 1, ..., \frac{N_s-1}{2}$. Furthermore, we note that for the special case $k = 0$ we get

$$\phi^{(0)}_{k=0,+}(x) = \phi^{(0)}_{k=0}(x), \qquad \phi^{(0)}_{k=0,-}(x) = 0. \tag{5.11}$$

Remembering the symmetry relations of the unperturbed Bloch functions (2.43a) and (2.43b), it turns out that the new Bloch functions have special properties, as well: $\phi^{(0)}_{k,+}(x)$ is real and symmetric, while $\phi^{(0)}_{k,-}(x)$ is imaginary and anti-symmetric.

For consistency reasons we check the orthonormality relation of the Bloch functions (5.10) and (5.11). For the calculation we have to distinguish between $k = 0$ and $k \neq 0$ as well as $\phi^{(0)}_{k,+}(x)$ and $\phi^{(0)}_{k,-}(x)$. For $k = 0$ and the Bloch functions $\phi^{(0)}_{k,+}$ we get due to (5.11)

$$\int \mathrm{d}x\ \phi^{(0)\star}_{k=0,+}(x)\phi^{(0)}_{k'=0,+}(x) = \int \mathrm{d}x\ \phi^{(0)\star}_{k=0}(x)\phi^{(0)}_{k'=0}(x) = 1, \tag{5.12}$$

where we exploit the orthonormality relation of the initial Bloch functions $\phi_k(x)$ (2.37) in the last step. For $k \neq 0$ we have to insert (5.10)

$$\begin{aligned}
&\int \mathrm{d}x\ \phi^{(0)\star}_{k,+}(x)\phi^{(0)}_{k',+}(x) \\
&\quad = \int \mathrm{d}x\ \frac{1}{2}\Big[\phi^{(0)\star}_k(x)\phi^{(0)}_{k'}(x) + \phi^{(0)\star}_k(x)\phi^{(0)}_{-k'}(x) + \phi^{(0)\star}_{-k}(x)\phi^{(0)}_{k'}(x) + \phi^{(0)\star}_{-k}(x)\phi^{(0)}_{-k'}(x)\Big] \\
&\quad = \delta_{k,k'} + \delta_{k,-k'}.
\end{aligned} \tag{5.13}$$

Due to the assumption $k, k' \geq 0$ it follows that

$$\int \mathrm{d}x\ \phi_{k,+}^{(0)\star}(x)\phi_{k',+}^{(0)}(x) = \delta_{k,k'}, \tag{5.14}$$

thus the Bloch functions $\phi_{k,+}^{(0)}(x)$ are normalized and orthogonal. In an analogue way we can show for $\phi_{k,-}^{(0)}(x)$

$$\int \mathrm{d}x\ \phi_{k,-}^{(0)\star}(x)\phi_{k',-}^{(0)}(x) = \begin{cases} 0, & k, k' = 0 \\ \delta_{k,k'}, & k, k' \neq 0 \end{cases} \tag{5.15}$$

and for the mixed terms

$$\int \mathrm{d}x\ \phi_{k,\pm}^{(0)\star}(x)\phi_{k',\mp}^{(0)}(x) = 0 \tag{5.16}$$

due to the symmetries mentioned above.

Based on the unperturbed Bloch functions $\phi_{k,\pm}^{(0)}(x)$ we obtain an expression for the first-order correction for the Bloch functions by using the result (4.54) of non-degenerate perturbation theory as well as the scalar products (5.6) and (5.7)

$$\begin{aligned} \phi_{k,\pm}^{(1)}(x) = &\sum_{k' \neq k} \frac{1}{E_k^{(0)} - E_{k'}^{(0)}} \left[\int \mathrm{d}x'\ \phi_{k',\pm}^{(0)}(x') H_1 \phi_{k,\pm}^{(0)}(x') \right] \phi_{k',\pm}^{(0)}(x) \\ &- \frac{1}{4} \left[\int \mathrm{d}x'\ h(x') \phi_{k,\pm}^{(0)}(x') \phi_{k,\pm}^{(0)}(x') \right] \phi_{k,\pm}^{(0)}(x). \end{aligned} \tag{5.17}$$

Note that (5.17) depends on both the correction of the Hamiltonian H_1 given by (5.5) and the correction of the metric $h(x)$ from (5.2). Mixed terms like $\int \mathrm{d}x\ \phi_{k',+}^{(0)}(x) H_1 \phi_{k,-}^{(0)}$ vanish due to the symmetries of the Bloch functions. The perturbed Bloch functions then have the form

$$\phi_{k,\pm}(x) = \phi_{k,\pm}^{(0)}(x) + \phi_{k,\pm}^{(1)}(x) \tag{5.18}$$

like we supposed in (5.9) for the degenerate perturbation theory.

In Fig. 5.2 the perturbed Bloch functions $\phi_{k,+}(x)$ and $\phi_{k,-}(x)$ are compared to the unperturbed Bloch functions $\phi_k^{(0)}(x)$ for an exemplary number $p = 10$ with $N = 31$. As assumed in perturbation theory, we see that the perturbed Bloch functions slightly differ from the unperturbed Bloch functions, which are used in Chapter 2. Especially at the point $\tilde{x} = 0$ there are no changes between both perturbed and unperturbed functions

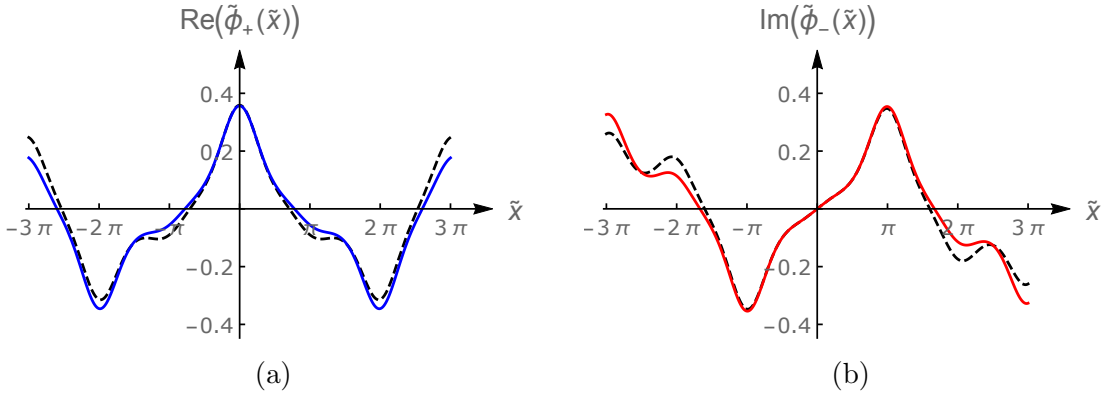

(a) (b)

Figure 5.2.: Real (a) and imaginary (b) part of the perturbed Bloch functions $\phi_{k,+}(x)$ and $\phi_{k,-}(x)$ for the lattice depth $\tilde{V}_0 = 3$ and with $p = 10$. Black dashed line shows the corresponding unperturbed Bloch function $\phi_k^{(0)}(x)$.

but the differences appear at $\tilde{x} = \pi$ and $\tilde{x} = 2\pi$.

5.3. Perturbed Wannier functions

Now we derive the Wannier functions, which are given according to (2.44) as

$$w(x - x_i) = \frac{1}{\sqrt{N_s}} \sum_{k \in 1.\mathrm{BZ}} \phi_k(x) e^{-ikx_i}. \tag{5.19}$$

Inserting the ansatz of the perturbed Bloch functions (5.9) into (5.19) gives us

$$w(x - x_i) = w^{(0)}(x - x_i) + w^{(1)}(x - x_i), \tag{5.20}$$

where we define

$$w^{(0)}(x - x_i) = \frac{1}{\sqrt{N_s}} \sum_{k \in 1.\mathrm{BZ}} \phi_k^{(0)}(x) e^{-ikx_i}, \tag{5.21}$$

$$w^{(1)}(x - x_i) = \frac{1}{\sqrt{N_s}} \sum_{k \in 1.\mathrm{BZ}} \phi_k^{(1)}(x) e^{-ikx_i}. \tag{5.22}$$

We derive now an expression for the unperturbed Wannier function $w^{(0)}(x - x_i)$ depending on the Bloch functions $\phi_{k,+}^{(0)}(x)$ and $\phi_{k,-}^{(0)}(x)$. To this end we rewrite the sum

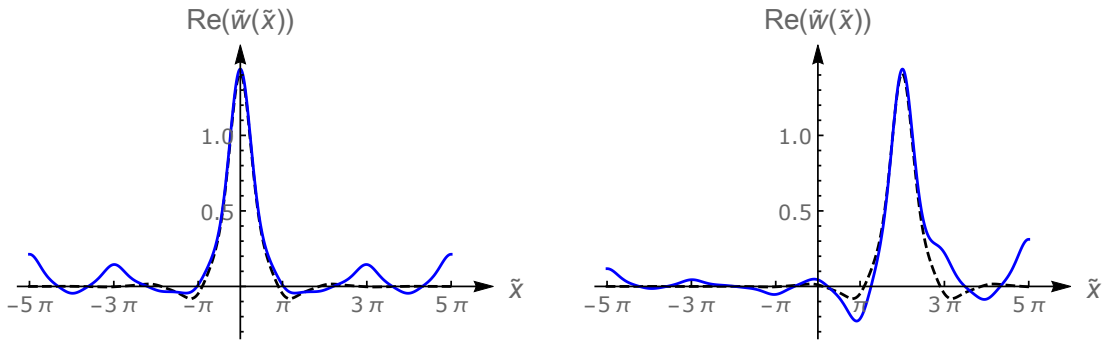

Figure 5.3.: Comparison between perturbed and unperturbed Wannier functions for $\tilde{V}_0 = 3$ and (a) $\tilde{x}_i = 0$ as well as (b) $\tilde{x}_i = 2\pi$. Blue line shows the perturbed Wannier function and black dashed line denotes the unperturbed function.

over all values of k according to

$$w^{(0)}(x - x_i) = \frac{1}{\sqrt{N_s}} \left[\sum_{k>0} \phi_k^{(0)}(x) e^{-ikx_i} + \sum_{k<0} \phi_k^{(0)}(x) e^{-ikx_i} + \phi_{k=0}^{(0)}(x) \right], \tag{5.23}$$

where the upper and lower bound of the values of k is still limited by the first Brillouin zone. In the second sum we change the sign of k and we rewrite the two exponential functions with the Euler formula, yielding

$$\begin{aligned} w^{(0)}(x - x_i) =& \frac{1}{\sqrt{N_s}} \sum_{k>0} \left\{ \cos(kx_i) \left[\phi_k^{(0)}(x) + \phi_{-k}^{(0)}(x) \right] - i \sin(kx_i) \left[\phi_k^{(0)}(x) - \phi_{-k}^{(0)}(x) \right] \right\} \\ &+ \frac{1}{\sqrt{N_s}} \phi_{k=0}^{(0)}(x). \end{aligned} \tag{5.24}$$

Here we use the definitions of the new Bloch functions (5.10), (5.11) and obtain

$$w^{(0)}(x - x_i) = \frac{1}{\sqrt{N_s}} \left\{ \phi_{k=0,+}^{(0)}(x) + \sqrt{2} \sum_{k>0} \left[\cos(kx_i) \phi_{k,+}^{(0)}(x) - i \sin(kx_i) \phi_{k,-}^{(0)}(x) \right] \right\}. \tag{5.25}$$

Now we also check the orthonormality relation for the unperturbed Wannier functions (5.25) for consistency reasons. To this end we have to prove

$$\int \mathrm{d}x \; w^{(0)\star}(x - x_i) w^{(0)}(x - x_j) = \delta(x_i - x_j). \tag{5.26}$$

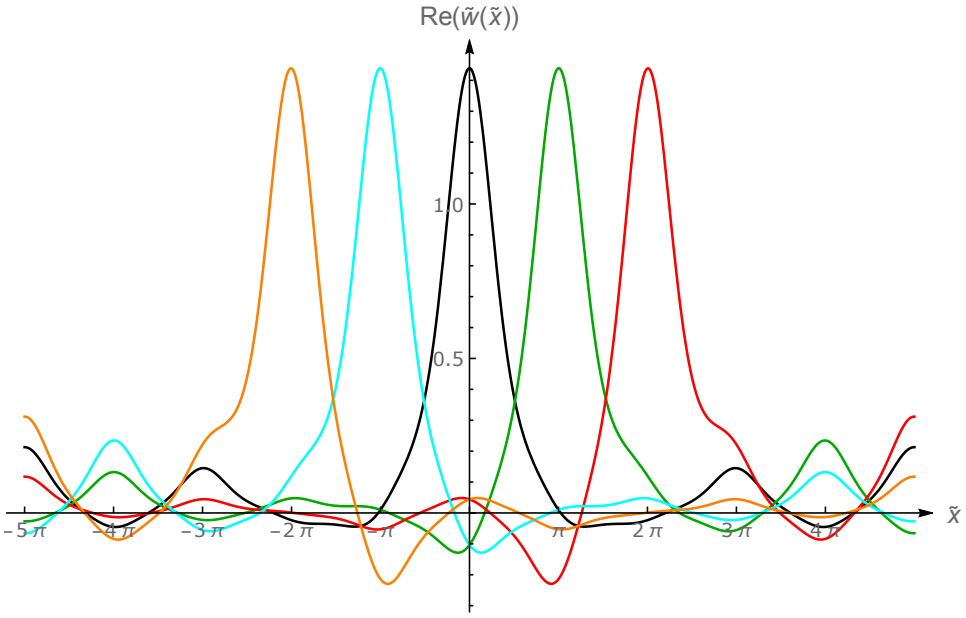

Figure 5.4.: Perturbed Wannier functions for $\tilde{V}_0 = 3$ for different x_i: $\tilde{x}_i = 0$ (blue), $\tilde{x}_i = +\pi$ (green), $\tilde{x}_i = -\pi$ (cyan), $\tilde{x}_i = +2\pi$ (red), $\tilde{x}_i = -2\pi$ (orange).

We insert (5.25) into (5.26) and multiply out the product, where mixed terms involving $\phi^{(0)}_{k,\pm}(x)$ and $\phi^{(0)}_{k',\mp}(x)$ vanish due to (5.16). An intermediate expression is

$$\int \mathrm{d}x\; w^{(0)\star}(x-x_i)w^{(0)}(x-x_j) = \frac{1}{N_s}\int \mathrm{d}x\; \phi^{(0)\star}_{k=0,+}(x)\phi^{(0)}_{k'=0,+}(x)$$
$$+\frac{2}{N_s}\sum_{k,k'}\int \mathrm{d}x\Big[\cos(kx_i)\cos(k'x_j)\phi^{(0)\star}_{k,+}(x)\phi^{(0)}_{k',+}(x) + \sin(kx_i)\sin(k'x_j)\phi^{(0)\star}_{k,+}(x)\phi^{(0)}_{k',+}(x)\Big]. \tag{5.27}$$

Here we see that for $k' \neq k$ the integrals vanish due to the orthonormality of the Bloch functions (5.14). In the case $k' = k$ we use the addition theorem $\cos(x)\cos(y) + \sin(x)\sin(y) = \cos(x-y)$, thus (5.27) reduces to

$$\int \mathrm{d}x\; w^{(0)\star}(x-x_i)w^{(0)}(x-x_j) = \frac{1}{N_s}\Big\{1 + 2\sum_{k>0}\cos\big[k(x_i-x_j)\big]\Big\}. \tag{5.28}$$

We rewrite this expression by using the symmetry of the cosine function

$$\int \mathrm{d}x\; w^{(0)\star}(x-x_i)w^{(0)}(x-x_j) = \frac{1}{N_s}\sum_{k\in 1.\mathrm{BZ}}\cos\big[k(x_i-x_j)\big]. \tag{5.29}$$

With the Euler formula we get

$$\int \mathrm{d}x\; w^{(0)\star}(x-x_i)w^{(0)}(x-x_j) = \frac{1}{N_s}\sum_{k\in 1.\mathrm{BZ}} \frac{1}{2}\left[e^{ik(x_i-x_j)} + e^{-ik(x_i-x_j)}\right], \tag{5.30}$$

which can be expressed using the Kronecker symbol, yielding indeed (5.26).

An expression of the first-order correction of the Wannier functions $w^{(1)}(x-x_i)$ can be derived analogue to the unperturbed Wannier function (5.25). It reads

$$w^{(1)}(x-x_i) = \frac{1}{\sqrt{N_s}}\left\{\phi^{(1)}_{k=0,+} + \sqrt{2}\sum_{k>0}\left[\cos(kx_i)\phi^{(1)}_{k,+}(x) - i\sin(kx_i)\phi^{(1)}_{k,-}(x)\right]\right\}. \tag{5.31}$$

In Fig. 5.3 we compare the perturbed Wannier function (5.20) with the unperturbed function (5.25), which coincides with the Wannier function (2.44) used in Chapter 2. We see that the perturbation mainly influences the values of the function for higher x_i. Figure 5.4 shows the perturbed Wannier functions $w(x-x_i)$ for different values of x_i. The perturbation is locally dependent as expected, as well as symmetric around $x=0$ due to the symmetry of the Lorentz function (5.2) shown in Fig. 5.1.

5.4. Perturbed hopping parameter

Now we analyze corrections to the hopping parameter J_{ij} for the slightly bent chain model. According to the definition of the hopping parameter in the flat case given by (2.12a), we can rewrite this expression by

$$J_{ij} = -\langle w_i|H|w_j\rangle, \tag{5.32}$$

where w_i is the abbreviation of the Wannier function $w(x-x_i)$. Inserting the perturbed scalar product (4.14), the perturbed Hamiltonian (4.11), and the perturbed Wannier functions (5.20) leads to a hopping parameter of the following form

$$J_{ij} = J^{(0)}_{ij} + J^{(1)}_{ij} + J^{(2)}_{ij} + J^{(3)}_{ij} + J^{(4)}_{ij} \tag{5.33}$$

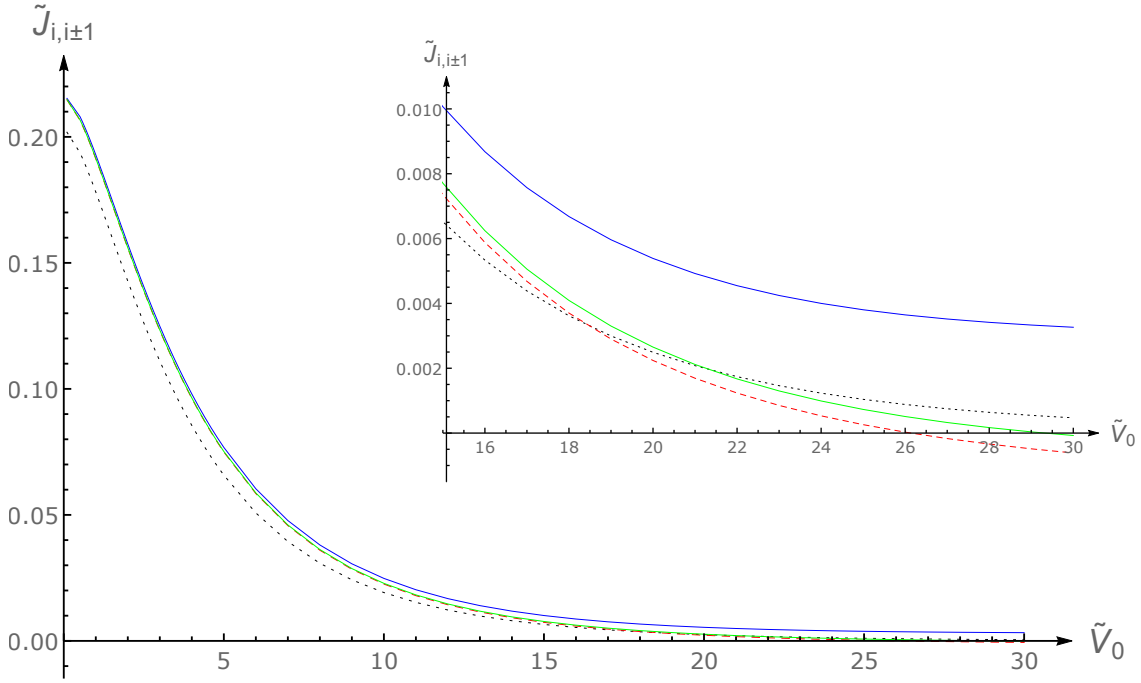

Figure 5.5.: Perturbed hopping parameter of the slightly bent chain model as a function of the lattice depth $\tilde{V}_0$. Black-dashed line shows the unperturbed limit of Chapter 2. Blue line shows the hopping parameter $\tilde{J}_{0,1}$, red-dashed line stands for $\tilde{J}_{10,11}$ and green line for $\tilde{J}_{10,9}$.

with the respective terms

$$J_{ij}^{(0)} = -\int \mathrm{d}x\; w^{(0)}(x-x_i)\; H_0\; w^{(0)}(x-x_j) \tag{5.34a}$$

$$J_{ij}^{(1)} = -\int \mathrm{d}x\; w^{(1)}(x-x_i)\; H_0\; w^{(0)}(x-x_j) \tag{5.34b}$$

$$J_{ij}^{(2)} = -\int \mathrm{d}x\; w^{(0)}(x-x_i)\; H_1\; w^{(0)}(x-x_j) \tag{5.34c}$$

$$J_{ij}^{(3)} = -\int \mathrm{d}x\; w^{(0)}(x-x_i)\; H_0\; w^{(1)}(x-x_j) \tag{5.34d}$$

$$J_{ij}^{(4)} = -\int \mathrm{d}x\; \frac{1}{2}h(x)w^{(0)}(x-x_i)\; H_0\; w^{(0)}(x-x_j). \tag{5.34e}$$

Higher order corrections are neglected. We recognize that the first part $J_{ij}^{(0)}$ is the unperturbed hopping parameter, which we already determined and discussed in Section 2.4. The other four terms are first-order corrections, so $J_{ij}^{(2)}$ means the second part of the first-order correction. Note that $J_{ij}^{(3)} = J_{ji}^{(1)}$ due to the hermiticity of the Hamiltonian H_0 with respect to the scalar product $\langle\cdot|\cdot\rangle_0$.

We calculate numerically the five parts of the hopping parameter J_{ij} (5.34a)–(5.34e) separately and then sum over all parts according to (5.33). For the numeric calculation we consider the metric (5.1) with the Lorentz connection (5.2) as well as the values $N_s = 31$, $\alpha = 0.1$ and $\tilde{\rho} = 10\pi$. The numerical results for nearest neighbor hopping $J_{i,i\pm1}$ are shown in Fig. 5.5 for different points x_i. We see that the perturbed hopping parameter is larger than the unperturbed one while having quite the same form. Additionally the perturbed hopping parameter is locally dependent and the curve for $x_i = 0$, which marks the center of the curvature, seems to be the upper limit. In the inlet of Fig. 5.5 the curves for the different hopping parameters are enlarged for $V_0 \geq 15$. We see clearly a difference between the nearest neighbors hopping terms $\tilde{J}_{10,11}$ and $\tilde{J}_{10,9}$. Furthermore, we obtain a sign change for both of the hopping parameters for deep lattices.

5.5. Perturbed onsite energy

In this short section we give the numerical results for the onsite energy in the curved case based on the definition (2.12b) in the flat case. The perturbed onsite energy is defined by

$$\epsilon_i = \langle w_i | H | w_i \rangle \tag{5.35}$$

in analogy to (5.32). This leads to the expression

$$\epsilon_i = \epsilon_i^{(0)} + \epsilon_i^{(1)} + \epsilon_i^{(2)} + \epsilon_i^{(3)} + \epsilon_i^{(4)}, \tag{5.36}$$

where the five terms are analogue to (5.34a)–(5.34e) given by

$$\epsilon_i^{(0)} = \int \mathrm{d}x \; w^{(0)}(x - x_i) \; H_0 \; w^{(0)}(x - x_i) \tag{5.37a}$$

$$\epsilon_i^{(1)} = \int \mathrm{d}x \; w^{(1)}(x - x_i) \; H_0 \; w^{(0)}(x - x_i) \tag{5.37b}$$

$$\epsilon_i^{(2)} = \int \mathrm{d}x \; w^{(0)}(x - x_i) \; H_1 \; w^{(0)}(x - x_i) \tag{5.37c}$$

$$\epsilon_i^{(3)} = \int \mathrm{d}x \; w^{(0)}(x - x_i) \; H_0 \; w^{(1)}(x - x_i) \tag{5.37d}$$

$$\epsilon_i^{(4)} = \int \mathrm{d}x \; \frac{1}{2} h(x) w^{(0)}(x - x_i) \; H_0 \; w^{(0)}(x - x_i). \tag{5.37e}$$

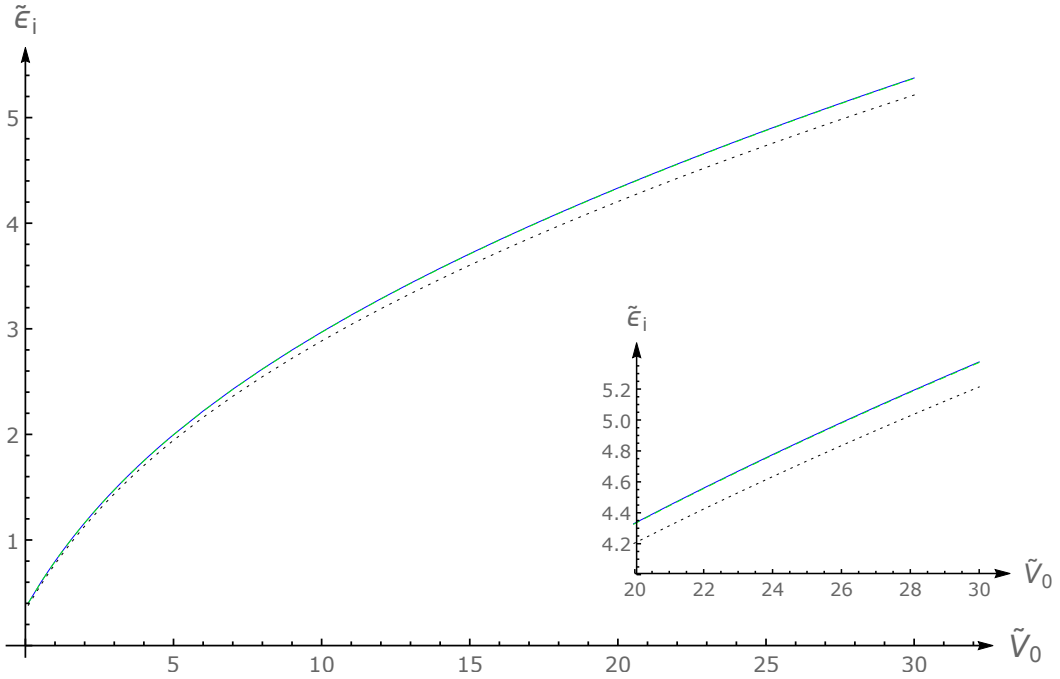

Figure 5.6.: Onsite energy of the perturbed model depending on the lattice depth $\tilde{V}_0$. The black-dashed line shows the unperturbed limit of Chapter 2, the blue line is the energy for $x_i = 0$, and the green dashed line for $x_i = 10\pi$.

Due to the hermiticity of H_0 we obtain $\epsilon_i^{(3)} = \epsilon_i^{(1)}$. For the numerical calculation we assume the same values for the parameters as in Section 5.4.

Figure 5.6 shows the perturbed onsite energy for different x_i compared to the unperturbed onsite energy treated in Section 2.4. In contrast to the hopping parameter in Fig 5.5 the curve seems to be independent from x_i as shown in the inlet but also larger than the unperturbed onsite energy.

5.6. Continuum limit

In Section 2.5 we have calculated analytically the many-body Hamiltonian in second quantization in the continuum starting with the Bose-Hubbard Hamiltonian on the lattice. We now derive the many-body Hamiltonian in curved space containing (5.3) and (5.5) with the same method. To this end we first derive the Hamiltonian in second quantization. Afterwards we have to find the limits of both the Bloch functions (5.10) and the Wannier functions (5.25) for vanishing lattice depth V_0 analogue to the procedure of Section 2.5. Then we calculate the perturbed hopping parameter J_{ij} for this special case and by using the Bose-Hubbard Hamiltonian (2.13) we derive the many-

body Hamiltonian for the slightly bent chain model.

First of all we derive the second quantized Hamiltonian on a curved manifold. To this end we start with

$$\hat{H} = \langle \hat{\psi} | H | \hat{\psi} \rangle \,, \tag{5.38}$$

where the single particle Hamiltonian H is given by the sum over (5.3) and (5.5). With these expressions as well as the scalar products (5.6) and (5.8) we obtain

$$\begin{aligned} \hat{H} = \int \mathrm{d}x \; \hat{\psi}^\dagger(x) \Bigg\{ & -\frac{\hbar^2}{2m}\partial_x^2 + V(x) + \frac{\hbar^2}{2m}\left[h(x)\partial_x^2 + \frac{1}{2}h'(x)\partial_x \right] \Bigg\} \hat{\psi}(x) \\ & + \frac{1}{2}\int \mathrm{d}x \; h(x)\hat{\psi}^\dagger(x) \left[-\frac{\hbar^2}{2m}\partial_x^2 \right] \hat{\psi}(x) + \mathcal{O}(h^2). \end{aligned} \tag{5.39}$$

Inserting the perturbation $h(x)$ of the metric from (5.2) leads to the second quantized Hamiltonian

$$\hat{H} = \int \mathrm{d}x \; \hat{\psi}^\dagger(x) \left\{ -\frac{\hbar^2}{2m} \left[\partial_x^2 + \frac{1}{2}\alpha\rho^2 \frac{1}{x^2+\rho^2}\partial_x^2 - \alpha\rho^2 \frac{x}{(x^2+\rho^2)^2}\partial_x \right] + V(x) \right\} \hat{\psi}(x). \tag{5.40}$$

In the following we reconstruct this continuum Hamiltonian from the corresponding lattice model by evaluating the hopping parameter of the Bose-Hubbard Hamiltonian (2.13) for vanishing lattice depth. But first we have to investigate both the Bloch and the Wannier functions for the limit of vanishing lattice depth.

We start with the Bloch functions $\phi_{k\pm}^{(0)}(x)$. According to Section 2.5 the limit of the initial functions $\phi_k(x)$ for vanishing lattice depth is given by a plane wave (2.48). We insert this in the definition of the unperturbed Bloch functions (5.10) and obtain

$$\phi_{k,+}^{(0)}(x) = \frac{1}{\sqrt{2N_s a}} \left(e^{ikx} + e^{-ikx} \right) = \frac{2}{\sqrt{2N_s a}} \cos(kx), \tag{5.41a}$$

$$\phi_{k,-}^{(0)}(x) = \frac{1}{\sqrt{2N_s a}} \left(e^{ikx} - e^{-ikx} \right) = \frac{2i}{\sqrt{2N_s a}} \sin(kx). \tag{5.41b}$$

Here we see that for the limit $V_0 \to 0$ the Bloch functions $\phi_{k,+}^{(0)}(x)$ are real while the Bloch functions $\phi_{k,-}^{(0)}(x)$ are imaginary functions as already explained in Section 5.3.

The next step is to investigate the limit for the unperturbed Wannier functions

$w^{(0)}(x-x_i)$. For this, we have to apply the equations (5.41a) and (5.41b) to the definition of the Wannier function (5.25). Thus we get for vanishing lattice depth

$$w^{(0)}(x-x_i) = \frac{1}{N_s}\frac{2}{\sqrt{2N_s a}}\Big\{1+\sqrt{2}\sum_{k>0}\Big[\cos(kx_i)\cos(kx)+\sin(kx_i)\sin(kx)\Big]\Big\}. \quad (5.42)$$

We simplify this expression by using the addition theorem

$$\cos(kx_i)\cos(kx)+\sin(kx_i)\sin(kx) = \cos\Big(k(x-x_i)\Big). \quad (5.43)$$

Furthermore we apply the limit of infinitely large number of lattice sites, i.e. $N_s \to \infty$ according to (2.50) and replace the sum over k by the corresponding integral. The first part of the equation is still proportional to $1/N_s$, thus this term vanishes due to the used limit. As result we obtain after integrating

$$w^{(0)}(x-x_i) = \frac{1}{\sqrt{a}}\frac{\sin\left(\frac{\pi}{a}(x-x_i)\right)}{\frac{\pi}{a}(x-x_i)}. \quad (5.44)$$

This agrees with the result in the flat case (2.52). Thus, this calculation confirms once again our definition of the unperturbed Bloch and Wannier functions as discussed in Section 5.2 and Section 5.3.

For the calculation of the hopping parameter we also need the first-order correction of the Wannier function $w^{(1)}(x-x_i)$. Therefore we insert the formula for the correction of the Bloch function $\phi^{(1)}_{k,\pm}(x)$ (5.17) with the limits for the unperturbed Bloch functions $\phi^{(0)}_{k,+}(x)$ (5.41a) and $\phi^{(0)}_{k,-}(x)$ (5.41b) in the correction of the Wannier function (5.31). In this long expression we replace the sum over k and k' with the corresponding integrals multiplied with the prefactor $N_s a/(2\pi)$ due to (2.50). The appearing equation contains terms of the orders N_s^0, N_s^{-1}, and N_s^{-2}, thus in the limit of infinitely large number of lattice sites $N_s \to \infty$ only the terms proportional to N_s^0 remain.

$$\begin{aligned} w^{(1)}(x-x_i) = {} & \frac{1}{\sqrt{a}}\frac{a}{\pi^2} \\ & \cdot \int_0^{\frac{\pi}{a}} \mathrm{d}k \left[\cos(kx_i)\int_0^{\frac{\pi}{a}} \mathrm{d}k' \, \frac{\cos(kx)}{E^{(0)}_k - E^{(0)}_{k'}} \int_{-\infty}^{\infty} \mathrm{d}x' \, \cos(k'x')H_1(x',\partial_{x'})\cos(kx') \right. \\ & \left. - \sin(kx_i)\int_0^{\frac{\pi}{a}} \mathrm{d}k' \, \frac{\sin(kx)}{E^{(0)}_k - E^{(0)}_{k'}} \int_{-\infty}^{\infty} \mathrm{d}x' \, \sin(k'x')H_1(x',\partial_{x'})\sin(kx')\right]. \end{aligned} \quad (5.45)$$

For vanishing lattice depth we expect to have a Bloch function, which describes a free

particle. In the same way we are then able to approximate the energy with the relation $E_k^{(0)} = \hbar^2 k^2/(2m)$. However, it is difficult to evaluate the equation (5.45) analytically due to the finite integrals over k and k'. Thus we stop here the analytic calculations for the correction of the Wannier function.

We continue with the evaluation of the hopping parameter for vanishing lattice depth. To this end we have to evaluate the expressions (5.34a)–(5.34e), where we already know the result for the unperturbed hopping parameter $J_{ij}^{(0)}$. Due to the calculations in Section 2.4 we obtain for an arbitrary hopping distance expressed in dimensionless units through an integer s

$$\tilde{J}_{i,i+s}^{(0)} = (-1)^{s+1} \frac{2}{s^2\pi^2} \tag{5.46}$$

as the continuum limit of the first part $J_{ij}^{(0)}$ of the perturbed hopping parameter J_{ij}. Now we have to find the limits for the first-order correction terms.

Because of the lack of an easier expression for the perturbed Wannier function we are not able to calculate analytically the limits for the parts $J_{ij}^{(1)}$ and $J_{ij}^{(3)}$. Nonetheless we calculate the limits for the remaining two parts starting with $J_{ij}^{(2)}$. Inserting both the Hamiltonian H_1 from (5.5) and the limit of the unperturbed Wannier functions (5.44) into (5.34c) leads to

$$\begin{aligned} J_{ij}^{(2)} = + \int \mathrm{d}x \; & \frac{1}{\sqrt{a}} \frac{\sin\left(\frac{\pi}{a}(x-x_i)\right)}{\frac{\pi}{a}(x-x_i)} \\ & \cdot \left[\frac{\hbar^2}{2m}\alpha\rho^2 \left(\frac{1}{x^2+\rho^2}\partial_x^2 - \frac{x}{(x^2+\rho^2)^2}\partial_x\right)\right] \frac{1}{\sqrt{a}} \frac{\sin\left(\frac{\pi}{a}(x-x_j)\right)}{\frac{\pi}{a}(x-x_j)}. \end{aligned} \tag{5.47}$$

We use dimensionless units $\tilde{x} = \pi/a \; x$, $\tilde{x_i} = \pi/a \; x_i$, and $\tilde{\rho} = \pi/a \; \rho$ and get

$$J_{ij}^{(2)} = E_\mathrm{R} \frac{1}{\pi} \alpha\tilde{\rho}^2 \int \mathrm{d}\tilde{x} \; \frac{\sin(\tilde{x}-\tilde{x}_i)}{\tilde{x}-\tilde{x}_i} \left[\frac{1}{\tilde{x}^2+\tilde{\rho}^2}\partial_{\tilde{x}}^2 - \frac{\tilde{x}}{(\tilde{x}^2+\tilde{\rho}^2)^2}\partial_{\tilde{x}}\right] \frac{\sin(\tilde{x}-\tilde{x}_j)}{\tilde{x}-\tilde{x}_j}. \tag{5.48}$$

Dividing by the recoil energy E_R gives us the dimensionless hopping parameter $\tilde{J}_{ij}^{(2)}$.

Before we evaluate this expression, we compute the last part of the first-order correction $J_{ij}^{(4)}$ by the definition (5.34e). Here we insert the perturbation $h(x)$ of the metric according to (5.2), the unperturbed Hamiltonian H_0 of (5.5) and the limit of the Wannier

functions (5.44) to obtain

$$J_{ij}^{(4)} = + \int \mathrm{d}x \, \frac{1}{2} \, \frac{\alpha\rho^2}{x^2+\rho^2} \frac{1}{\sqrt{a}} \frac{\sin\left(\frac{\pi}{a}(x-x_i)\right)}{\frac{\pi}{a}(x-x_i)} \cdot \left[-\frac{\hbar^2}{2m}\partial_x^2 + V_0 \sin^2\left(\frac{\pi}{a}x\right) \right] \frac{1}{\sqrt{a}} \frac{\sin\left(\frac{\pi}{a}(x-x_j)\right)}{\frac{\pi}{a}(x-x_j)}. \tag{5.49}$$

In the limit $V_0 \to 0$ the second part vanishes. We use the same dimensionless units like above and get

$$J_{ij}^{(4)} = -\frac{E_\mathrm{R}}{2\pi}\alpha\tilde{\rho}^2 \int \mathrm{d}\tilde{x} \, \frac{\sin(\tilde{x}-\tilde{x}_i)}{\tilde{x}-\tilde{x}_i} \left[\frac{1}{\tilde{x}^2+\tilde{\rho}^2}\partial_{\tilde{x}}^2 \right] \frac{\sin(\tilde{x}-\tilde{x}_j)}{\tilde{x}-\tilde{x}_j}. \tag{5.50}$$

This looks quite similar to the first part of $J_{ij}^{(2)}$ in (5.48). Thus we evaluate the sum over both parts because we are only interested in the whole correction. The sum over $J_{ij}^{(2)}$ and $J_{ij}^{(4)}$ is then given as

$$\tilde{J}_{ij}^{(2)} + \tilde{J}_{ij}^{(4)} = \frac{1}{\pi}\alpha\tilde{\rho}^2 \int \mathrm{d}\tilde{x} \, \frac{\sin(\tilde{x}-\tilde{x}_i)}{\tilde{x}-\tilde{x}_i} \left[\frac{1}{2} \, \frac{1}{\tilde{x}^2+\tilde{\rho}^2}\partial_{\tilde{x}}^2 - \frac{\tilde{x}}{(\tilde{x}^2-\tilde{\rho}^2)^2}\partial_{\tilde{x}} \right] \frac{\sin(\tilde{x}-\tilde{x}_j)}{\tilde{x}-\tilde{x}_j}. \tag{5.51}$$

Here we substitute $\tilde{x}' = \tilde{x} - \tilde{x}_i$ and in the last term we rewrite the appearing argument of the diffraction function analogue to Section 2.4

$$\tilde{x}' - (\tilde{x}_j - \tilde{x}_i) = \tilde{x}' - s\pi \tag{5.52}$$

$$\sin(\tilde{x}' - s\pi) = (-1)^s \sin(\tilde{x}'). \tag{5.53}$$

We obtain then

$$\tilde{J}_{i,i+s}^{(2)} + \tilde{J}_{i,i+s}^{(4)} = \alpha\tilde{\rho}^2 \frac{1}{\pi}(-1)^s \cdot \int \mathrm{d}\tilde{x}' \, \frac{\sin(\tilde{x}')}{\tilde{x}'} \left[\frac{1}{2} \, \frac{1}{(\tilde{x}'+\tilde{x}_i)^2+\tilde{\rho}^2}\partial_{\tilde{x}'}^2 - \frac{\tilde{x}'+\tilde{x}_i}{[(\tilde{x}'+\tilde{x}_i)^2+\tilde{\rho}^2]^2}\partial_{\tilde{x}'} \right] \frac{\sin(\tilde{x}')}{\tilde{x}'-s\pi}. \tag{5.54}$$

The derivatives and the addition theorem $2\sin(x)\cos(x) = \sin(2x)$ lead us to a long expression which can be solved by using the partial fraction expansion. After a straightforward, long calculation the result up to first order in the lattice constant a reads

$$J_{i,i+s}^{(2)} + J_{i,i+s}^{(4)} = -(-1)^s \alpha\rho^2 E_\mathrm{R} \left[\frac{1}{s^2\pi^2(x_i^2+\rho^2)} + \frac{x_i a}{s\pi^2(x_i^2+\rho^2)^2} \right]. \tag{5.55}$$

Note that we do not use here the dimensionless units, thus the variables are written without a tilde symbol. With the recoil energy $E_{\mathrm{R}} = \hbar^2\pi^2/(2ma^2)$ we obtain

$$J^{(2)}_{i,i+s} + J^{(4)}_{i,i+s} = (-1)^s \frac{\hbar^2}{2m}\alpha\rho^2 \left[\frac{1}{s^2(x_i^2+\rho^2)}\frac{1}{a^2} + \frac{x_i}{s(x_i^2+\rho^2)^2}\frac{1}{a}\right]. \tag{5.56}$$

An important point is included in the second term. Due to x_i the correction is locally dependent and because of the linear dependence of the hopping distance s we can observe an asymmetric behavior. Thus we obtain in general different values for the hopping parameters $J_{i,i+s}$ and $J_{i,i-s}$.

Now we apply the hopping parameter (5.56) to the Bose-Hubbard Hamiltonian (2.67) in the nearest neighbor approximation

$$H_{\mathrm{BHM}} = -\sum_i \left(J_{i,i+1}\, a_i^\dagger\, a_{i+1} + J_{i,i-1}\, a_i^\dagger\, a_{i-1}\right) + \sum_i \epsilon_i a_i^\dagger a_i, \tag{5.57}$$

where we still neglect the interaction term. The nearest neighbor hopping parameter $J_{i,i\pm1}$ with $s = 1$ is now given by the unperturbed hopping parameter and both calculated corrections read

$$\begin{aligned} J_{i,i\pm1} &= J^{(0)}_{i,i\pm1} + J^{(2)}_{i,i\pm1} + J^{(4)}_{i,i\pm1} \\ &= \frac{\hbar^2}{m}\left[\frac{1}{a^2} + \frac{1}{2}\alpha\rho^2\left(\frac{1}{x_i^2+\rho^2}\frac{1}{a^2} \pm \frac{x_i}{(x_i^2+\rho^2)^2}\frac{1}{a}\right)\right] \\ &= J_\pm. \end{aligned} \tag{5.58}$$

Like in Section 2.5 we perform now the limit $a \to 0$. To this end we rewrite the sum over the lattice sites i as an integral over x and express the creation and annihilation operators $a_i^\dagger$ and a_i in terms of the field operators $\psi^\dagger(x)$ and $\psi(x)$ according to (2.68a) and (2.68b). We obtain then

$$H = \int \mathrm{d}x\, \left\{-\Big[J_+(x)\psi^\dagger(x)\psi(x+a) + J_-(x)\psi^\dagger(x)\psi(x-a)\Big] + \epsilon(x)\psi^\dagger(x)\psi(x)\right\}. \tag{5.59}$$

The Taylor expansion

$$\psi(x \pm a) = \psi(x) \pm a\partial_x\psi(x) + \frac{a^2}{2}\partial_x^2\psi(x) \tag{5.60}$$

leads us to

$$H = \int \mathrm{d}x \left\{ -\frac{a^2}{2}\Big[J_+(x) + J_-(x)\Big]\psi^\dagger(x)\partial_x^2\psi(x) - a\Big[J_+(x) - J_-(x)\Big]\psi^\dagger(x)\partial_x\psi(x) + \Big(\epsilon(x) - \Big[J_+(x) + J_-(x)\Big]\Big)\psi^\dagger(x)\psi(x)\right\}. \tag{5.61}$$

The last part can be absorbed in some potential term like in the flat case. We compute the prefactors of the field operators with (5.58)

$$\Big[J_+(x) + J_-(x)\Big] = \frac{\hbar^2}{m}\left[\frac{2}{a^2} + \alpha\rho^2\frac{1}{x^2+\rho^2}\frac{1}{a^2}\right] \tag{5.62a}$$

$$\Big[J_+(x) - J_-(x)\Big] = \frac{\hbar^2}{m}\alpha\rho^2\frac{x}{(x^2+\rho^2)^2}\frac{1}{a}. \tag{5.62b}$$

By inserting (5.62a) and (5.62b) in (5.61) we get

$$H = \int \mathrm{d}x\ \psi^\dagger(x)\left\{-\frac{\hbar^2}{m}\left[\partial_x^2 + \frac{1}{2}\alpha\rho^2\frac{1}{x^2+\rho^2}\partial_x^2 - \alpha\rho^2\frac{x}{(x^2+\rho^2)^2}\partial_x\right] + V(x)\right\}\psi(x). \tag{5.63}$$

Compared to the second quantized Hamiltonian on curved manifolds (5.40), we find out that besides a missing factor of 2 like in Sec. 2.5 for the hopping parameter derived by Bloch functions only the sign of the third term of the perturbed Hamiltonian is not correct. We assume that this is due to the fact that the additional corrections $J_{ij}^{(1)}$ and $J_{ij}^{(3)}$ have not yet been taken into account. Nevertheless we are able to derive the correct form meaning one additional part including the second derivative and one spatially depending part, which contains the first derivative of x.

5.7. Effective potential

At the end of this chapter, we check the previous calculation as follows. Due to the special case of one dimension, we know from Section 3.2.3 that we are able to express the one dimensional Hamiltonian (3.73) of the bent chain model by using a general coordinate transformation (3.76) as a flat Hamiltonian with an effective potential according to (3.78). This effective potential $V_{\text{eff}}\big(x(u)\big)$ is then depending on the coordinate

transformation $x(u)$, where we choose in Section 3.2.3 the condition

$$x'(u) = \sqrt{g\big(x(u)\big)} = 1 - \frac{1}{2}h\big(x(u)\big). \tag{5.64}$$

By inserting the perturbation $h(x)$ of the metric (5.2) and integrating we get as coordinate transformation

$$x(u) = u + \frac{1}{2}\alpha\rho \arctan\left(\frac{u}{\rho}\right). \tag{5.65}$$

Thus the effective potential is given as

$$V\big(x(u)\big) = V_0 \sin^2\left[\frac{\pi}{a}\left\{u + \frac{1}{2}\alpha\rho \arctan\left(\frac{u}{\rho}\right)\right\}\right], \tag{5.66}$$

which we can simplify with the dimensionless units $\tilde{u} = \frac{\pi}{a}u$, $\tilde{\rho} = \frac{\pi}{a}\rho$ and a Taylor expansion to

$$V(\tilde{u}) = V_0\left[\sin^2(\tilde{u}) + \frac{1}{2}\alpha\tilde{\rho} \arctan\left(\frac{\tilde{u}}{\tilde{\rho}}\right)\sin(2\tilde{u})\right]. \tag{5.67}$$

This potential is interpreted as the sum over an unperturbed potential and a correction, thus we get for the Hamiltonian the form (4.11) with

$$H_0 = -\frac{\hbar^2}{2m}\partial_u^2 + V_0 \sin^2\left(\frac{\pi}{a}u\right), \tag{5.68}$$

$$H_1 = \frac{1}{2}V_0\alpha\frac{\pi}{a}\rho \arctan\left(\frac{u}{\rho}\right)\sin(2u). \tag{5.69}$$

The unperturbed eigenenergies $E_k^{(0)}$ are still the same as in the beginning of this chapter, thus due to the degeneracy we have to define the unperturbed Bloch functions $\phi_{k,\pm}^{(0)}(x)$ as in Eqs. (5.10) and (5.11). But the correction of the Bloch functions $\phi_{k,\pm}^{(1)}(x)$ is determined by the common Rayleigh-Schrödinger theory since we have no longer a perturbation of the scalar product. So we get instead of (5.17)

$$\phi_{k,\pm}^{(1)}(x) = \sum_{k'\neq k} \frac{1}{E_k^{(0)} - E_{k'}^{(0)}}\left[\int \mathrm{d}x'\ \phi_{k',\pm}^{(0)}(x')H_1\phi_{k,\pm}^{(0)}(x')\right]\phi_{k',\pm}^{(0)}(x). \tag{5.70}$$

The Wannier functions are calculated analogue to (5.25) and (5.31) with the corresponding Bloch functions.

The perturbed hopping parameter and the perturbed onsite energy are given by

$$J_{ij} = J_{ij}^{(0)} + J_{ij}^{(1)} + J_{ij}^{(2)} + J_{ij}^{(3)}, \tag{5.71}$$

$$\epsilon_i = \epsilon_i^{(0)} + \epsilon_i^{(1)} + \epsilon_i^{(2)} + \epsilon_i^{(3)}, \tag{5.72}$$

where the corresponding terms are given by (5.34a)–(5.34d) and (5.37a)–(5.37d) with the corresponding Wannier function. The last terms of each quantity, see (5.34e) and (5.37e) do not appear due to the unperturbed scalar product.

Due to the lack of time we are not able to calculate numerically the hopping parameter and the onsite energy. But we expect due to the derivation in Section 3.2.3 to reobtain the results of the previous sections.

6. Conclusions

In the last chapter of this thesis we conclude this diploma thesis. To this end we summarize the main results in Section 6.1. Afterwards, in Section 6.2 we give an outlook about further possible research. Points of interest are e.g. the phase transition between the superfluid phase and the Mott-insulating phase on curved manifolds as well as the problems of curved two- and three-dimensional optical lattices.

6.1. Summary

In this thesis we developed a one-dimensional mathematical model for quantum particles in a slightly curved optical lattice based on the Bose-Hubbard model and treated it within perturbation theory.

After a general introduction into the modern research field of ultracold quantum gases in Chapter 1, we revisited the flat Bose-Hubbard model in Chapter 2. By applying the method of continued fraction for determining both the Bloch and the Wannier functions we calculated numerically the hopping parameter for multiple hopping distances. The corresponding results in Fig. 2.5 show that the hopping parameter is exponentially decreasing and alternating with the hopping distance. An alternative equivalent way to compute the hopping parameter relies on the Fourier transformation of the lattice dispersion and is derived in the Appendix in Eq. (A.10). Furthermore, we derived analytically the continuum limit of the Bose-Hubbard model at the end of Chapter 2. We found out that we can perform two different limits. The first one is based on the analytically exact results of the Bloch functions, while the second one uses the effective mass approximation. For both limits we have to calculate the special case of a vanishing lattice depth as an intermediate step. Assuming a free particle and thus plane waves as Bloch functions leads to the diffraction function for the Wannier function (2.52) and to Eq. (2.57) for the hopping parameter, which agrees with the numeric results concerning both the absolute value and the alternating sign. With this formula we were able to reconstruct the second quantized Hamiltonian (2.72) up to a factor 2. On the other

hand, the effective mass approximation of the hopping parameter (2.65) leads to the correct Hamiltonian.

To be able to describe curved optical lattices we provided a brief introduction on Riemannian differential geometry in Chapter 3 based on Ref. [49]. By using the Laplace-Beltrami operator as the extension of the common Laplace operator we generalized the single-particle Hamiltonian on curved manifolds (3.56). On the other hand we also generalized the scalar product (3.62) by using the general volume element on curved manifolds (3.61). Afterwards, we proved with an appropriate coordinate transformation that in one dimension no physical curvature occurs.

In Chapter 4 we dealt with a perturbation of the metric itself to describe the curvature, which leads to both a perturbation in the Hamiltonian due to the Laplace-Beltrami operator and a perturbation in the scalar product due to the volume element. This implies to work out a new form of Rayleigh-Schrödinger perturbation theory on curved manifolds. As a result we obtained additional correction terms for the eigenenergy (4.34) as well as for the eigenstates (4.44).

This perturbation theory was applied in Chapter 5 to the Bose-Hubbard model, where we restricted the problem to one dimension. The perturbed Hamiltonian is then given by the Eqs. (5.3) and (5.5) and the perturbed scalar product by (5.6) and (5.8). Due to the degeneracy of the energy shown in Fig. 2.1 we had to define new unperturbed Bloch functions (5.10) and (5.11). With the perturbation theory we then determined numerically for a Lorentzian deformation of the optical lattice the correction to the Bloch functions as well as the Wannier functions, see Fig. 5.4 and analogues to the flat Bose-Hubbard model the hopping parameter and the onsite energy. It turned out that both the hopping term and the onsite energy become spatially dependent as shown in Fig. 5.5 and Fig. 5.6. Analogue to the flat Bose-Hubbard model we also performed the continuum limit. To this end we determined as an intermediate step the unperturbed Bloch functions for vanishing lattice depth in the Eqs. (5.41a) and (5.41b) and afterwards the limit of the unperturbed Wannier functions (5.44), which agrees with the Wannier function in the flat model. The limits of the corrections were difficult to calculate analytically, so that we could not finalize that due to the lack of time. Instead, we continued deriving the continuum limit of the hopping parameter by taking into account of most of the corrections in (5.33). As result we were able to derive the correct form of the perturbed Hamiltonian (5.63), where we obtain a difference by a factor of 2 like in Chapter 2 as well as a sign change in one term, which is assumed to be a consequence of the lack of two correction terms. Especially we were able to reconstruct the spatially

depending part including the first derivative with respect to the spatial coordinate.

6.2. Outlook

Now at the end of this thesis we point out some interesting possibilities for further research.

First of all, one can check the results of 5 by determining the energy correction according to the extended perturbation theory (4.33) due to the perturbed metric. With this one is able to calculate the hopping parameter by using a Fourier transformation analogue to Eq. (A.10) in the Appendix. The resulting hopping parameter should coincide with the results of Chapter 5. Another application of the perturbed energy is the continuum limit by using the effective mass approximation. This should lead to an expression of the hopping parameter, which is supposed to get the correct continuous Hamiltonian as in Chapter 2 in the flat case.

Furthermore, in the whole thesis we have neglected interactions between the quantum particles. This would lead to an essential distinction between bosonic and fermionic particles. For bosonic gases the interaction term U_i in the Bose-Hubbard model depends on the dimensionality of the system, see e.g. [42], thus one has to apply the perturbation theory on curved manifolds developed in Chapter 4 to two- and three-dimensional models, where a physical curvature is possible. To this end one has to specify which type of lattice is used, because depending on the perturbation of the metric it is possible that the nearest neighborhood of an arbitrary lattice well could change.

With the interaction term U_i and the hopping parameter J_{ij} one can investigate the transition between the superfluid phase and the Mott-insulating phase in curved optical lattices. Depending on the perturbation one can imagine that a more complex structure of phases can occur, where it can be possible that in one direction a Mott-insulating phase dominates while in the other direction a superfluid phase is formed. Thus it can be even possible to generate bands or rings of one phase surrounded by the other. In order to investigate the quantum phase transition including the degeneracy between two neighboring Mott phases, one can also apply the Brillouin-Wigner perturbation theory treated in [58], which then has to be extended on curved manifolds.

Finally, the theory developed in this thesis as well as all further theoretical researches have to be experimentally realized and verified. This can be done with a Digital Mirror Device (DMD), which contains multiple small mirrors to generate spatially and temporally varying optical lattices.

A. Hopping parameter as Fourier transformed energy

In this section we will discuss an alternative way to calculate the hopping parameter via the eigenvalues $E_n(k)$ of the Schrödinger equation. This way is worked out in Ref. [45]. We expand this calculation to arbitrary hopping distances and a formula for the onsite energy. Therefore we test our results of Section 2 for the hopping parameter as well as the onsite energy.

Starting point is the definition of the hopping parameter (2.12a)

$$J_{ij} = -\int \mathrm{d}^3x \; w^\star(\mathbf{x}-\mathbf{x}_i) H w(\mathbf{x}-\mathbf{x}_j). \tag{A.1}$$

The Wannier functions are separable in the spatial coordinates

$$w(\mathbf{x}-\mathbf{x}_i) = w(x-x_i)w(y-y_i)w(z-z_i) \tag{A.2}$$

so the first quantized Hamiltonian of a point mass in an optical lattice reads

$$\begin{aligned} H &= -\frac{\hbar^2}{2m}\Delta + V_{\text{ext}} \\ &= -\frac{\hbar^2}{2m}(\partial_x^2+\partial_y^2+\partial_z^2) + V_0\Big[\sin^2(\frac{\pi}{a}x)+\sin^2(\frac{\pi}{b}y)+\sin^2(\frac{\pi}{c}z)\Big] \\ &= h_x + h_y + h_z, \end{aligned} \tag{A.3}$$

where a, b, and c are the lattice constants in the three different directions x, y, and z.

Inserting (A.3) and (A.2) in (A.1) yields

$$\begin{aligned} J_{ij} = &- \int_{-\infty}^{\infty} dx\; w^{\star}(x-x_i) h_x w(x-x_j) \int_{-\infty}^{\infty} dy\; w^{\star}(y-y_i) w(y-y_j) \\ &\cdot \int_{-\infty}^{\infty} dz\; w^{\star}(z-z_i) w(z-z_j) \\ &- \int_{-\infty}^{\infty} dx\; w^{\star}(x-x_i) w(x-x_j) \int_{-\infty}^{\infty} dy\; w^{\star}(y-y_i) h_y w(y-y_j) \\ &\cdot \int_{-\infty}^{\infty} dz\; w^{\star}(z-z_i) w(z-z_j) \\ &- \int_{-\infty}^{\infty} dx\; w^{\star}(x-x_i) w(x-x_j) \int_{-\infty}^{\infty} dy\; w^{\star}(y-y_i) w(y-y_j) \\ &\cdot \int_{-\infty}^{\infty} dz\; w^{\star}(z-z_i) h_z w(z-z_j). \end{aligned} \tag{A.4}$$

We assume the nearest neighbor approximation and the fact that one particle can then only hop in one spatial direction, say x, so that $x_i - x_j \neq 0$ we have $y_i = y_j$ and $z_i = z_j$. Using the orthonormality relation of the Wannier functions (2.8), (A.4) simplifies then to

$$J_{ij} = - \int_{-\infty}^{+\infty} dx\; w^{\star}(x-x_i) h_x w(x-x_j). \tag{A.5}$$

Thus the hopping parameter is a one-dimensional quantity, meaning a real number, which does not dependent on the dimensionality of the system.

With the definition of the Wannier function (2.44) we can express the hopping parameter in terms of the Bloch functions

$$J_{ij} = - \int \mathrm{d}x\; \frac{1}{\sqrt{N_s}} \sum_k e^{+ikx_i} \phi_k^{\star}(x) h_x \frac{1}{\sqrt{N_s}} \sum_{k'} e^{-ik'x_j} \phi_{k'}(x). \tag{A.6}$$

Here we use the one-dimensional Schrödinger equation

$$h_x \phi_k(x) = E(k) \phi_k(x). \tag{A.7}$$

Like in Section 2.2 we set the band index n equal to zero due to the low temperatures and neglect it in the notation. With the orthonormality relation of the Bloch functions (2.37)

we simplify (A.6) to

$$J_{ij} = -\frac{1}{N_s} \sum_k E(k) e^{+ik(x_i - x_j)}. \tag{A.8}$$

This equation shows that the hopping parameter J_{ij} can also be evaluated as the Fourier transformation of the eigenenergies $E(k)$.

In a one-dimensional chain we are also able to calculate the hopping parameter for next nearest neighbor, and so on by supposing an arbitrary hopping distance $x_j - x_i = sa$, where a is the lattice constant and s an integer. Due to the homogenuity, we know that

$$J_{i,j} = J_{0,j-i} = J_{0,s} \tag{A.9}$$

thus (A.8) becomes

$$J_{0,s} = -\frac{1}{N_s} \sum_k E(k) e^{iksa}, \tag{A.10}$$

where $s = 1$ stands for the nearest neighbor, $s = 2$ for the next nearest neighbor, and so on.

We can do an analogue calculation for the onsite energy (2.12b) or alternatively we set in (A.8) $x_j = x_i$ and change the sign due to the definition (2.12b). In both cases we get an equation for the onsite energy ϵ_i depending on the eigenenergies $E(k)$ according to

$$\epsilon_i = \frac{1}{N_s} \sum_k E(k). \tag{A.11}$$

Applying (A.8) and (A.11) leads to the same results as shown in Fig. 2.5 and Fig. 2.7 by using the definition of the hopping parameter (2.12a) and the onsite energy (2.12b) via the Wannier functions (2.44). But note that from a numerical point of view, the Fourier transformed equations are easier to calculate because we just have to calculate the eigenvalues of the matrix equation (2.34) of the method of continued fraction mentioned in Section 2.2 instead of the eigenvectors and then the lattice periodic function $u_k(x)$, the Bloch functions $\phi_k(x)$, and finally the Wannier function $w(x - x_i)$.

Additionally, we are able to compute the continuum limit of the hopping parameter with (A.10) for the next neighbor approximation $s = 1$. To this end we use the limit of infinitely large number of lattice sites $N_s \to \infty$ explained in Section 2.5. Thus the sum

over the wave number k in (A.10) can be expressed as an integral, where we have to add a prefactor according to (2.50), so we get

$$J_{0,1} = -\frac{1}{N_s}\frac{N_s a}{2\pi}\int_{\frac{-\pi}{a}}^{\frac{+\pi}{a}} \mathrm{d}k\; E(k)e^{ika}. \tag{A.12}$$

Since we are interested in the limit of vanishing lattice depth $V_0 \to 0$ we approximate the energy $E(k)$ by the free particle dispersion relation in one dimension

$$E(k) = \frac{\hbar^2 k^2}{2m} \tag{A.13}$$

and insert this in (A.12) to get

$$J_{0,1} = -\frac{\hbar^2}{2ma^2}\frac{a}{2\pi}\int_{\frac{-\pi}{a}}^{\frac{+\pi}{a}} \mathrm{d}k\; k^2 a^2 e^{ika}. \tag{A.14}$$

After the substitution $k' = ka$ and using the partial integration twice, the integral yields

$$\int_{-\pi}^{+\pi} \mathrm{d}k'\; k'^2 e^{ik'} = -4\pi, \tag{A.15}$$

thus it follows for the continuum limit of the hopping parameter

$$J_{0,1} = \frac{\hbar^2}{ma^2}, \tag{A.16}$$

which is equal to the limit (2.59) derived via the Wannier functions. Note that the optical lattice is assumed to be homogeneous in this calculation, thus $J_{0,1} = J_{i,i+1}$ for every lattice site i.

List of Figures

Bibliography

[1] A. Einstein. Quantentheorie des einatomigen idealen Gases, 1925. Handwritten manuscript, Leiden University, Instituut-Lorentz. http://www.lorentz.leidenuniv.nl/history/Einstein_archive/.

[2] S. Bose. Plancks Gesetz und Lichtquantenhypothese. *Springer*, **26**, 178, 1924. http://link.springer.com/article/10.1007%2FBF01327326.

[3] M. H. Anderson, J. R. Ensher, M. R. Matthews, C. E. Wieman, E. A. Cornell. Observation of Bose-Einstein Condensation in a Dilute Atomic Vapor. *Science*, **269**, 198, 1995. http://sites.fas.harvard.edu/~phys191r/References/a10/Anderson1995.pdf.

[4] C. C. Bradley, C. A. Sackett, J. J. Tollett, and R. G. Hulet. Evidence of Bose-Einstein Condensation in an Atomic Gas with Attractive Interactions. *Physical Review Letters*, **75**, 1687, 1995. http://journals.aps.org/prl/pdf/10.1103/PhysRevLett.75.1687.

[5] C. C. Bradley, C. A. Sackett, J. J. Tollett, and R. G. Hulet. Errata - Evidence of Bose-Einstein Condensation in an Atomic Gas with Attractive Interactions. *Physical Review Letters*, **79**, 1170, 1997. http://journals.aps.org/prl/pdf/10.1103/PhysRevLett.79.1170.

[6] K. B. Davis, M.-O. Mewes, M. R. Andrews, N. J. van Druten, D. S. Durfee, D. M. Kurn, and W. Ketterle. Bose-Einstein Condensation in a Gas of Sodium Atoms. *Physical Review Letters*, **75**, 3969, 1995. http://journals.aps.org/prl/pdf/10.1103/PhysRevLett.75.3969.

[7] T. Fukuhara, S. Sugawa, M. Sugimoto, S. Taie, and Y. Takahashi. Mott insulator of ultracold alkaline-earth-metal-like atoms. *Physical Review A*, **79**, 041604, 2009. http://journals.aps.org/pra/pdf/10.1103/PhysRevA.79.041604.

[8] A. Griesmaier, J. Werner, S. Hensler, J. Stuhler, and T. Pfau. Bose-Einstein Condensation of Chromium. *Physical Review Letters*, **94**, 160401, 2005. `http://journals.aps.org/prl/pdf/10.1103/PhysRevLett.94.160401`.

[9] F. Dalfovo, S. Giorgini, L. P. Pitaevskii, and S. Stringari. Theory of Bose-Einstein condensation in trapped gases. *Review of Modern Physics*, **71**, 463, 1999. `http://journals.aps.org/rmp/pdf/10.1103/RevModPhys.71.463`.

[10] S. Giorgini, L. P. Pitaevskii, and S. Stringari. Theory of ultracold atomic Fermi gases. *Review of Modern Physics*, **80**, 1215, 2008. `http://journals.aps.org/rmp/pdf/10.1103/RevModPhys.80.1215`.

[11] C. Chin, R. Grimm, P. Julienne, and E. Tiesinga. Feshbach resonances in ultracold gases. *Review of Modern Physics*, **82**, 1225, 2010. `https://journals.aps.org/rmp/pdf/10.1103/RevModPhys.82.1225`.

[12] D. Jaksch, C. Bruder, J. I. Cirac, C. W. Gardiner, and P. Zoller. Cold bosonic atoms in optical lattices. *Physical Review Letters*, **81**, 3108, 1998. `http://journals.aps.org/prl/pdf/10.1103/PhysRevLett.81.3108`.

[13] M. Greiner, O. Mandel, T. Esslinger, T. W. Hänsch, and I. Bloch. Quantum phase transition from a superfluid to a Mott insulator in a gas of ultracold atoms. *Nature*, **415**, 39, 2002. `http://www.nature.com/nature/journal/v415/n6867/full/415039a.html`.

[14] J. P. Ronzheimer, M. Schreiber, S. Braun, S. S. Hodgman, S. Langer, I. P. McCulloch, F. Heidrich-Meisner, I. Bloch, and U. Schneider. Expansion Dynamics of Interacting Bosons in Homogeneous Lattices in One and Two Dimensions. *Physical Review Letters*, **110**, 205301, 2013. `http://journals.aps.org/prl/pdf/10.1103/PhysRevLett.110.205301`.

[15] I. Bloch. Ultracold quantum gases in optical lattices. *Nature Physics*, **1**, 23, 2005. `http://www.nature.com/nphys/journal/v1/n1/full/nphys138.html`.

[16] G.-B. Jo, J. Guzman, C. K. Thomas, P. Hosur, A. Vishwanath, and D. M. Stamper-Kurn. Ultracold Atoms in a Tunable Optical Kagome Lattice. *Physical Review Letters*, **108**, 045305, 2012. `http://journals.aps.org/prl/pdf/10.1103/PhysRevLett.108.045305`.

[17] T. Gericke, P. Würtz, D. Reitz, T. Langen, and H. Ott. High-resolution scanning electron microscopy of an ultracold quantum gas. *Nature Physics*, **4**, 949, 2008. http://www.nature.com/nphys/journal/v4/n12/pdf/nphys1102.pdf.

[18] B. Santra and H. Ott. Scanning electron microscopy of cold gases. *Journal of Physics B*, **48**, 122001, 2015. http://iopscience.iop.org/article/10.1088/0953-4075/48/12/122001/meta.

[19] H. Ott. Single atom detection in ultracold quantum gases: a review of current progress. *Reports on Progress in Physics*, **79**, 5, 2016. http://iopscience.iop.org/article/10.1088/0034-4885/79/5/054401/meta.

[20] M. P. A. Fisher, P. B. Weichman, G. Grintstein, and D. S. Fisher. Boson localization and the superfluid-insulator transition. *Physical Review B*, **40**, 546, 1988. http://journals.aps.org/prb/pdf/10.1103/PhysRevB.40.546.

[21] H. Kleinert, S. Schmidt, and A. Pelster. Reentrant Phenomenon in the Quantum Phase Transitions of a Gas of Bosons Trapped in an Optical Lattice. *Physical Review Letters*, **93**, 160402, 2004. http://journals.aps.org/prl/pdf/10.1103/PhysRevLett.93.160402.

[22] A. Hoffmann and A. Pelster. Visibility of cold atomic gases in optical lattices for finite temperatures. *Physical Review A*, **79**, 053623, 2009. http://journals.aps.org/pra/pdf/10.1103/PhysRevA.79.053623.

[23] G. P. Bewley, D. P. Lathrop, and K. R. Sreenivasan. Superfluid Helium: Visualization of quantized vortices. *Nature*, **441**, 588, 2006. https://www.nature.com/nature/journal/v441/n7093/pdf/441588a.pdf.

[24] C. T. Lane. Resource Letter LH-1 on Liquid Helium. *American Journal of Physics*, **35**, 5, 1967. http://sites.fas.harvard.edu/~phys191r/References/e1/lane1967.pdf.

[25] H. Pu and N. P. Bigelow. Properties of Two-Species Bose Condensates. *Physical Review Letters*, **80**, 1130, 1998. http://journals.aps.org/prl/pdf/10.1103/PhysRevLett.80.1130.

[26] D. M. Stamper-Kurn, M. R. Andrews, A. P. Chikkatur, S. Inouye, H.-J. Miesner, J. Stenger, and W. Ketterle. Optical Confinement of a Bose-Einstein Condensate.

Physical Review Letters, **80**, 2027, 1998. http://journals.aps.org/prl/pdf/10.1103/PhysRevLett.80.2027.

[27] S. Ospelkaus, C. Ospelkaus, O. Wille, M. Succo, P. Ernst, K. Sengstock, and K. Bongs. Localization of Bosonic Atoms by Fermionic Impurities in a Three-Dimensional Optical Lattice. *Physical Review Letters*, **96**, 180403, 2006. http://journals.aps.org/prl/pdf/10.1103/PhysRevLett.96.180403.

[28] K. Günter, T. Stöferle, H. Moritz, M. Köhl, and T. Esslinger. Bose-Fermi Mixtures in a Three-Dimensional Optical Lattice. *Physical Review Letters*, **96**, 180402, 2006. http://journals.aps.org/prl/pdf/10.1103/PhysRevLett.96.180402.

[29] D. J. Bishop, J. E. Berthold, J. M. Parpia, and J. D. Reppy. Superfluid density of thin He-4 films adsorbed in porous Vycor glass. *Physical Review B*, **24**, 9, 1981. https://journals.aps.org/prb/pdf/10.1103/PhysRevB.24.5047.

[30] C. Wang, L. Yu. Vortex dynamics of superfluid helium films on spherical surfaces. *Physical Review B*, **33**, 1, 1986. https://journals.aps.org/prb/pdf/10.1103/PhysRevB.33.599.

[31] R. Fan, P. Zhang, and Z.-Y. Shi. Curvature Induced Topological Defects of p-wave Superfluid on a Sphere. *arXiv*, 1612.03380, 2016. https://arxiv.org/pdf/1612.03380.pdf.

[32] C. M. Herdman, P.-N. Roy, R. G. Melko, and A. Del Maestro. Entanglement area law in superfluid He-4. *Nature Physics*, 2017. http://www.nature.com/nphys/journal/vaop/ncurrent/full/nphys4075.html.

[33] S. W. Hawking. Black hole explosions? *Nature*, **248**, 30, 1974. https://www.nature.com/nature/journal/v248/n5443/pdf/248030a0.pdf.

[34] J. D. Bekenstein. Black Holes and Entropy. *Physical Review D*, **7**, 8, 1972. https://journals.aps.org/prd/pdf/10.1103/PhysRevD.7.2333.

[35] N. Szpak. Curved spacetimes in the lab. *arXiv*, 1410.1567, 2014. https://arxiv.org/pdf/1410.1567.pdf.

[36] W. H. Zurek. Cosmological experiments in superfluid helium? *Nature*, **317**, 505, 1985. https://www.nature.com/nature/journal/v317/n6037/pdf/317505a0.pdf.

[37] M. Novello, M. Visser, and G. Volovik, editor. *Artifical Black Holes*. World Scientific Publishing Co. Pte. Ltd., New Jersey, London, Singapore, Hong Kong, 2002.

[38] S. W. Hawking. Particle creation by black holes. *Communications in Mathematical Physics*, **43**, 3, 1975. https://projecteuclid.org/download/pdf_1/euclid.cmp/1103899181.

[39] J. Anglin. Theoretical physics: Why trapped atoms are attractive. *Nature*, **406**, 29, 2000. http://www.nature.com/nature/journal/v406/n6791/full/406029a0.html#B1.

[40] D. O'Dell, S. Giovanazzi, G. Kurizki, and V. M. Akulin. Bose-Einstein Condensates with 1/r Interatomic Attraction: Electromagnetically Induced Gravity. *Physical Review Letters*, **84**, 5687, 2000. https://journals.aps.org/prl/pdf/10.1103/PhysRevLett.84.5687.

[41] J. Stuhler, A. Griesmaier, T. Koch, M. Fattori, T. Pfau, S. Giovanazzi, P. Pedri, and L. Santos. Observation of Dipole-Dipole Interaction in a Degenerate Quantum Gas. *Physical Review Letters*, **95**, 150406, 2005. https://journals.aps.org/prl/abstract/10.1103/PhysRevLett.95.150406.

[42] A. Hoffmann. Bosonen im optischen Gitter. Diploma thesis (German), Freie Universität Berlin, 2007. http://users.physik.fu-berlin.de/~pelster/Theses/hoffmann.pdf.

[43] W. Demtröder. *Experimentalphysik 3 - Atome, Moleküle und Festkörper*. Springer-Verlag, Berlin Heidelberg New York, 4. edition, 2010.

[44] K. V. Krutitsky. Ultracold bosons with short-range interaction in regular optical lattices. *Physics Reports*, **607**, 1, 2016. http://www.sciencedirect.com/science/article/pii/S0370157315004366.

[45] T. Graß. Real-Time Ginzburg-Landau Theory for Bosonic Gases in Optical Lattices. Diploma thesis, Freie Universität Berlin, 2009. http://users.physik.fu-berlin.de/~pelster/Theses/tobiasgrass.pdf.

[46] W. Zwerger. MottHubbard transition of cold atoms in optical lattices. *Journal of Optics B: Quantum and Semiclassical Optics*, **5**, 2, 2003. http://iopscience.iop.org/article/10.1088/1464-4266/5/2/352/meta.

[47] B. Irsigler. Dimensional Phase Transition in an Ultracold Bose Gas. Master thesis, Freie Universität Berlin, 2016. `http://users.physik.fu-berlin.de/~pelster/Theses/irsigler.pdf`.

[48] W. Demtröder. *Experimentalphysik 2 - Elektrizität und Optik*. Springer-Verlag, Berlin Heidelberg, 5. edition, 2009.

[49] E. Schrödinger. *Space-Time Structure*. The syndics of the Cambridge University Press, 1. edition, 1950.

[50] A. Pelster. Zur Theorie und Anwendung nicht-integrabler Raum-Zeit-Transformationen in der klassischen Mechanik und in der Quantenmechanik. PhD Thesis (German), Universität Stuttgart, 1996. `http://users.physik.fu-berlin.de/~pelster/Theses/dissertation.pdf`.

[51] T. Fließbach. *Allgemeine Relativitätstheorie*. Springer Spektrum, Berlin Heidelberg, 6. edition, 2012.

[52] N. Straumann. *Allgemeine Relativitätstheorie und relativistische Astrophysik*. Springer-Verlag, Berlin Heidelberg, 1981.

[53] A. Einstein. Über Gravitationswellen, 1918. ECHO - cutural heritage online, Max Planck Institute for the History of Science. `http://echo.mpiwg-berlin.mpg.de/ECHOdocuView?url=/permanent/echo/einstein/sitzungsberichte/W7ZU8V1E/index.meta`.

[54] E. Rebhan. *Theoretische Physik: Relativitätstheorie und Kosmologie*. Springer-Verlag, Berlin Heidelberg, 2012.

[55] W. Nolting. *Grundkurs Theoretische Physik 5/2 - Quantenmechanik - Methoden und Anwendungen*. Springer-Verlag, Berlin Heidelberg New York, 6. edition, 2006.

[56] F. Schwabl. *Quantenmechanik (QM I) - Eine Einführung*. Springer-Verlag, Berlin Heidelberg New York, 7. edition, 2007.

[57] C. Cohen-Tannoudji, B. Diu, F. Laloë. *Quantum Mechanics - Volume Two*. John Wiley & Sons, New York London Sydney Toronto, 2. edition, 1977.

[58] M. Kübler. Improving Mean-Field Theory for Bosons in Optical Lattices via Degenerate Perturbation Theory. Diploma thesis, Technische Universität Kaiserslautern, 2016. `http://users.physik.fu-berlin.de/~pelster/Theses/kuebler.pdf`.

Acknowledgements

First of all, I want to thank Prof. Dr. James Anglin for giving me the possibility to work in his group. I am thankful for all the long discussions, for the ideas of alternative calculations, and for the hints about useful methods and writing a diploma thesis itself.

I also want to thank Prof. Dr. Herwig Ott for being the second corrector.

Especially Priv.-Doz. Dr. Axel Pelster I would like to give my greatest thanks for supervising this thesis the whole year. Although having a very tight time schedule, he always spends time for detailed calculations and discussions. I thank him for all the patience and for making it possible to connect his research topic to my personal interest.

Special thanks go to my office colleague Alexej Gaidoukov who has had to offer one of his two desks. Nevertheless he helped me with all smaller and bigger problems whether they are of physical, mathematical or numerical nature.

Many thanks go to Ralf Bürkle for answering my questions in the last few weeks of this work, for the careful proofreading and for lots of proposals to improve this thesis.

Furthermore, I am grateful for the introduction to the Bose-Hubbard model by Martin Bonkhoff and Martin Kübler right at the beginning of my thesis.

In addition, Malte Koster and Manuel Schmitt were a great help with many basic questions and calculations especially at the beginning of my work.

Finally, I want to thank Manfred Berg and my whole family for all the support and patience over many years. All of them succeeded in distracting me from my problems when I needed that and motivated me by their own way to finish my studies.

Ich versichere, dass ich die Arbeit selbstständig verfasst und keine anderen als die angegebenen Hilfsmittel verwendet habe.

Sandro Gödtel